DISS. ETH NO. 22437

Methods for Synaptic Connectivity Mapping, Neuronal Stimulation and Spike Sorting Using High-density Microelectrode Arrays and Patch Clamp Recordings

A thesis submitted to attain the degree of DOCTOR OF SCIENCES of ETH ZURICH

(Dr. sc. ETH Zurich)

presented by

David Jäckel

MSc. ETH in Electrical Engineering, Switzerland

born on 04.11.1980

Citizen of Geroldswil ZH, Switzerland

accepted on the recommendation of

Prof. Dr. Andreas Hierlemann
Prof. Dr. Ulrich Egert
Dr. Urs Frey

2014

CONTENTS

Abstract

Recent advances in microelectronics and microfabrication technology have allowed for developing novel high-density microelectrode arrays, incorporating thousands of densely-arrayed microelectrodes for measuring and stimulating neuronal activity. The high spatiotemporal resolution of high-density microelectrode array (HD-MEA) technology offers possibilities to conduct novel experiments, which are not possible by using traditional techniques. At the same time, the vast amount of data, recorded by hundreds to thousands of electrodes, also poses new challenges to performing signal processing and data analysis. This thesis presents the development and evaluation of spike sorting techniques, as well as experiments on targeted stimulation and mapping postsynaptic signals by combining the HD-MEA technology with the traditional patch clamp technique.

For observed signals that constitute a linear mixture of a set of source signals, independent component analysis (ICA) can be used to blindly deconvolve the data and to extract the individual source signals. ICA offers great potential to alleviate the problem of spike sorting in HD-MEA recordings, as it represents an unsupervised method to separate the neuronal sources. The characteristics of extracellular signals of retinal ganglion cells (RGCs), recorded at high spatiotemporal resolution by HD-MEAs, were analyzed. This analysis revealed that the recorded data cannot be modeled as a purely linear mixture. Artificial realistic HD-MEA recordings of RGC activity were simulated for different neuronal densities and used to evaluate the performance of ICA as a stand-alone tool for spike sorting. In order to overcome the limitations arising from the nonlinearity of the sources, an iterative algorithm combining PCA and clustering techniques with ICA was developed. The spike sorting performance of the unsupervised ICA-based algorithm was found to strongly depend on cell density and spike amplitudes.

A system combining an upright microscope, the HD-MEA, and a conventional patch clamp setup was built. Image alignment software was developed to automatically detect the electrode identities on acquired images. Hardware and software components of the HD-MEA system were modified in order to route the signals of the patch clamp

amplifiers through the HD-MEA recording and acquisition system, which facilitated the experiments. The system was complemented with software tools, which were developed to combine optical, extracellular and intracellular data, and which allowed for performing more complex experiments.

Simultaneous intra- and extracellular recordings of embryonic rat neurons, cultured on the HD-MEA chips, were performed and combined with optical staining techniques. These combined measurements allowed for mapping the extracellular signals to the neuronal morphology, as well as to reveal the relative timings between the extracellular and intracellular action potentials (APs).

The experimental set-up was also used to record and to map individual inhibitory and excitatory postsynaptic potentials (PSPs). Spontaneous extracellular activity from multiple neurons was recorded with the HD-MEA, while the membrane potential of an individual patched cell was measured. Average PSPs between pre- and postsynaptic cells were obtained by spike-triggered averaging of the postsynaptic intracellular signals, based on the presynaptic spike times. Alternatively, presynaptic APs were evoked by stimulation through the HD-MEA electrodes, and the resulting PSPs were measured at the patched neuron. Stimulation pulses of different amplitudes were sequentially applied at subsets of electrodes in order to identify stimuli, which evoked individual monosynaptic PSPs. The identified stimuli could be used to evoke PSPs from multiple presynaptic neurons in arbitrary patterns, in order to study interactions between different presynaptic inputs under controlled conditions.

By using a combination of intra- and extracellular recordings and optical imaging, the effects of HD-MEA stimulation on cultured neurons were investigated. Many stimulation electrodes in different locations could be used to evoke activity of individual neurons. While the somato-dendritic neuronal compartment was identified as a region of low excitability, regions in which large extracellular neuronal signals could be recorded were comparably efficient in exciting the respective neurons through subsets of electrodes. Immunohistochemical imaging, combined with extracellular spontaneous recordings, indicated that the largest extracellular signals of cultured neurons on HD-MEAs can be recorded near the axonal initial segment (AIS), which also is an area

of high neuronal excitability. Therefore, the region of large extracellular signals is highly suitable for targeted stimulation of identified neurons.

Zusammenfassung

Die Herstellung neuartiger, hochauflösender Mikroelektrodenarrays (HD-MEAs) mit tausenden von Mikroelektroden zum Messen und Stimulieren neuronaler Aktivität wurde durch Entwicklungen in den Bereichen der Mikroelektronik und Mikrofabrikation ermöglicht. Die hohe räumliche und zeitliche Auflösung von HD-MEAs kann für neue Experimente genutzt werden, die mit konventionellen Methoden nicht durchführbar waren. Die grossen Datenmengen, welche durch gleichzeitiges Messen von Signalen hunderter bis tausender Elektroden generiert werden, erfordern allerdings auch neue Ansätze zur Signalverarbeitung und Datenanalyse. Die vorliegende Arbeit enthält Konzepte zur Entwicklung und Evaluierung von Klassifizierungsalgorithmen gemessener Aktionspotentiale. Weiterhin werden Experimente zur Stimulierbarkeit von Hirnzellen sowie zum Messen postsynaptischer Potentiale mittels einer Kombination von HD-MEAs und der Patch Clamp Technik aufgeführt.

Besteht ein Messsignal aus der linearen Mischung von Ursprungsignalen, so kann die Methode der Independent Component Analysis (ICA) dazu benutzt werden, die Signale automatisch zu entmischen und die Ursprungsignale wiederherzustellen. Könnten die gemessenen Signale der HD-MEAs mittels ICA entmischt werden, um die ursprünglichen neuronalen Signale wiederherzustellen, würde dies die Analyse bedeutend erleichtern. Die Eigenschaften der mittels HD-MEA gemessenen extrazellulären Signale von retinalen Ganglionzellen (RGC) wurden hinsichtlich ihrer Linearität analysiert, und entsprachen nur bedingt den Anforderungen der ICA Methode. Die Leistungsfähigkeit der ICA Methode zur Entmischung von gemessenen HD-MEA Signalen wurde mittels simulierter künstlicher RGC-Messdaten evaluiert. Ein iterativer Algorithmus, welcher ICA mit der Hauptkomponentenanalyse und Clustering Technik kombiniert wurde entwickelt, um die Limitierungen der ICA-Methode zu umgehen. Die Resultate der Evaluierung des automatischen Algorithmus zur Klassifizierung von Aktionspotentialen zeigen, dass dessen Leistungsfähigkeit stark von der Zelldichte sowie von den Signalamplituden abhängt.

Ein System wurde realisiert, welches ein Mikroskop mit dem HD-MEA und der Patch Clamp Technik verbindet. Mittels automatischer Zuordnung konnten die individuellen Elektroden auf Mikroskopiebildern identifiziert werden. Hardware- und Softwarekomponenten des HD-MEA Systems wurden modifiziert, um die Patch Clamp Signale direkt in das HD-MEA System einlesen zu können, was die Experimente erheblich erleichterte. Verschiedene Softwareprogramme zur Kombination optischer, intrazellulärer, sowie extrazellulärer Daten wurden entwickelt, die dann komplexere Experimente ermöglichten.

Hirnzellen von embryonalen Ratten wurden auf den HD-MEA-Chips kultiviert. Intrazelluläre und extrazelluläre Messungen wurden simultan durchgeführt und mit Mikroskopiebildern kombiniert. Diese Messungen gaben Aufschluss über die Positionen extrazellulärer Signale mit Hinsicht auf die Morphologie der Hirnzellen, sowie über das relative Timing intrazellulärer und extrazellulärer Aktionspotentiale.

Inhibitorische und exzitatorische postsynaptische Potentiale (PSPs) wurden mit dem realisierten System gemessen und zugeordnet. Während das intrazelluläre Signal einer Hirnzelle mit der Patch-Clamp-Methode gemessen wurde, wurden gleichzeitig die spontanen extrazellulären Signale von mehreren Zellen aufgezeichnet. Die durchschnittlichen PSPs wurden berechnet, in dem das intrazelluläre Signal der postsynaptischen Zelle während der Aktionspotentiale der einzelnen präsynaptischen Zellen gemittelt wurde. Alternativ wurden präsynaptische Zellen elektrisch stimuliert und die dadurch ausgelösten PSPs an der postsynaptischen Zelle gemessen. An mehreren Elektroden wurde mit unterschiedlichen Amplituden stimuliert, um Stimuli zu identifizieren, die PSPs durch unterschiedliche präsynaptische Zellen auslösten. Die so identifizierten Stimuli können dazu benutzt werden, PSPs in beliebigen Mustern auszulösen, um die Wechselwirkungen zwischen den verschiedenen synaptischen Signalen zu studieren.

Die Effekte elektrischer Stimulation kultivierter Hirnzellen durch das HD-MEA wurden mithilfe einer Kombination intrazellulärer, extrazellulärer und optischer Daten untersucht. Aktionspotentiale einzelner Neuronen konnten durch Stimulation an mehreren verschiedenen Elektroden ausgelöst werden. Während Hirnzellen in

der somato-dendritischen Region nur sehr beschränkt stimulierbar waren, konnten die Zellen in Regionen, in denen grosse extrazelluläre Signalamplituden gemessen wurden durch einige Elektroden vergleichbar effizient stimuliert werden. Immunohistochemische Untersuchungen ergaben, dass diese Regionen mit grossen Signalamplituden um das Initialsegment des Axons angeordnet waren. Diese Regionen mit grossen extrazellulären Amplituden sind in hohem Masse geeignet, um identifizierte Hirnzellen gezielt zu stimulieren.

CHAPTER 1 Introduction

Two fundamentally different approaches to directly measure electrical signals from neurons have been established and extensively used to study brain function and underlying mechanisms: intracellular and extracellular recordings. In intracellular recordings, the voltage across the cell membrane is measured. Intracellular recordings are typically performed using the patch clamp technique (Neher and Sakmann, 1976), where a glass micropipette is placed close to the neuronal membrane, and a high-resistance seal between the micropipette and the cell membrane is formed by the applied negative pressure. By further applying pulses of negative pressure, the membrane between the micropipette and the cell is then disrupted and the pipette solution comes into contact with the intracellular volume (Molleman, 2003). In extracellular recordings, a metal electrode is placed near a neuron. The electrode measures brief deflections of the electrode potential, whenever the neuron fires an action potential (AP).

Intracellular recordings feature an excellent signal-to-noise-ratio (SNR) and can be used to record subthreshold signals, such as postsynaptic potentials. The method is, however, time consuming, laborious and low-throughput, as one individual cell is measured per micropipette. As it is an invasive method, the time of the experiment is limited to a few hours. Extracellular recordings, in contrast, represent a noninvasive method and can be carried out over long time scales. As opposed to intracellular recording techniques, extracellular electrodes record the electrical activity of multiple cells in their surroundings. Therefore, to extract the spike times of individual measured neurons, spikes in the extracellular signals have to be assigned to individual neurons, a complex process referred to as 'spike sorting'.

Extracellular recordings from many small-size electrodes can be carried out in parallel. This is the concept of planar microelectrode arrays (MEAs), arrangements of electrodes for recording from multiple cells on a chip surface simultaneously (Pine, 1980). Complementary metal-oxide-semiconductor (CMOS) technology has allowed for the development of novel high-density MEAs (HD-MEAs), which feature integrated addressing, recording, and stimulation circuitry and thereby can provide much larger electrode densities (L Berdondini et al. 2005; Luca Berdondini et al. 2009; Eversmann, Jenkner, Hofmann, et al. 2003; Hutzler et al. 2006 with recording only and Ballini et al. 2014; Bjorn Eversmann et al. 2011; Frey et al. 2010 with recording and stimulation capabilities).

This thesis describes theoretical and experimental work towards the development of novel tools and methods for electrophysiological experiments while using HD-MEAs.

Proper spike sorting is fundamental to extract the spike times of individual neurons from HD-MEA recordings, and, therefore, constitutes a requirement for many experiments (Einevoll et al., 2012). In the first, theoretical part of this thesis, the usability and limitations of Independent Component Analysis (ICA) for automatic spike sorting of HD-MEA data are evaluated.

In the second, experimental part, the potentials of combining the extracellular HD-MEA technique with the intracellular patch clamp technique are explored.

1.1 Structure of this Thesis

This thesis consists of three papers:

1. *Applicability of Independent Component Analysis on High-Density Microelectrode Array Recordings*

   David Jäckel, Urs Frey, Michele Fiscella, Felix Franke, and Andreas Hierlemann

   Journal of Neurophysiology Volume 108, Issue 1, 1 July 2012, Pages 334–348.

2. *Mapping Synaptic Connections by Using Combined High-density Microelectrode Array and Patch Clamp Recordings*

   David Jäckel, Thomas Russell, Douglas Bakkum, Jan Müller, Felix Franke, Urs Frey, and Andreas Hierlemann

   In preparation

3. *Highly Localized Extracellular Stimulation of Cultured Cortical Neurons using High-density Arrays of Subcellular-size Microelectrodes*

   David Jäckel, Milos Radivojevic, Douglas Bakkum, Jan Müller, Thomas Russel, Felix Franke, Urs Frey, and Andreas Hierlemann

   In preparation

1.1.1 First aspect: Spike sorting techniques for HD-MEA recordings

Identifying the spike times of individual neurons is, in most cases, the goal of extracellular multi-unit recordings. In order to extract this information, spike sorting is absolutely required. Accordingly, a wide range of methods has been developed to address this problem (Lewicki, 1998), and many laboratories spend significant efforts to improve these methods. Spike sorting techniques have to face the challenges of low SNR recordings and the presence of overlapping spikes from multiple neurons.

For *in vivo*, as well as for *in vitro* applications, two classes of recording devices can be distinguished from the spike sorting perspective. In the first type of devices, neurons are recorded by single electrodes. In the *in vivo* case, such devices can be single extracellular electrodes or implantable needle arrays with large electrode distances. In *in vitro* research, planar MEAs with electrode distances larger than 60 µm typically record spikes from individual neurons only through single electrodes. The spike sorting performance is oftentimes very limited in such recordings, as spikes from multiple neurons that have been recorded by a single electrode may feature very similar spike waveforms and cannot be unambiguously assigned to the respective neurons.

CHAPTER 1

The second type of devices allows for simultaneous recording of spikes of individual neurons by multiple electrodes, such as tetrodes and implantable high-density MEAs for *in vivo*, or planar HD-MEAs for *in vitro* applications. It has been shown that recording with two or more, closely-spaced microelectrodes greatly improves the spike sorting performance (Gray et al., 1995; Einevoll et al., 2012; Fiscella et al., 2012).

For this reason, tetrodes have been widely used to record multi-unit activity, as they are easy to produce and yield acceptable spike sorting results. As a consequence, many spike sorting methods for this technique have been published (Takahashi et al., 2003). A particular challenge for spike sorting with tetrodes is how to select optimal features from the multichannel data, which are then used to separate the spikes into neuronal units.

For this particular problem of multichannel feature selection, and also for the clustering procedure, the spike sorting of HD-MEAs and tetrode recordings are partly related, which allows to adapt concepts from the literature for one method to the respective other method. However, simultaneous recordings of neuronal activity with hundreds to thousands of electrodes pose new challenges, and strategies for spike detection in highly redundant data and for how to deal with spike overlaps for very large numbers of recording sites are to be developed.

Since the first HD-MEA recordings, these challenges have been approached by different groups (Litke et al., 2004; Segev et al., 2004; Prentice et al., 2011). However, with the increasing developmental progress of HD-MEAs featuring thousands of densely-arranged recording sites, novel effective spike sorting approaches for such devices are highly demanded.

Chapter 2 of this thesis presents a study on the suitability and applicability of independent component analysis (ICA), an automatic method for blind source separation, to the problem of spike sorting of HD-MEA data. It is shown that the characteristics of neuronal signals as recorded with HD-MEAs do not fully meet the ICA requirement of representing linearly mixed source signals. Realistic HD-MEA data were simulated in order to evaluate the ICA performance. It was found that ICA does not yield complete separation of the neuronal signals, but

can still serve as a valuable preprocessing method prior to spike sorting. The simulated datasets were also used for evaluating spike sorting performances in another project (Dragas et al., 2014).

1.1.2 Second aspect: Combined HD-MEA and Patch Clamp recordings

The combination of HD-MEA technology with the patch clamp technique can be used for different purposes:

1. Use of the intracellular signal to understand and validate extracellular features and characteristics of extracellular data (Henze et al., 2000)
2. Evaluation of spike sorting algorithms (Harris et al., 2000; Hill et al., 2010)
3. Monitoring of effects of HD-MEA stimulation on cultured neurons (Chapter 4)
4. Recording and evoking of individual PSPs and mapping the presynaptic neurons (Chapter 3)
5. Using combined intra/ and extracellular recordings for detailed computational modelling studies

The advantages and disadvantages of intracellular and extracellular recordings have been mentioned above. An important advantage of the intracellular technique is the capability to measure subthreshold synaptic signals, since understanding synaptic transmission is the key to understanding the functioning of neural circuits. At the same time, the main advantage of HD-MEAs is to measure and to stimulate large numbers of neurons simultaneously. The experiments presented in Chapter 3 make use of the individual strengths of each technique and effectively combine both methods to measure spontaneous and stimulation-triggered synaptic signals of patched neurons.

From an experimental point of view, three individual techniques had to be brought together, namely optical imaging (which is required visualize and to patch a neuron), patch clamp and HD-MEAs. A first requirement was to map between acquired images of neurons on the array and their positioning in terms of HD-MEA electrodes. This was necessary in order to identify which electrodes were located underneath patched neurons, and to select these electrodes for

recording or stimulation. An automatic method to transform between the coordinate systems of the microscope and the HD-MEA and to align the obtained images was developed. Also, intra- and extracellular recordings needed to be combined and synchronized. This was achieved by employing additional analog-to-digital inputs to the HD-MEA system. The experimental setup was further complemented with a variety of software tools, which were essential for performing complex experiments.

1.1.3 Third Aspect: HD-MEA Stimulation for Cultured Neurons

For many electrophysiological experiments, it is not only necessary to record neuronal activity but to also evoke activity in a controlled manner. Targeted stimulation of previously identified, cultured neurons on HD-MEAs would offer the possibility to control neuronal activity of defined cells. In combination with the capability to record from multiple cells, the system would be highly suitable for experiments in the field of long-term plasticity and homeostatic regulation in neuronal networks.

Chapter 4 describes experimental approaches to analyzing the effects of HD-MEA stimulation on cultured neurons. Upon placement on HD-MEAs with sub-cellular size microelectrodes, cells can be stimulated through electrodes at many different locations so as to find the optimal stimulation electrode.

1.2 Summary of Major Results

Spatiotemporal analysis of retinal ganglion cell extracellular signals. To what extent neuronal signals, recorded with HD-MEAs, match the characteristics of a purely linear mixture is unknown. The analysis showed that somatic AP signals, recorded at high spatiotemporal resolution, contain significant propagation delays and, thus, cannot be regarded as an instantaneous mixture (Figure 2.3 on page 38).
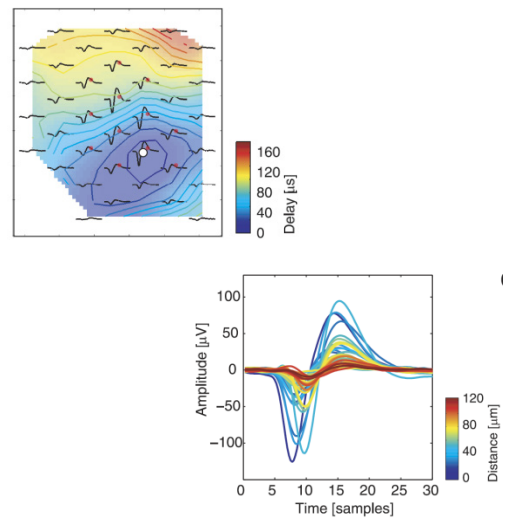
Spike sorting performance evaluation using simulated data. Simulated data were generated and used to evaluate the performance of ICA as a stand-alone method and of an ICA-based spike sorting algorithm. (Sections 2.3.4 - 2.3.6 on pages 44 - 47)
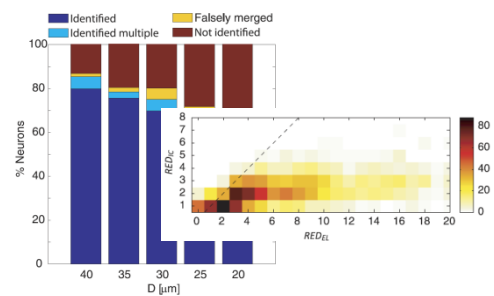
Intra- and extracellular recordings combined with optical imaging. A set-up combining an upright microscope, the HD-MEA, and a conventional patch clamp setup was built. Simultaneous intra- and extracellular recordings from spontaneous activity and from intracellularly-evoked activity were performed and combined with optical neuron imaging (Figure 3.1 on page 70).
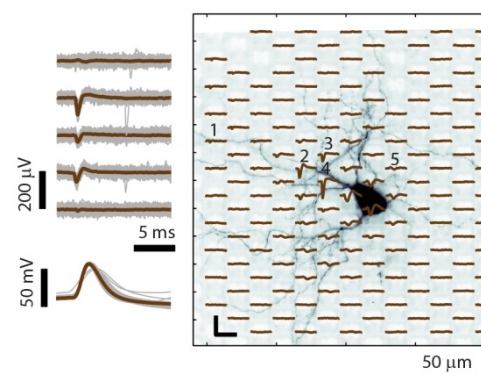
Spontaneous and stimulation-triggered mapping of postsynaptic potentials. Postsynaptic potentials (PSPs) in spontaneous recordings were identified by spike-triggered averaging based on presynaptic spike times. Furthermore, HD-MEA stimulation was used to evoke individual PSPs by stimulating presynaptic neurons (Figure 3.3 on page 77, Figure 3.5 on page 81).
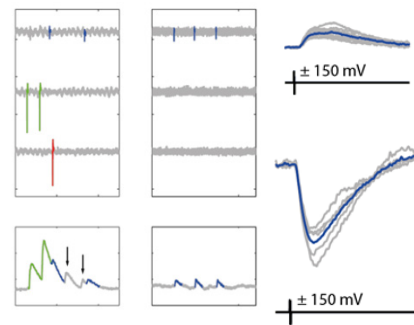
Identifying multiple presynaptic inputs. An automated method was used to identify sets of stimuli, which activated PSPs through multiple presynaptic neurons (Figure 3.6 on page 83).
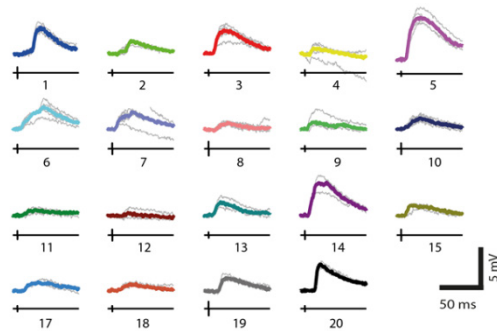
Intracellular responses to extracellular stimulation. Intracellular recordings were used to investigate effects of extracellular HD-MEA stimulation (Figure 4.4 on page 105).
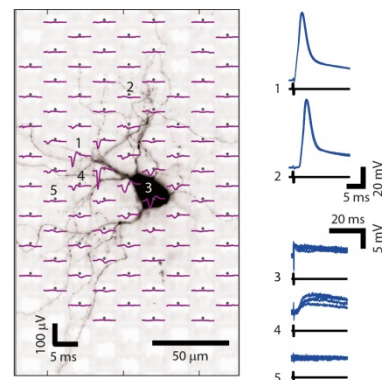
Excitability profiles. Excitability of neurons across many electrodes was measured and compared to their extracellular signals recorded at the respective electrodes (Figure 4.6 on page 109).
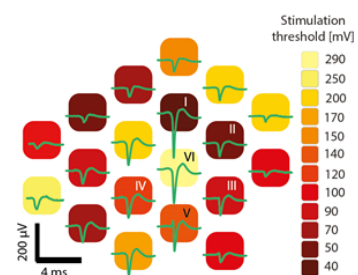
1.3 Author contributions

People involved in the project included:

Urs Frey

Hardware and software design of the HD-MEA system. Support for HD-MEA system. Concept and implementation of the ICA-spike sorter. Design of spike sorting experiments. Interpretation of spike sorting results. Editing of scientific manuscripts.

Michele Fiscella: Performed retina experiments.

Felix Franke: Design of the spike sorting experiments. Interpretation of spike sorting results. Visualization tools and software for HD-MEA and patch clamp setup. Editing of scientific manuscripts.

Thomas Russell: Support for patch clamp experiments. Editing of scientific manuscripts.

Douglas Bakkum: Software tools for combined HD-MEA and patch clamp setup. Editing of scientific manuscripts. Immunohistochemistry staining of axon initial segment combined with extracellular signal recordings. Dissection of embryonic rats.

Jan Müller: Design and realization of analog interface for patch clamp data acquisition. Design and support for stimulation software tools. Support for HD-MEA system.

Milos Radivojevic: Design of stimulation experiments. Performed experiments and data analysis of excitability maps. Dissection of embryonic rats. Support with culturing techniques. Built experimental setup for recordings from cultured neurons.

David Jäckel: Built the experimental setup for combined HD-MEA and patch clamp recordings. Developed software and spike sorting tools. Simulation of artificial data. Design of experiments. HD-MEA and patch clamp experiments. Data analysis and interpretation of results. Writing of scientific manuscripts.

CHAPTER 2 Applicability of Independent Component Analysis on High-density Microelectrode Array Recordings

David Jäckel[1], Urs Frey[2], Michele Fiscella[1], Felix Franke[1], Andreas Hierlemann[1]

1 Bio Engineering Laboratory, ETH Zurich, Basel, Switzerland.

2 Riken Quantitative Biology Center, Kobe, Japan.

Abstract

Emerging complementary metal oxide semiconductor (CMOS)-based, high-density microelectrode array (HD-MEA) devices provide high spatial resolution at subcellular level and a large number of readout channels. These devices allow for simultaneous recording of extracellular activity of a large number of neurons with every neuron being detected by multiple electrodes. To analyze the recorded signals, spiking events have to be assigned to individual neurons, a process referred to as "spike sorting." For a set of observed signals, which constitute a linear mixture of a set of source signals, independent component (IC) analysis (ICA) can be used to demix blindly the data and extract the individual source signals. This technique offers great potential to alleviate the problem of spike sorting in HD-MEA recordings, as it represents an unsupervised method to separate the neuronal sources. The separated sources or ICs then constitute estimates of single-neuron signals, and threshold detection on the ICs yields the sorted spike times. However, it is unknown to what extent extracellular neuronal recordings meet the requirements of ICA. In this paper, we evaluate the applicability of ICA to spike sorting of HD-MEA recordings. The analysis of extracellular neuronal signals, recorded at high spatiotemporal resolution, reveals that the recorded data cannot be modeled as a purely linear mixture. As a consequence, ICA fails to separate completely the neuronal signals and cannot be used as a stand-alone method for spike sorting in HD-MEA recordings. We assessed the demixing performance of ICA using simulated data sets and found that the performance strongly depends on neuronal density and spike amplitude. Furthermore, we show how postprocessing techniques can be used to overcome the most severe limitations of ICA. In combination with these postprocessing techniques, ICA represents a viable method to facilitate rapid spike sorting of multidimensional neuronal recordings.

2.1 Introduction

In the field of neurophysiology research, extracellular recordings of neural activity have become an important means to study intercell interaction and firing patterns to understand better the physiology and the information processing of neuronal networks. In multiunit recordings, the electrodes monitor the simultaneous activity of a large number of individual neurons. For the analysis, the spike trains of the individual neurons then have to be extracted from the recorded data, a process usually referred to as "spike sorting" (Lewicki, 1998). Generally, the spike-sorting task consists of two fundamental steps: to *1*) detect action potential (AP) events in the data; and *2*) classify them into groups. Whereas a main problem for the spike detection task is to deal with data recorded under low signal-to-noise-ratio (SNR) conditions, the most severe challenge to the classification problem is the presence of overlapping spikes from different neurons. The sorting performance can be drastically increased by using multielectrode devices such as tetrodes (Gray et al., 1995). In these systems, which feature several closely spaced electrodes, an AP is simultaneously measured on more than one electrode. In addition to the temporal cues of the waveform, these multielectrode devices reveal information about the spatial cues of the spike shape distribution. This additional information can be efficiently used to separate units.

Planar microelectrode arrays (MEAs) are arrangements of electrodes for extracellular measurements of multiple cells on a chip surface. They are widely used to study the dynamics of the neuronal networks, as they enable simultaneous access to a large number of neurons. Traditional MEA systems incorporate 60–200 passive metal electrodes on a silicon or glass surface, which are connected to external circuitry and typically feature interelectrode distances of 100–200 µm (Stett et al., 2003). Since the signal of a neuron is detected by at most one electrode on such MEAs, the spike-sorting problem is the same as for single-electrode recordings (Shoham et al., 2003; Zhang et al., 2003).

Recently, "active" MEAs based on complementary metal oxide semiconductor (CMOS) technology have been developed (Eversmann et al., 2003; Berdondini et al., 2005; Hutzler et al., 2006; Frey et al., 2010). These devices feature signal-conditioning circuitry on-chip and provide much larger electrode densities and, thereby, enable to conduct

electrophysiological experiments at cellular or subcellular level. The MEA used for our experiments (Frey et al., 2010) features 11,011 electrodes (3,161 electrodes/mm^2) as well as 126 read-out channels. The possibility to select arbitrarily a subset of electrodes for recording or stimulation entails the possibility to use different electrode configurations, such as high-density (HD) or sparse arrangements.

The HD of the electrodes on the array enables recordings at subcellular resolution, with the activity of every neuron being measured by multiple electrodes. Although this feature improves sorting capabilities, the large number of channels and the highly redundant nature of HD-MEA data pose challenges to the strategies for event detection and classification. Particularly, two issues arise when applying standard analysis techniques to HD-MEA data.

How to Perform Event Detection in Redundant Data?

A neuronal AP will produce spikes on several electrodes, leading to threshold crossing events (TCEs) on these electrodes. Ideally, these events should be grouped and considered as one single spiking event, since their origin is the same AP of the same cell. This could be performed by merging TCEs, which are spatially and temporally closely aligned. However, this task gets challenging for large numbers of spatially highly overlapping neurons.

Which Features Should be Used for Unit Separation?

For recordings with hundreds to thousands of electrodes, the feature space needs to be reduced in a way that only the electrodes are used that prominently contribute to unit separation.

Only a few methods have been published that specifically target spike sorting of HD, redundant recordings. A sequential approach that targets one electrode at a time is proposed in Litke et al. (2004). This simple and robust method lacks efficiency by repeating the clustering of the same cells many times and does not handle the overlap problem. Another approach based on template matching has been presented in Segev et al. (2004), using data from MEA recordings with up to 30 electrodes. The overlap problem is addressed by this approach; this method, however, is formulated for a limited number of electrodes and templates and requires prior knowledge of the neurons and their waveforms. The challenges of efficient, automatic spike-sorting and validation techniques for multielectrode systems have been discussed in Einevoll et al. (2012).

Independent component (IC) analysis (ICA) (Hyvärinen and Oja, 2000; Stone, 2002) is a blind source separation technique that can be used to demix a set of independent source signals that were linearly mixed across a number of observed signals.

The high potential of ICA to be applied to spike-sorting problems has been discussed in Brown et al. (2001). Neurons have been regarded as independent signal sources, which are linearly mixed across the recording electrodes. ICA has the following requirements:

1) The source signals are non-Gaussian and statistically independent.
2) A linear, instantaneous mixture of the source signals is assumed to produce the observed signals.
3) The number of observed signals needs to be equal to or larger than the number of source signals.

Although neurons are not independent from each other, as they can be synaptically connected or may receive common input, the individual spike trains can be regarded as statistically independent, since dependence in this context refers to instantaneous overlaps rather than time-delayed dependence (Brown et al., 2001). Therefore, concerning the first requirement, ICA will only fail to separate two neurons if they fire always precisely at the same time.

Recently, some studies attempted to combine closely spaced electrode recording techniques with computationally efficient ICA algorithms such as FastICA (Hyvärinen, 1999). In Hermle et al. (2004) and Snellings et al. (2006), ICA is applied as a preprocessing step on recorded data to reduce cross talk and increase data quality. The major obstacle for an efficient use of ICA has been, however, requirement 3. In standard in vivo experiments with tetrodes, the number of neurons is likely to be larger than the number of recording sites. One attempt to overcome this restriction for ICA included to perform k-means clustering of detected waveforms in a preprocessing step and to decompose the waveforms of each cluster individually with ICA (Takahashi et al., 2003), since the number of neurons in the clusters is expected to be lower than the number of recording sites. A second approach included to increase the number of recording sites to 12 (Takahashi and Sakurai, 2005).

The large number of electrodes of HD-MEAs is suited to meet requirement 3, which renders ICA a good candidate to separate HD-MEA data. Ideally,

the independent source signals, found by ICA, correspond to individual activity signals of neurons. Applying threshold detection on each source signal then yields the sorted spike times of the neurons that have been recorded on the array. Making use of the redundancy in the data, ICA should also provide an increase in the SNR of the demixed signal compared with the recorded signals and, therefore, improve the spike detection performance. By separating the neuronal sources, it also holds promise to solve the problem of overlapping spikes.

In this study, we explore the applicability of ICA for blind and rapid spike sorting of HD-MEA recordings.

2.2 Methods

2.2.1 Data Acquisition System

Recordings were made with the HD-MEA recording system described by Frey et al. (2009, 2010). The array is integrated into a microsystem chip, fabricated in a 0.6-µm CMOS process. It accommodates a total of 11,011 electrodes of 7-µm diameter on an area of 2.00×1.75 mm^2 (18-µm hexagonal center-to-center pitch, density of 3,161 electrodes/mm^2). One hundred twenty-six bidirectional channels are implemented on-chip, featuring recording and stimulation electronics. The channels are connected to the electrodes via a flexible switch matrix lying underneath the array. This system provides routing flexibility to select almost arbitrary electrode configurations, which can be changed within milliseconds.

The programmable gain amplifiers (0–80 dB) allow for recording neuronal signals throughout a wide range of amplitudes, which depend on the respective cell type. Offset and fluctuations resulting from the electrode-saline interface are removed by first-order high-pass filtering the analog signals (tunable cutoff frequency 0.3–100 Hz). The frequency range is limited toward the high-frequency end by means of a tunable second-order low-pass filter (3.5–14 kHz). The signals are multiplexed and digitalized with 8-bit analog-to-digital converters with a sampling rate of 20 kHz. The data were stored on a standard PC, and the analysis was conducted using MATLAB. Before postprocessing, all the data were digitally band-pass filtered (500–3,000 Hz).

2.2.2 Extracellular Recordings from Retinal Ganglion Cells

We used the rd1 mouse retina to record spontaneous activity (Stasheff, 2008) from retinal ganglion cells (RGCs). All animal experiments and procedures were approved by the Swiss Federal Veterinary Office. The retinae were isolated at ambient light from the C3H/HeNCrl (*rd1*) mouse strain at P80 in Ringer medium (in mM: 110 NaCl, 2.5 KCl, 1 $CaCl_2$, 1.6 $MgCl_2$, 10 D-glucose, 22 $NaHCO_3$, bubbled with 5% CO_2-95% O_2). Once a piece of the retina was isolated, it was placed with the RGC layer adjacent to the MEA. The retina was fixed on the array by a permeable membrane (polyester, 10-μm thickness, 0.4-μm pore size) and superfused with Ringer medium at 36 °C.

All recordings shown in this study were done with electrode configurations of blocks at highest possible spatial resolution. The largest HD block that can be simultaneously read in the configurable array is 6 × 17 electrodes and covers an area of approximately 80 × 320 μm^2.
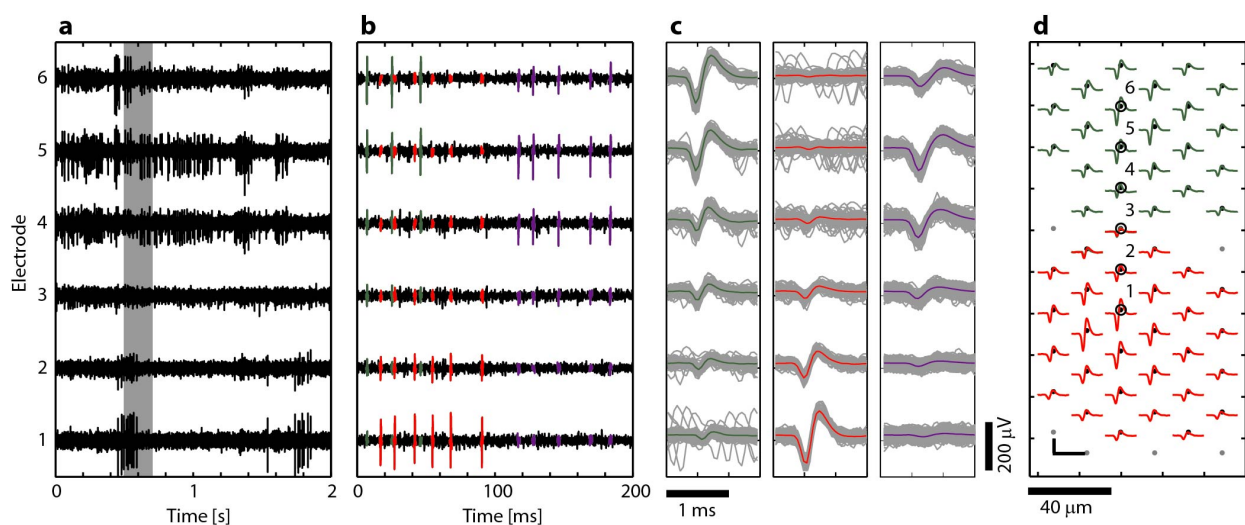
Figure 2.1 Example of raw data and neuronal templates.

(a) 2 s of recorded data from 6 selected electrodes, labeled in a. (b) Data segment indicated by a gray rectangle in a. The spikes of 3 retinal ganglion cells (RGCs) that were identified by supervised spike sorting were colored (red, green, and violet). (c) Superposition of all detected spike waveforms within 50 s of data (green neuron: 187 spikes; red neuron: 191 spikes; violet neuron: 1,046 spikes). The colored line shows the averaged waveform [spike-triggered averaging (STA)]. (d) Cell-specific templates (only green and red neuron shown for visualization purposes). Black dots indicate electrode positions on the microelectrode array (MEA). Colored waveforms correspond to the STA of the neuron on the respective electrode. The numbered electrodes refer to those in a-c. Scale bar: 100 μV/1.8 ms.

An example of recorded RGC activity is shown in Figure **2.1**. Three neurons were identified in an HD block, using a manually supervised custom-designed spike-sorting method based on principal component analysis (PCA) and expectation-maximization (EM) clustering (KlustaKwik; Harris et al. 2000). The characteristic multichannel signature of the neurons is obtained by spike-triggered averaging (STA) of the individual aligned traces (Figure 2.1c). This cell-specific footprint will be referred to as template, namely the distribution of the average spike shape across the electrodes. Figure 2.1d shows the templates of two cells that have significant energy on a large number of electrodes.

Templates and firing characteristics of recorded neurons were found to be very similar across several recording experiments ($n = 10$).

2.2.3 Assumption of Linear Dependence

ICA requires a linear and instantaneous mixture of the source signals across the electrodes. This requirement implies that the signals of the sources (neurons) on the different electrodes are linearly dependent and do not contain phase shifts. The assumption of linear dependence can be validated by testing the degree of linearity within the waveforms of the neuron template.

We measure the linearity between two vectors, $\boldsymbol{a}$ and $\boldsymbol{b}$, using the normalized cross-correlation coefficient (CC):

$$\mathrm{CC}_{ab} = \frac{\langle \boldsymbol{a}, \boldsymbol{b} \rangle}{\|\boldsymbol{a}\|\|\boldsymbol{b}\|} \qquad (1)$$

The CC can range from −1 to 1, where two vectors with a CC of 1 are perfectly linearly dependent and two vectors with a CC of −1 are inversely linearly dependent. A CC of 0 indicates that the vectors are orthogonal. Therefore, the linearity assumption is met if the absolute CC values of the spike waveforms of the individual neuron templates are close to 1.

2.2.4 ICA

Let the recorded time-series signals on M electrodes be $\boldsymbol{X} = [x_1(t), \dots, x_M(t)]^T$ and $\tilde{\boldsymbol{S}} = [\tilde{s}_1(t), \dots, \tilde{s}_N(t)]^T$ be the intrinsic signals generated by N single neurons. Given the assumption of linearity,

stated in the previous section, we can model the recordings as a linear mixture of the neuronal signals:

$$X = A \cdot \tilde{S}. \tag{2}$$

Under the additional assumptions that the individual signals are non-Gaussian and statistically independent and that there are more recording sites than neurons, the mixing matrix A can be estimated blindly by applying ICA (FastICA; Hyvärinen 1999) directly to the recorded data. The ICs, which ideally represent individual-neuron signals, are obtained by:

$$S = W \cdot X. \tag{3}$$

The ICs are the rows in $S = [s_1(t), \dots, s_M(t)]^T$, and $W = A^{-1}$ is the demixing matrix. In the following, we will refer to the columns of A as the mixing coefficient vectors (MCVs), whereas the rows of W will be called demixing coefficient vectors (DCVs). Note, that the estimated mixing matrix has a dimension of $M \times M$.

If the individual templates are known, we can evaluate the separation by directly demixing the templates with W. For a given neuron, i, consider the template matrix $F^i = \left[f_1^i, \dots, f_M^i \right]^T$, for which the jth row is the STA waveform f_j^i at the electrode j. Then the demixed template is:

$$H^i = W \cdot F^i. \tag{4}$$

In the case of perfect separation, H^i contains the intrinsic neuron waveform in the ith row and zeros in all the other rows. ICA offers three main features if all the assumptions are met:

1) The redundancy is reduced so that only ICs $1, \dots, N$ contain significant signals (spikes), whereas ICs $N + 1, \dots, M$ contain only noise. This allows for extracting the number of neurons from the number of ICs containing spikes.
2) The recordings are demixed in a way that every IC only contains the spikes of one corresponding neuronal source. Consequently, applying threshold detection to the ICs yields the sorted spike times.
3) ICA achieves an increase in SNR compared with single-channel signals by accumulating signals of several electrodes in the ICs.

The use of ICA, however, typically entails two major problems if the linearity assumption is not totally fulfilled:

1) One IC can contain signals from more than one neuron. In that case, demixing does not achieve perfect separation.
2) A neuron can contribute signals to two or more ICs. In that case, more than N ICs contain neuronal signals, and ICA does not completely reduce the redundancy.

2.2.5 Evaluation Criteria

In the following, we formulate several evaluation metrics to characterize the performance of ICA with regard to the points elaborated in the previous section.

SNR

We define the SNR of neuron i in the recorded signal $\boldsymbol{X}$ as

$$\mathrm{SNR}^i_{\mathrm{EL}} = \frac{\max(\mathrm{abs}(\boldsymbol{f}^i_j))}{\sigma_j} \qquad (5)$$

where j is the electrode on which the template $\boldsymbol{F}^i$ has its highest peak value, and where σ_j is the standard deviation of the noise signal on that electrode. The $\mathrm{SNR}_{\mathrm{EL}}$ thus denotes the peak value in the template divided by the noise standard deviation.

Next, we define the SNR of the neurons in the ICs. FastICA normalizes the DCVs so that every IC signal has unit variance. Instead, we want the noise on the ICs to have unit variance. Therefore, we first normalize all the DCVs:

$$\widehat{\boldsymbol{w}}^k = \frac{\boldsymbol{w}^k}{\sqrt{(\boldsymbol{w}^k)^T \boldsymbol{C} \boldsymbol{w}^k}} \; ; \; k = 1, \dots, M \qquad (6)$$

Here, $\boldsymbol{w}^k$ is the kth row of $\boldsymbol{W}$, and $\boldsymbol{C}$ is the instantaneous noise covariance matrix between the electrodes. $\widehat{\boldsymbol{W}}$ is the new demixing matrix with normalized DCVs, having $\widehat{\boldsymbol{w}}^k$ on its kth row. This normalization ensures equivalent noise levels on all the ICs and allows for comparison of their signals. The SNR of neuron i in the ICs is the peak value of the demixed template $\widehat{\boldsymbol{H}}^i = \widehat{\boldsymbol{W}} \cdot \boldsymbol{F}^i$:

$$\text{SNR}^i_{\text{IC}} = \max\left(\left|\widehat{\boldsymbol{H}}^i\right|\right). \qquad (7)$$

Redundancy

Another important ICA performance measure is how well redundancy in the ICs is reduced compared with the recorded signals. Therefore, the redundancies RED^i_{EL} and RED^i_{IC} are defined, where the first denotes the number of electrodes and the latter denotes the number of ICs, on which the signal of neuron i exceeds the threshold value of five times the noise standard deviation.

Separability

We also introduce a measure for the separability of the neurons on the ICs. A neuron i with high separability must have a high peak signal on an IC k, on which all other neurons have only low peak signals. Thus its separability is the difference between its peak on IC k and the highest peak of any other neuron on IC k. We determine k by maximizing the separability, taking into account that the relevant peak can feature either positive- or negative-sign amplitude.

$$\text{SEP}^i_{\text{IC}} = \max_{k=1,..,M}\left(\delta^k_{\text{IC,pos}}, \delta^k_{\text{IC,neg}}\right);$$

$$\delta^k_{\text{IC,pos}} = \max(\widehat{\boldsymbol{w}}^k \boldsymbol{F}^i) - \max_{q \neq i}(\widehat{\boldsymbol{w}}^k \boldsymbol{F}^q) \qquad (8)$$

$$\delta^k_{\text{IC,neg}} = \min_{q \neq i}(\widehat{\boldsymbol{w}}^k \boldsymbol{F}^q) - \min(\widehat{\boldsymbol{w}}^k \boldsymbol{F}^i)$$

Analogously, we define the separability of a neuron in the recorded signals as the difference between the peak of its template and the highest peak of any other neuron template on the same electrode, divided by the noise standard deviation on that electrode.

$$\text{SEP}^i_{\text{EL}} = \max_{j=1,..,M}\left(\frac{\delta^j_{\text{EL,pos}}}{\sigma_j}, \frac{\delta^j_{\text{EL,neg}}}{\sigma_j}\right);$$

$$\delta^j_{\text{EL,pos}} = \max\left(\boldsymbol{f}^i_j\right) - \max_{q \neq i}\left(\boldsymbol{f}^q_j\right) \qquad (9)$$

$$\delta^j_{\text{EL,neg}} = \min_{q \neq i}\left(\boldsymbol{f}^q_j\right) - \min\left(\boldsymbol{f}^i_j\right)$$

Configu-ration	Average neuron distance, [μm]	Cell density [neurons/mm^2]	Approximate number of neurons per simulation (incl. in analysis/ simulated)	Number of simulations used	Neurons considered in analysis
1	40	722	18 / 32	20	358
2	35	943	24 / 40	15	358
3	30	1283	30 / 50	12	358
4	25	1848	46 / 77	8	358
5	20	2887	71 / 111	5	358

Table 2.1 Simulation overview for configurations in *data set B*.

Different numbers of simulations were considered for different configurations to have equal sample sizes in the analysis. For comparison of these values, please keep in mind that the average electrode distance is 18 μm, the electrode density is 3,161 mm^2, and the number of electrodes used in the simulations is 90 (high-density arrangement of 9 × 10 electrodes).

2.2.6 Simulation of Recorded Neuronal Activity

For evaluation purposes, simulated data were generated. In this study, we used two types of simulated data sets. *Data set A* contained simulated activity of three neurons that had spatially overlapping templates that were extracted from digitally unfiltered, recorded data. This data set is mainly used for visualization purposes. Spike sorting to extract the templates for data simulation was performed using manually supervised PCA and EM clustering.

For a systematic analysis, we simulated RGC activity at different cell densities in *data set B*. Therefore, we used eight well-isolated, manually selected neuronal templates extracted from recorded unfiltered data as model templates. Higher spatial resolution was obtained by interpolating the model templates on a grid (5-μm pitch). By modifying position, orientation, amplitude, and spatial extension of the model templates, individual neuron templates were simulated. The modified templates were positioned on a gridlike structure with equidistant points. Peak-to-peak amplitudes were set randomly (uniformly distributed between 50 and 300 μV). The grid of neurons covered an HD block of 90 electrodes on an area of 130 × 185 μm^2.
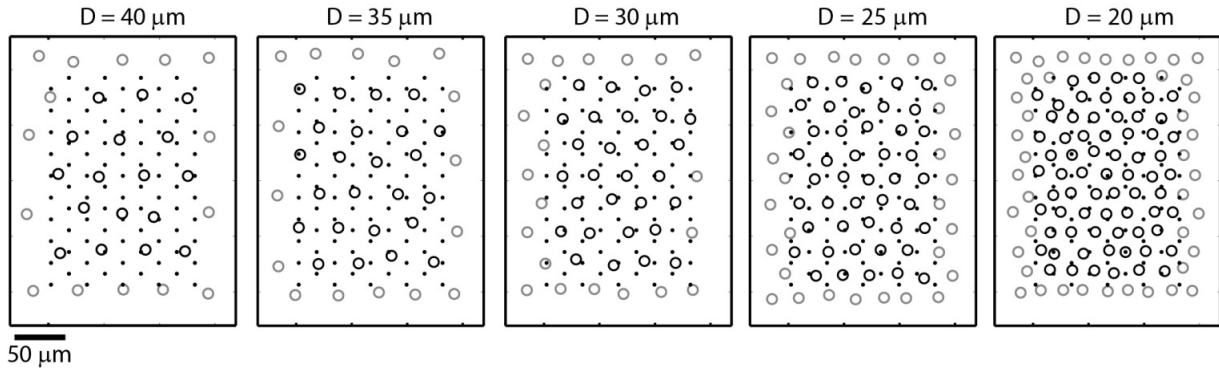
Figure 2.2

Sample arrangements of neurons (circles) and electrodes (black dots) for the 5 configurations in *data set B*. Neurons lying outside the electrode block (gray) were also simulated, but only neurons inside the electrode block (black circles) were considered for the evaluation. D, average neuron distance.

We simulated 5 different configurations with average neuron distances (D) between 40 and 20 μm (average distance to the 6 neighboring neurons in a hexagonal arrangement). Out of 20 simulations of 30 s each, which were generated for each configuration, a subset of 358 neurons per configuration was considered for the analysis. Surrounding neurons outside the electrode block were simulated but not included in the analysis. An overview of the different configurations represented in *data set B* is given in Table 2.1 and illustrated in Figure 2.2.

Individual, uncorrelated spike trains were simulated for both data sets using sets of γ-distributed interspike intervals (ISI), which proved to be a good model for the spiking behavior of RGCs (Levine, 1991). The mean firing rates ranged between 30 and 50 Hz for *data set A* and between 5 and 50 Hz for *data set B*. A refractory period of 2 ms was introduced. We upsampled the template waveforms to 160 kHz and then randomly downsampled them to the respective sampling frequency for every simulated AP, this way imitating recording conditions, under which the spikes are not always digitalized at the exact same position (Pouzat, 2002; Quiroga et al., 2004). Spike shape variability (Fee et al., 1996a) was induced by multiplying the template waveforms of every spiking event on all electrodes with a random factor (normally distributed $\mu = 1$, $\sigma = 0.1$). A digitally unfiltered noise signal, which was recorded under experimental conditions with a retina preparation on the array that had no visible spiking activity, was added to the simulated spike data. The resulting signal was quantified to a least

significant bit, similar to the one used in the measurements (5 μV). This way, the simulated data had similar characteristics as recorded data, and the same data handling and processing steps could be used.

2.3 Results

2.3.1 Spatiotemporal Template Analysis

A main requirement for ICA is that the independent sources (i.e., the neuron templates) are linearly mixed over all recording electrodes. This requirement implies that the waveforms of a neuron on the different recording electrodes are linearly dependent. Therefore, the degree of linear dependence between the waveforms of a RGC template was analyzed.

A single neuron template was reconstructed from two overlapping blocks, recorded at highest spatial resolution (Figure 2.3a). Because of the chip architecture, the electrodes are not sampled at the same point in time. We corrected for this by upsampling (160 kHz) and resampling the recorded data at defined time points (20 kHz). After spike detection, the multichannel spike traces of the identified neuron were again upsampled by a factor of 4 to allow a more precise spike alignment and averaging (upsampled resolution: 12.5 μs).

Figure 2.3b shows the superimposed waveforms from 40 electrodes, illustrating that they are not exactly in phase but shifted by up to 3 samples (150 μs). The electrode position where the AP wave appears 1st (dark blue wave in Figure 2.3b) will be referred to as AP reference (white marker in Figure 2.3c). The color of each waveform indicates the distance between the corresponding electrode and the AP reference. An increase in the phase shift is observed for increasing distance. This phase shift is due to the AP propagation delay.

The spatial extent of the propagation delay is visualized in Figure 2.3c. For every electrode, the precise position of the negative peak in the upsampled averaged waveform was used to determine the temporal delay compared with the AP reference. After emergence close to this reference point, the AP spreads into all directions. The timing delays vs. the travelling distances for the individual waveforms, shown in Figure 2.3d, give an estimate of the propagation speed. The slope of the linear fit corresponds to a velocity of 0.55 m/s.

For better visibility, we focus in the following on the waveforms recorded from the 12 electrodes providing the highest signals (peak-to-peak voltages > 60 μV, marked with a red dot in Figure 2.3, a and c). In any case, signals with low amplitude only moderately influence ICA compared with high amplitude signals. The CC matrix (Figure 2.3e, *left*) contains the CC values (see Eq. 1 in Methods) for the waveforms of all electrode pair combinations of the selected electrodes. The electrodes were arranged in the matrix with respect to ascending time delay, which is displayed in the inset above the matrix plot. Electrodes 1–7 (electrodes in purple, bluish area in Figure 2.3c) as well as 8–12 (electrodes in green, yellowish area in Figure 2.3c) form electrode groups with high CC values for electrode pairs within each group but relatively small CC values for electrode pairs between both groups. The decrease in linearity is caused by a relatively large phase shift between electrodes 7 and 8. Similar abrupt phase shifts were observed for many RGCs and are presumably a characteristic physiological feature of these neurons. For electrode pairs without significant phase shift, such as for electrodes 5 and 6 or for electrodes 10–12, the resulting CCs are very close to 1.

This example shows that somatic AP signals, recorded at high spatiotemporal resolution, contain significant propagation delays and thus cannot be regarded as an instantaneous mixture. However, even if there was no propagation delay, we could not assume a perfect linear mixture for a second reason. The complex physiological structure of the neurons has effects on the spike waveforms. To analyze this, the waveforms were temporally aligned according to the occurrence of their negative peak value, and the resulting CC matrix was determined (Figure 2.3e, *right*). For this case, the interelectrode CC values have a mean of 0.97 and a smallest value of 0.89, compared with a mean of 0.89 and smallest CC value of 0.61 in the nonaligned case.

These characteristics of limited linear dependence between the waveforms of a neuronal unit on different recording electrodes, mainly caused by the phase shift due to the AP propagation delay, imply that the linearity assumption of ICA is not fulfilled.
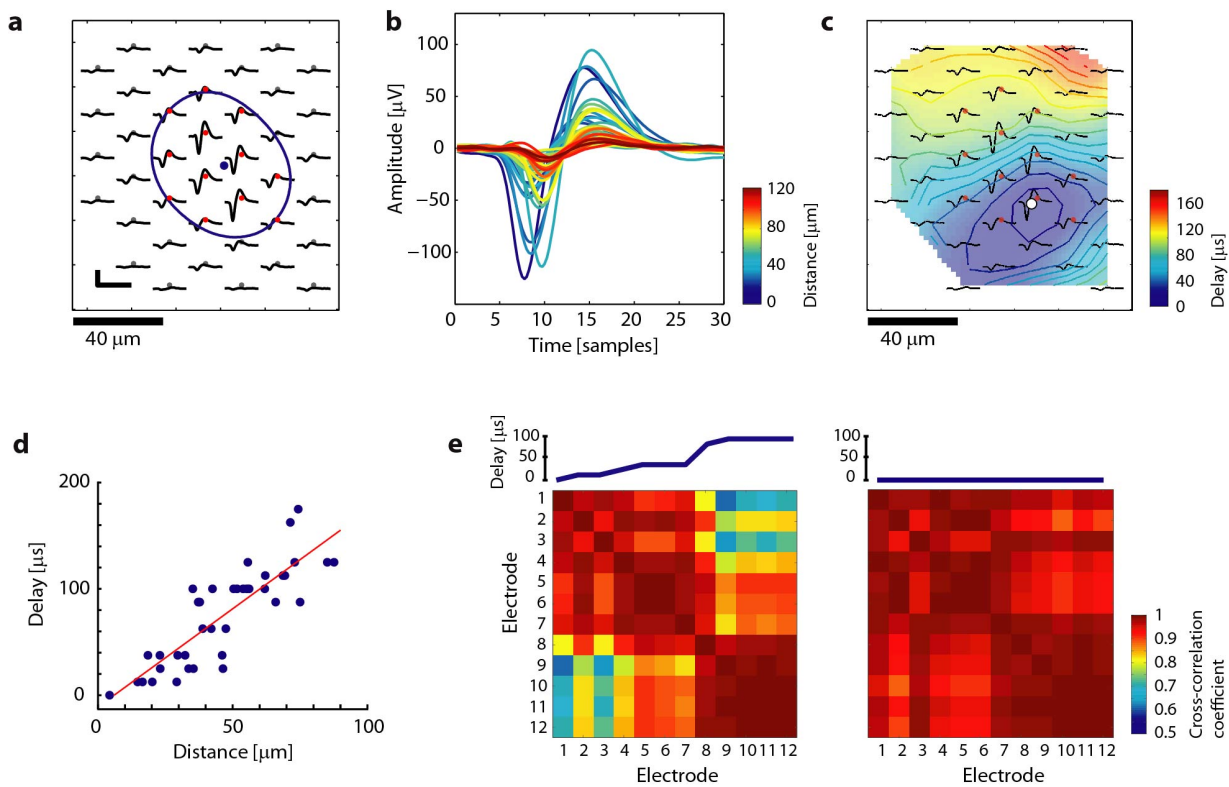
Figure 2.3 Ganglion cell template analysis at high spatiotemporal resolution.

(a) RGC template; the blue point indicates the center of gravity, and the blue line shows a Gaussian-fit equipotential line; scale bar: 100 µV/1.6 ms. (b) Superimposed averaged waveforms with the color code indicating the distance to the reference point marked in c. The phase shift grows with increasing distance. (c) For every averaged waveform, the action potential (AP) timing was determined based on the occurrence of the respective negative peak value. The position of the earliest AP occurrence (AP reference) is indicated by the white dot, and the background color shows AP delay with respect to this reference point. (d) Distance to reference point vs. AP delay for all recorded waveforms (blue points) of the RGC. The red line shows a linear fit with a slope of 1.8, corresponding to a velocity of 0.55 m/s. (e) *Left*: cross-correlation coefficient (CC) matrix for waveforms on 12 electrodes with highest amplitude (red dots in a and c), arranged according to AP delay in ascending order. The increasing delay (shown at the *top*) causes a decrease in the CC, with values as low as 0.61. Two main groups with high intragroup but low intergroup CCs appear, particularly electrodes 1–7 and 8–12. *Right*: CC matrix for the same 12 waveforms, however, with the phase shift being corrected by alignment according to the occurrence of the negative peak value. The resulting CCs range between 0.89 and 1.

2.3.2 Nonlinearity Effects on Linear Demixing and ICA

Next, we investigated how nonlinearity in the neuronal templates affects the possibilities of separating neuronal signals by means of linear demixing and ICA. For this, we used *data set A*, which contained simulated activity of three spatially overlapping neuronal templates (Figure 2.4, a and b) extracted from a retinal recording.

In a first trial, the template of every neuron was manipulated to achieve linearity across the electrodes. This was realized by replacing the template waveform in each channel by scaled versions of the waveform observed on the electrode with maximum signal so that the peak-to-peak amplitude value at each electrode was preserved. The DCVs, directly derived from the manipulated templates (see Eqs. 10–11 in Appendix) led to perfect separation in the demixed templates (Figure 2.4c, *top*), which means that there is only one high peak signal in each component (row). This shows that neuronal templates can be completely separated by means of linear demixing, given the assumption of perfect linear mixtures under the boundary condition that there are more electrodes than neurons.

The DCVs were extracted in the same way from the realistic templates, and the demixed templates were computed (Figure 2.4c, *bottom*). The signals along the diagonal of both plots have similar magnitudes, suggesting that the accumulation of the template energies in the components leads to a similar SNR increase for the linearized and the real case. However, compared with the linearized ideal case, there is significant cross talk. As a result, e.g., neuron 3, having the smallest spike amplitudes and being therefore the most challenging to demix, fails to be separated.

In a next step, ICA was applied to the simulated *data set A*, which contained spikes from these three neurons. The demixed templates and corresponding DCVs maps (Figure 2.4d) show that some of the responses (i.e., for ICs 1, 3, 5, and 6) feature a reversed sign, which is due to the fact that ICA cannot derive the correct sign of the source signals. Besides this, ICA leads to comparable SNR and separability on the first three ICs as the demixing using directly derived DCVs from the templates.
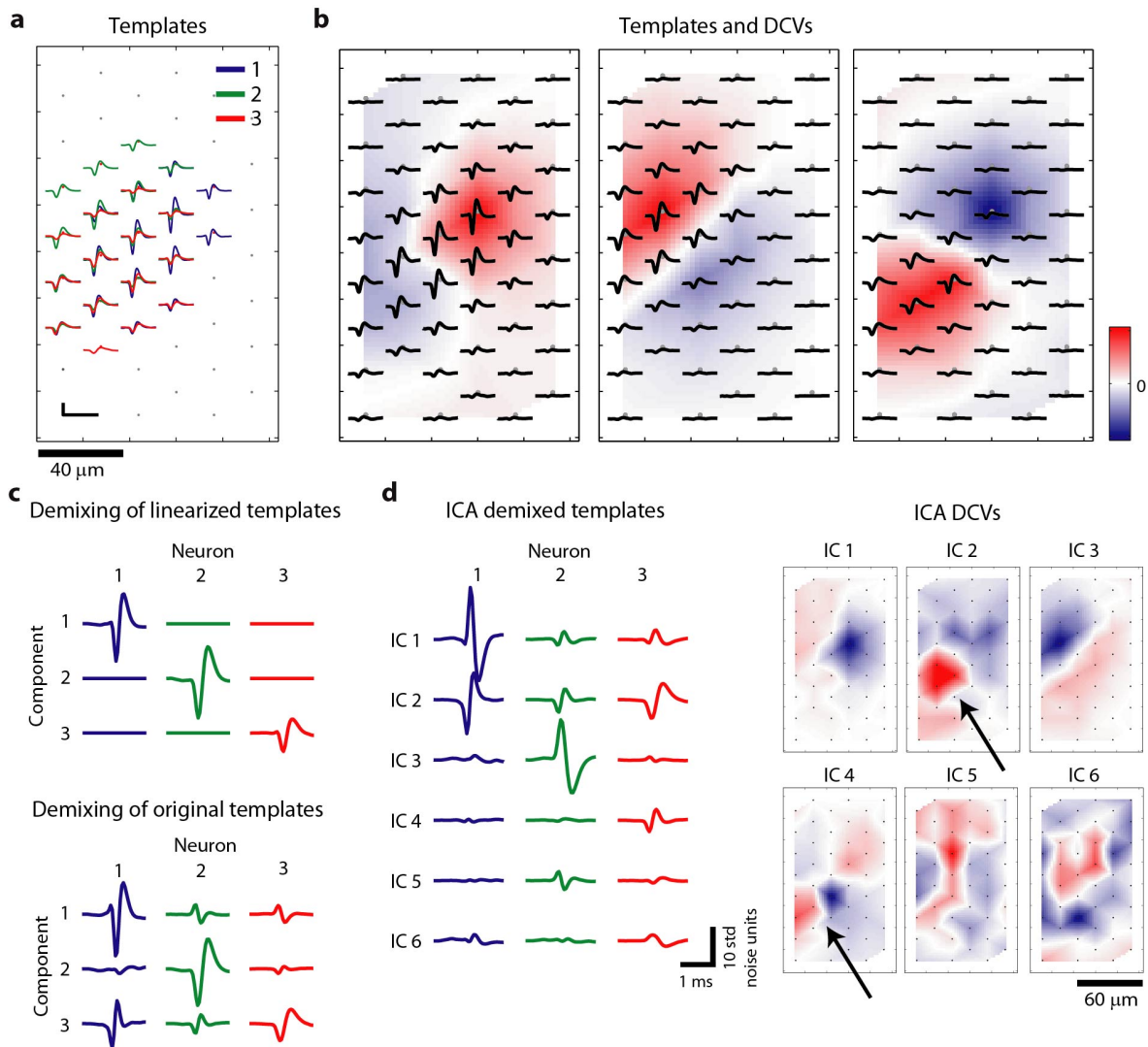
Figure 2.4 Nonlinearity effects on linear demixing and ICA.

(a) STA templates of 3 spatially overlapping neurons identified and extracted from retinal recordings. Scale bar: 100 µV/1.8 ms. (b) Individual templates and respective demixing coefficient vectors (DCVs), directly derived from the templates (see appendix). (c) Demixed templates using the DCVs, which were directly derived from the templates. In this representation, the rows refer to the demixing components, and the columns refer to the neuron templates. *Top*: the manipulated, idealized case where linearity across each template is given. *Bottom*: the realistic case where linearity is not given. The DCVs used here are shown in b. (d) *Left*: template responses for the 1st 6 independent components (ICs) obtained by applying IC analysis (ICA) on the simulated data set. *Right*: corresponding DCV maps. The arrows indicate an example where significant weightings for demixing 1 source (neuron 3) are found on 2 ICs (ICs 2 and 4).

If the linearity criterion of ICA would be met, we would not only achieve perfect separation, but also redundancy reduction so that the number of ICs with significant signals would be equal to the number of neurons. This would imply that we find only one high peak signal per column of the demixed templates. Since there are still signals in the demixed templates for ICs 4–6, ICA does not completely reveal the right number of sources here.

We observe that ICs 2 and 4 have significant DCV weightings in the area of neuron 3 (black arrows in Figure 2.4d, *right*) while having nearly orthogonal MCVs (CC = 0.11). However, the positive weightings (red) in the DCV of IC 4 are centered around a subset of three electrodes, whereas one electrode has large negative weight (blue). The CC values of spike waveforms of the three electrodes with positive weights are >0.995, however, significantly lower for combinations with the waveform of the electrode with negative weight (CC values 0.79, 0.81, and 0.83). The effect of splitting the source between different ICs was also consistently found on simulated data sets containing spikes from only single neurons (data not shown). This suggests that ICA splits the source due to the phase shift between the waveforms across the electrodes described in the previous section. As a consequence, the similarity of MCVs, as used in (Takahashi and Sakurai, 2005), might be a poor indicator for determining if the sources underlying two ICs are coming from a single or two separate neurons.

Interestingly, there are cases where a neuron does not exhibit the best separation performance on the first IC on which its signal is visible. Whereas neuron 3 has a strong signal but no separability on IC 2, better separability is achieved on IC 4 ($\text{SEP}^3_{\text{IC2}} = 0$ vs. $\text{SEP}^3_{\text{IC4}} = 4.8$). At the same time, the DCV for IC 4 has large weights on a smaller area (Figure 2.4d, *right*), and therefore it features less template energy and a smaller SNR increase compared with IC 2 ($\text{SNR}^3_{\text{IC2}} = 9.7$ vs. $\text{SEP}^3_{\text{IC4}} = 5.6$).

2.3.3 Advantages of ICA for Resolving Overlapping Spikes

We have shown in the previous section that the violated linearity criterion complicates clean separation of the neuronal sources using ICA-based linear demixing. However, in the following, we show that ICA has substantial advantages compared with traditional PCA methods for dealing with overlapping spikes in the case of sufficient separability on the ICs.
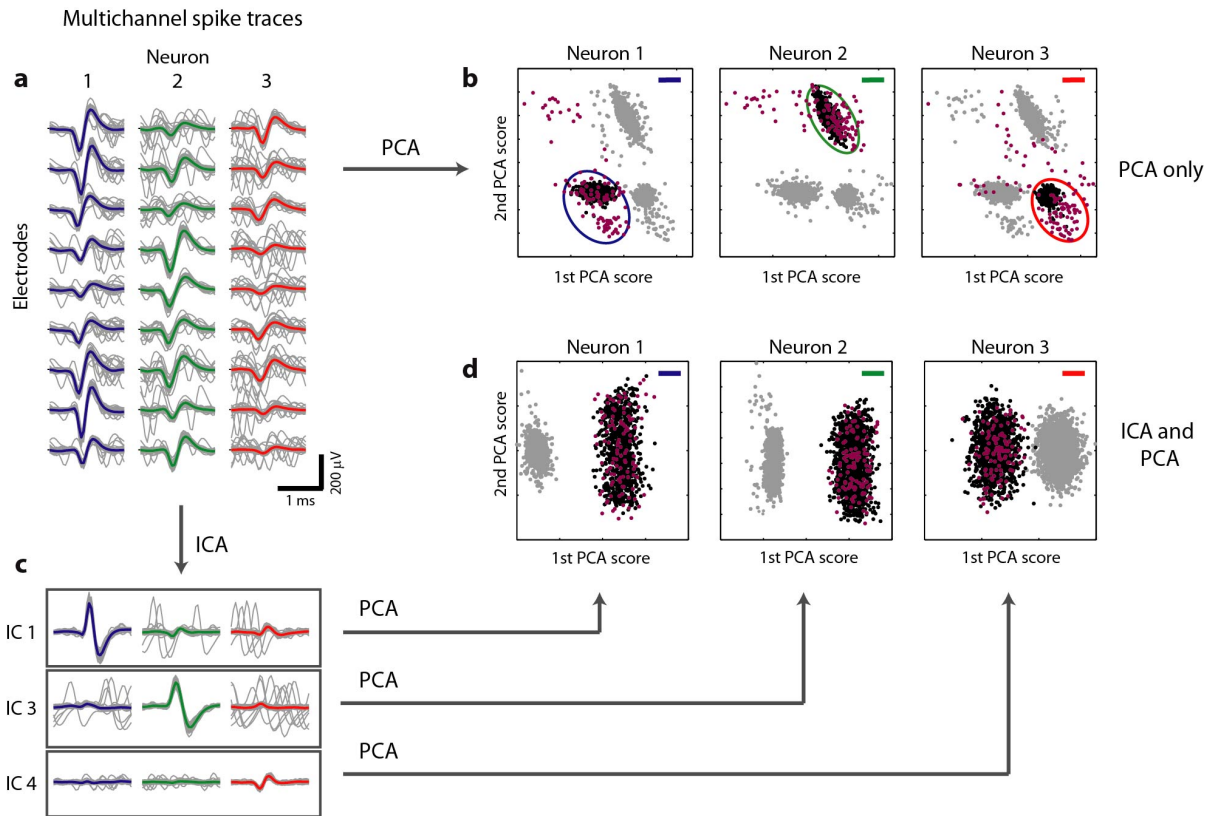
Figure 2.5 Using ICA to resolve overlaps.

(a) Template waveforms (colored) and individual spike traces (gray, only 80 traces are shown per neuron for better visualization) on 9 selected electrodes for the neurons shown in Figure 2.4. Many overlapping spikes are visible in the gray traces. (b) Principal component analysis (PCA) applied to the multichannel spike traces on the 9 selected electrodes in a. Black dots indicate spikes from the neuron of interest, and gray dots denote spikes from other neurons. Spikes, which temporally overlapped with a spike from another neuron (timing difference of 10 samples or less), are colored violet (the respective overlapping spikes from the other neurons are not shown). Note that overlaps mostly lie outside of the main cluster. (c) Spike traces on ICs 1, 3, and 4 after applying ICA. The clean waveforms along the diagonal indicate that separability is given and that overlaps have been resolved. (d) PCA applied individually to the IC spike traces on the 3 selected ICs.

Figure 2.5a shows individual spike traces and average waveforms of the neurons in Figure 2.4 on nine selected electrodes. The high firing rates of the simulated neurons caused many overlapping spikes, which evidently challenge alignment and classification of the spikes. To demonstrate this challenge, multichannel PCA (i.e., PCA performed on the concatenated single-channel waveform traces; see Litke et al. (2004)) was applied to the spike traces of the three neurons on the selected electrodes. Figure 2.5b shows the resulting PCA scores of the first two principal components for each individual neuron; the black dots indicate spikes of the neuron of interest, and the gray dots mark spikes of other neurons. Violet dots indicate spikes that overlapped with another neuron within a time frame of 10 samples (0.5 ms). The nonoverlapping events are located in different, defined regions of the PCA space (ellipses) and can thus be separated using the representation of the PCA scores. However, the overlapping events are distributed all over the space and cannot be correctly identified using standard clustering methods.

In the following, ICs 1, 3, and 4 (from Figure 2.4d) were considered for separating neurons 1–3 (Figure 2.4, a and b). The spike traces projected on the corresponding ICs (traces along the diagonal in Figure 2.5c) exhibit clean waveforms, which indicate that the overlaps shown in Figure 2.5a have been resolved. Therefore, the ICA separation for this example is sufficient to enable proper spike assignment based only on threshold detection on the ICs.

The capability to resolve overlaps is also demonstrated by applying PCA to the IC spike traces of the three neurons for each IC independently. The representation of the scores (Figure 2.5d) shows clear separation of the spikes of the respective neuron of interest (black dots) from the spikes of other neurons (gray dots). The overlapping spikes (violet dots) also lie within the cluster, which enables a correct assignment.

An important advantage of ICA usage for dealing with overlapping spikes appears here. Since the ICs can be treated independently, event detection is applied to the individual ICs. Thus two neurons that fire simultaneously evoke signals on two ICs and can also be detected as two independent spike sources.

It is important to mention in this context that, as shown in the previous section, ICA yields different separabilities on different ICs. However, it is not

known which of the IC achieves the best separability for every neuron. Therefore, the best IC cannot be selected blindly.

2.3.4 ICA Performance Evaluation

To use ICA, followed by simple threshold detection for spike sorting, the neuronal sources need to be well-separated, and each neuron needs to be prominent and detectable on exactly one IC. To evaluate the applicability of such an ICA-based spike-sorting method, we analyzed the performance of ICA with regard to achieving three goals: 1) SNR increase; 2) separation of the neuronal sources; and 3) redundancy reduction. For this purpose, we used the basic evaluation metrics, which were defined in Evaluation Criteria.

ICA was applied to simulated RGC activity at different cell densities (*data set B*; see Methods). For calculation of the evaluation criteria, the noise signals and the templates that were used in the simulations have been considered.

First, the SNR of the neurons on the raw data (SNR_{EL}) was compared with that on the ICs (SNR_{IC}; Figure 2.6a), whereat an overall increase in the SNR_{IC} was observed. The SNR ratio $r_{SNR} = SNR_{IC}/SNR_{EL}$ was found to be particularly large for neurons with high SNR_{EL}, which suggests that ICA is more effective in demixing signals of high-SNR neurons. However, the SNR increase drops for configurations with higher cell densities. Whereas for D = 40 μm, 82% of the neurons have $r_{SNR} > 1$, for D = 20 μm this is only the case for 44% of the neurons (Figure 2.6b).

Next, we addressed the question of how well the neuronal sources are separated in the representation of ICs. Separability SEP_{IC} denotes the difference between the peak of a neuron on an IC and the next highest peak of another neuron. If a neuron has a large enough SEP_{IC}, the sorted spikes can be obtained by simply applying threshold detection to the respective IC. We define the condition for a neuron to be separable if it has an SEP_{IC} above a threshold of 5. Note that the SEP_{IC} is given in units of standard deviations of the noise in the IC, like the SNR_{IC}, and, therefore, every neuron with an $SEP_{IC} > 5$ also has an $SNR_{IC} > 5$.
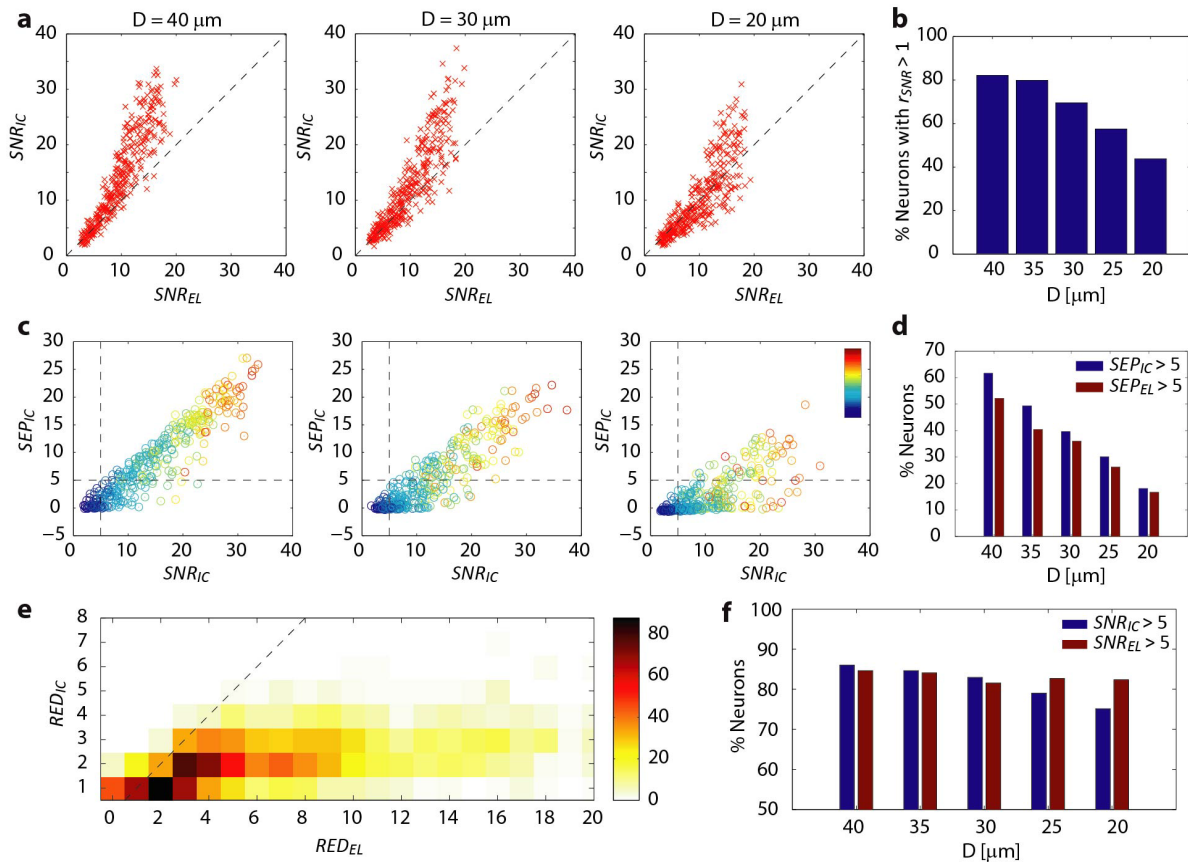
Figure 2.6 ICA performance evaluation.

(a) Signal-to-noise-ratio (SNR) conditions for electrodes (SNR_{EL}) vs. ICs (SNR_{IC}) for simulated neurons (red crosses) of 3 different configurations. The dashed line shows $SNR_{EL} = SNR_{IC}$. (b) Percentage of neurons, for which $SNR_{IC} > SNR_{EL}$ for the 5 configurations. (c) SNR vs. separability for neurons of 3 different configurations. The dashed lines indicate threshold values for separability of neurons ($SEP_{IC} = 5$ and $SNR_{IC} = 5$). The color code indicates the template energies. (d) Percentage of neurons with $SEP_{IC} > 5$ (blue) and $SEP_{EL} > 5$ (red). (e) Histogram showing the counts of redundancies RED_{EL} and RED_{IC} for a total of 1,130 neurons (330 neurons having $RED_{IC} = 0$ were excluded from the graphic representation). The dashed line indicates $RED_{EL} = RED_{IC}$. (f) Percentage of neurons that can be detected according to the criteria $SNR_{IC} > 5$ (blue) and $SNR_{EL} > 5$ (red) for the 5 configurations.

45

Figure 2.6c shows the separability and SNR values of the neurons for different configurations; the color code indicates the template energy. The dashed lines confine the thresholds with regard to detectability, and therefore all neurons positioned in the upper right area of the plot are detectable and separable according to the defined criteria. For largely spaced neurons, separability increases approximately linearly with the SNR. The overall separability drops for larger neuron densities, and several large-SNR neurons feature low separability for the most tightly spaced configuration $D = 20$ µm. ICA yields an increase in separability compared with the raw data (Figure 2.6d). However, a substantial decrease in separability is observed for tightly spaced neuron configurations, reflected by the low percentage of neurons featuring $SEP_{IC} > 5$ or $SEP_{EL} > 5$.

The third performance criterion is the reduction of redundancy in the IC space. The redundancies in the IC and electrode space were computed for a total of 1,460 simulated neurons in all configurations. Figure 2.6e shows the histogram counts for RED_{EL} and RED_{IC}. A majority of the neurons yields RED_{IC} values between 1 and 2, and thus ICA performs well in reducing the dimensionality of the data.

Note that the zero value in the y-axis is not shown, and thus neurons with $RED_{IC} = 0$ were excluded in this graphic. Whereas low RED_{IC} values are desired, as they mean that the individual neurons are not detected many times, $RED_{IC} = 0$ means that the neuron cannot be detected at any of the ICs.

Finally, the effect of an increased SNR (Figure 2.6, a and b) on the detection of the neurons was evaluated. We found that for the configurations with $D \geq 30$ µm, more neurons are detectable on the ICs (Figure 2.6f) due to the increase in SNR obtained by using ICA. One has to note, however, that the SNR increase, as shown in Figure 2.6a, is relatively small for low-SNR neurons. Therefore, ICA only slightly increases the percentage of detectable neurons. For configurations with $D < 30$ µm, the percentage of detectable neurons based on the ICs drops below the percentage of detectable neurons based on the raw signals, which is approximately constant across all configurations. We conclude that ICA fails to improve signal quality for very dense neuron populations but is beneficial for lower density populations.

The presented analyses revealed that ICA, applied to HD-MEA recordings, yields only limited separation performance and is, therefore, not suited to be used as a stand-alone spike-sorting tool in combination with threshold detection.

2.3.5 ICA Applied to Recorded Data

An example of ICA, applied to block recordings with spontaneous RGC activity is illustrated in Figure 2.7. The DCVs, depicted in Figure 2.7a, yield spatially localized high weightings. Note that the input to ICA is the multielectrode signal without any information on the electrode positions and that the neuronal templates are localized in space. Therefore, spatially localized high weighting values in the DCVs are a good indicator that the signals, underlying the ICs, originate from neuronal units.

In looking at the spike waveforms, some ICs (e.g., ICs 1 and 7 in Figure 2.7b) feature high separability and, practically, represent single-unit spike trains of neurons. However, the problems of limited separability and dimensionality reduction that were discussed in the previous sections are also visible in the IC signals. Several ICs (e.g., ICs 3–6 and 8) presumably contain spikes from multiple neurons as indicated by spike waveforms of different amplitudes on the IC. On the other hand, in some cases, spikes from a single neuron were observed on multiple components (red arrows in Figure 2.7b).

2.3.6 Approaches for ICA-Based Spike Sorting

Since most ICs do not represent single-unit spike trains (Figure 2.7b), the spikes cannot be sorted by just applying event detection to the ICs. The reduced redundancy in the data as well as the increased SNR and separability are, however, still valuable features of the IC representation. In this section, we propose to use postprocessing techniques to overcome the most severe limitations arising from the nonlinearity of the templates.

For the case that an IC contains spikes of multiple units, the spikes can be separated by means of PCA-based clustering of the IC spike waveforms. This is exemplarily shown for IC 4 in Figure 2.7, c-e. The green cluster, which exhibits large spike signals in this IC, corresponds most likely to the neuron that can be associated with this component. The smaller spikes, grouped into the red cluster, can be discarded and may be detected on other ICs.
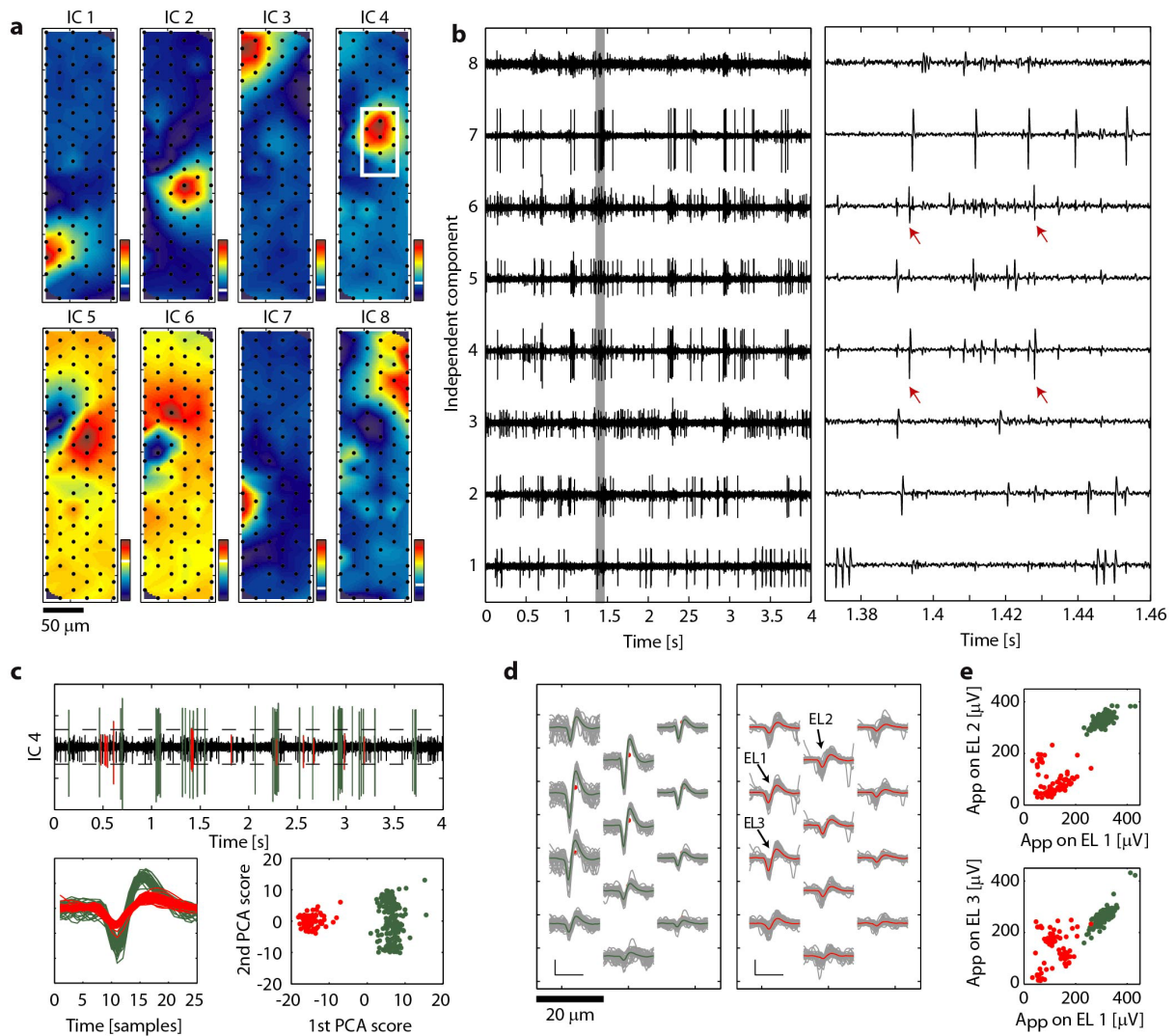
Figure 2.7 Example of ICA applied to retinal recordings.

(a) Spatial map of DCVs for the 1st 8 components. The coefficients are normalized with regard to the resulting IC signal having a standard deviation of 1; therefore, no absolute values are shown here. The white line in the corresponding color bars represents the 0 value. (b) Corresponding IC signals (*left*) and close-up (*right*, data segment is indicated by a gray rectangle on *left* plot). Except for the large spikes in *ICs 4* and *6*, which originate from the same neuron (red arrows), the spikes on different components belong to different neurons, as they are not correlated in their timing. (c) Threshold detection and clustering for *IC 4. Top*: dashed line representing the threshold level; detected events are colored. *Bottom left*: superimposed IC traces for all detected events above threshold within 20 s. *Bottom right*: 1st and 2nd PCA scores for detected events, which can be clustered (colors). (d) Spatial spike distributions for both clusters over selected electrodes marked by the white rectangle in a, showing the average spike shape (colored) and the individual traces (gray). Scale bar: 100 μV/1 ms. (e) Peak-to-peak amplitude values of the 2 clusters on pairs of electrodes. EL1–EL2 and EL1–EL3: the electrodes are indicated in d.

Note that the peak-to-peak amplitudes in the red cluster (Figure 2.7e) show large variability, suggesting that these spikes arise from multiple neurons.

The problem of multiple detection of neurons can be addressed by using an aggregation method, which, e.g., compares the identified spike times of the questionable neurons and merges them if they have a specific number of spike times in common (Litke et al., 2004). Additionally, waveform similarity and ISI statistics can be included as aggregation criteria (Fee et al., 1996b).

Furthermore, ICA-based spike sorting can be performed in an iterative procedure: ICA is applied to the data, and spikes are identified by applying threshold detection to the ICs. Following clustering and merging, the STA waveforms of identified neurons are subtracted from the raw data. In a next iteration, ICA is applied to the residual signals. Similar, subtractive methods were proposed for spike sorting using optimal filters (Gozani and Miller, 1994) and template matching (Vargas-Irwin and Donoghue, 2007).

This iterative scheme, which adds a nonlinear feature to the linear ICA approach, is motivated by two reasons. On the one hand, neurons featuring large signal amplitudes render the separation of neighboring, spatially overlapping neurons with smaller amplitudes difficult. Therefore, the identification and subtraction of dominant neuronal sources allows for identifying less dominant signals in the subsequent ICA iteration. On the other hand, ICA facilitates the detection and classification of a spike A even though it temporally overlaps with another spike B. The proper subtraction of spike A will improve detection and classification of spike B in the proximate iteration in case that it cannot be identified on another IC.

An algorithm based on the described approaches was implemented. ICA was applied to the band-pass filtered recordings, decomposing the data into ICs. AP events, identified by applying threshold detection to the IC signals, were clustered (KlustaKwik), based on the principal components of the IC spike traces. Clusters with high standard deviation on the multichannel spike traces were believed to be erroneous and discarded. After an intermediate merging step, during which clusters of multiple-detected neurons were aggregated, the STA spikes were subtracted from the raw data. In the next iteration, ICA was applied to the residual signal. This iterative scheme was repeated for a defined number of iterations. A detailed description of the individual algorithm steps is given in ICA-Based Spike-Sorting Algorithm in Appendix.
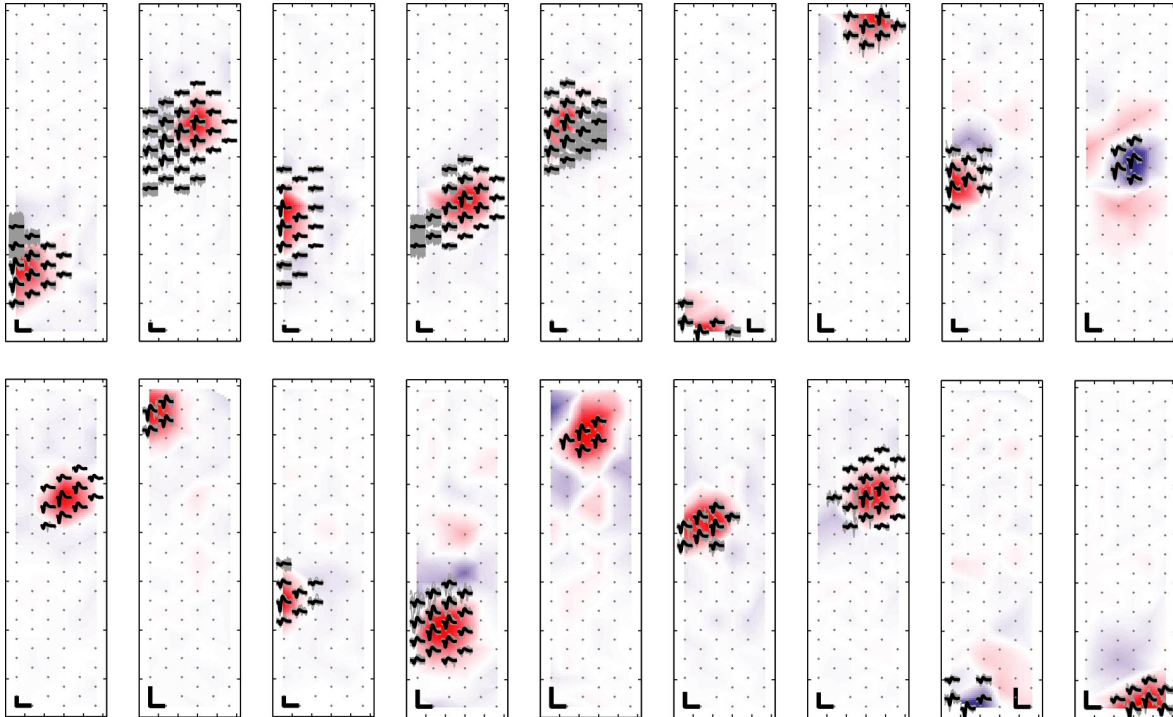
Figure 2.8 Automatically sorted neurons.

STA templates (black) and individual traces (gray) of neurons as identified using the iterative ICA-based approach. The DCVs are indicated through the color code in the background. Scale bars: 100 μV/1 ms. For visualization purposes, the templates were individually scaled, which results in variable-size scale bars.

Figure 2.8 shows the templates (black) of 18 sorted cells from recorded RGC activity on an HD block. The DCV weightings (background colors) largely overlap with the active electrodes of the neuron templates. The individual traces are depicted in gray. Concurrent high-amplitude spiking activity of neighboring neurons results in visible gray traces near the neuron template, which can be observed for several neurons (e.g., for templates 1, 2, 4, 5, and 6). These traces, which lie mostly outside the DCV active area, indicate that ICA allowed to classify correctly the spikes despite overlaps.

Finally, an unsupervised version of the spike-sorting algorithm was applied to the simulated *data set B*, and the sorting output was matched with the simulated data. A sorted neuron was assigned to a simulated neuron, if the number of matching spikes exceeded 10% of the total number of spikes of the simulated neuron. We classified the simulated neurons as identified (if detected as 1 neuron), identified multiple (if detected as 2 or more separate neurons), falsely merged (if detected but merged with 1 or more simulated neurons), or as not found (if not detected at all). The classification
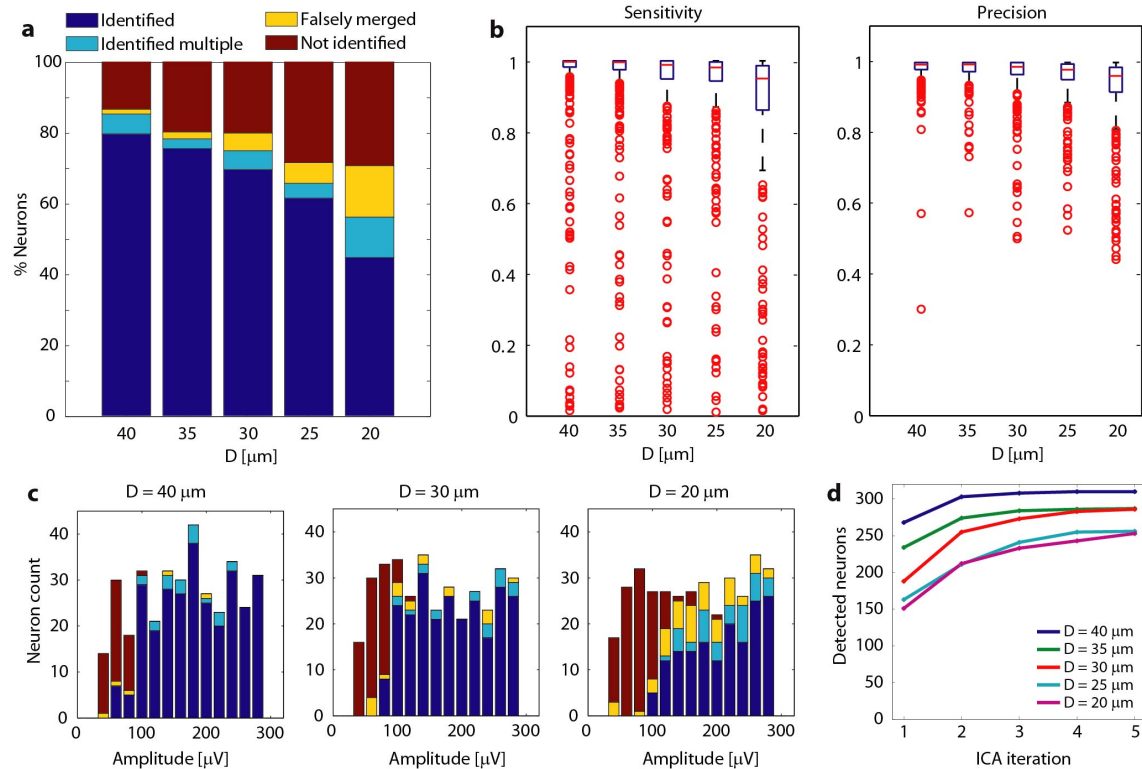
Figure 2.9 Evaluation of spike sorting as applied to simulated data sets.

(a) Percentage of simulated neurons classified as identified, identified multiple, falsely merged, and not identified for the different configurations. (b) Box plots of the sensitivity and precision values for all sorted neurons, showing the median values (red horizontal line), the interquartile ranges (IQR; blue boxes), highest and lowest data values that are within 1.5 times the IQR (black whiskers), and outliers outside 1.5 times the IQR (red circles). (c) Histogram counts of neuron classification vs. neuronal-signal peak-to-peak amplitude for 3 configurations. (d) Cumulative sum of detected neurons vs. ICA iterations.

percentages of the simulated neurons are depicted in Figure 2.9a. As for ICA alone, the sorting performance was found to depend on the cell density. Additionally, the neuronal signal amplitude played a dominant role. As shown in Figure 2.9c for the different configurations, most detected neurons featured a certain amplitude range, whereas neurons with lower amplitudes passed constantly undetected. This correlates to the observation that the separability of a neuron on the IC strongly depends on its SNR.

To quantify the sorting quality, each sorted neuron was assigned to a simulated neuron (based on the number of matching spikes), and the numbers of true-positive (TP), false-positive (FP), and false-negative (FN) events were computed. We used the performance measures "sensitivity"

D [µm]	Non-overlaps		Overlaps		Overlap specific error probability p_O
	Total	Missed (p_E)	Total	Missed (p_{OE})	
40	75824	1332 (1.8 %)	2507	81 (3.2 %)	1.4 %
35	63425	1282 (2.0 %)	2214	97 (4.4 %)	2.4 %
30	70797	1860 (2.6 %)	3158	204 (6.4 %)	3.9 %
25	57908	2220 (3.8 %)	4873	426 (8.7 %)	5.1 %
20	49803	2510 (5.0 %)	6311	694 (11 %)	6.3 %

Table 2.2 Classification performance (false-negative events) of nonoverlapping vs. overlapping Spikes.

For this particular analysis, all sorted neurons with sensitivities >0.6 were considered. Overlaps were defined as spikes featuring a time difference of 10 samples or less to spikes of other neurons that were closer than 50 µm. The observed error probabilities for nonoverlapping spikes (p_E) and for overlapping spikes (p_{OE}) were used to compute the probability associated with overlapping spikes p_O shown in the last column, using Eq. 16 in Appendix. *D*, distance.

[TP/(TP+FN)] and "precision" [TP/(TP+FP)]; a sensitivity value of 1 means that all spikes were detected (no FNs), and a precision value of 1 signifies that only correct spikes were detected (no FPs). Figure 2.9b shows box plots of the performance results. The blue boxes indicate the interquartile ranges (IQR), and the black whiskers the highest and lowest data values that are within 1.5 times the IQR. Therefore, the lower performance bounds are given by the lower border of the blue boxes (for 75% of the neurons) and by the lower whiskers (for 87.5% of the neurons). Although there were numerous neurons with poor performance (outliers: red circles), the majority of the sorted neurons (indicated by the medians: red lines) yielded sensitivity and precision values >0.95 throughout all configurations. The performance was again found to depend on the cell density. For configurations D ≥ 35 µm, 87.5% of the neurons yield in performance values >0.93.

The iterative approach allowed to increase the number of detected neurons (i.e., substantial increases for iterations 2 and 3). This is evident from the number of detected neurons after each ICA iteration, shown in Figure 2.9d.

We also compared the detection performance for overlapping and nonoverlapping spikes (Table 2.2). This analysis revealed that the ICA approach performs well in classifying spikes despite the fact that they are temporally overlapping with spikes from nearby neurons. The error

probability associated with overlaps (right column in Table 2.2) was determined using Eq. 16 in Appendix. These error probabilities varied between 1.4 and 6% for the different configurations and are on the same order as the probabilities for nonoverlap errors. Accordingly, even for the highest-density case, only 1 out of 16 overlapping spikes was missed due to spatiotemporal interference with a spike from another neuron.

2.4 Discussion

Recently, ICA has received increasing attention as a tool to analyze biomedical signals, such as EEG or functional MRI, as well as for spike sorting of optical brain recordings (Stone, 2002; Reidl et al., 2007; Mukamel et al., 2009; Hill et al., 2010). Being an automatic tool for source separation of redundant data sets, ICA represents a promising candidate to facilitate rapid spike sorting of HD-MEA data.

In this paper, the suitability of ICA for demixing HD-MEA recordings was evaluated for the first time. We analyzed neuronal activity, recorded at high spatiotemporal resolution, and found that the fundamental requirement for ICA, a linear mixture of the source signals, is not fully satisfied by the characteristics of the data. Instead, the linearity between the waveforms of a neuron on different electrodes is decreased, which is mainly due to AP propagation delays.[1] The compromised linearity was found to be a limiting factor already in sparse neuron arrangements, which impeded perfect source separation. As a consequence, ICA, followed by threshold detection, cannot be used as a stand-alone method for spike sorting of HD-MEA data. These findings presumably also hold for other devices and planar microelectrode systems (Csicsvari et al., 2003; Takahashi and Sakurai, 2005; Du et al., 2009). The limitations of the applicability of ICA as a consequence of the nonlinear characteristic of the neuronal signals, as shown for tetrode

---

[1] Additional analyses (data not shown) revealed that the most relevant frequency bands for the phase differences between the waveforms on different channels are in the range between 1 and 4 kHz (for digitally unfiltered data). Consequently, low-pass filtering the data before ICA with a cutoff frequency ≈1 kHz reduced the nonlinearity effect and led to an increased ICA performance with respect to finding efficient MCVs and reducing redundancy. However, the achieved source separation was still limited. Furthermore, by removing the frequencies 1 kHz, where spikes have a significant part of their energy, important information for discrimination gets lost, and the SNR decreases.

recordings in Shiraishi et al. 2009, cannot be completely compensated by spatial oversampling using high electrode density.

The analysis of ICA applicability using simulated data sets of RGC activity as presented here revealed that the ICA performance strongly depends on the neuronal density in the preparation. Particularly, when the neuronal density approached the electrode density (3,161 electrodes/mm^2) and the number of simulated neurons (111) exceeded the number of electrodes (90), the separation performance clearly decreased. Neurons that produced high-SNR signals entailed superior separation performance.

Except for very dense neuronal populations, ICA led to a significant overall SNR increase, which allowed for detecting more neurons. Moreover, the redundancy was clearly reduced in the ICs, which helps to overcome the problem of detecting the same APs multiple times on several electrode signals. For a limited number of neuronal sources, ICA automatically provided separation, which could serve to resolve efficiently overlapping spikes from these sources.

We showed that limitations arising from the nonlinearity of the sources could be addressed by combining the ICA output with postprocessing techniques. In particular, we proposed an algorithm, based on applying PCA and clustering, to the detected IC traces. For densities up to 1,300 neurons/mm^2, >80% of the neurons were detected (>70% correctly identified as single neurons) using the unsupervised, ICA-based algorithm. The detection of the majority of the neurons for these densities was highly accurate (87.5% of the neurons had sensitivity and precision values above 0.86 and 0.91). Additionally, the algorithm performed well in resolving overlapping spikes. The percentage of misclassified overlaps (FNs), compared with nonoverlaps, was increased by factors of up to 2, and the particular error probability associated with the overlaps was between 1.4 and 6.3%.

The method of combining ICA with the proposed postprocessing techniques was not efficient for sorting the complete neuronal population but yielded good results in sorting large fractions of the cells with high accuracy. By iteratively subtracting identified spike waveforms from the data and applying ICA, the number of detected neurons could be increased by 15-68% for the different simulated neuron densities.

In conclusion, our results suggest that ICA applied to HD-MEA data does not yield complete separation of the neuronal signals. However, the IC-representation of the data has some valuable features, e.g., the reduced redundancy, which entails that spikes from a neuron are only prominent on one or a few ICs. This allows for treating the individual ICs as separate signals, which facilitates spike detection in redundant MEA data. In addition, the increased separability contributes to resolving overlaps. These features make ICA a valuable tool to serve as a preprocessing step to spike sorting.

2.5 Appendix

2.5.1 Estimation of the demixing matrix based on the templates

The linearity assumption implies that the template waveforms can be viewed as scaled versions of an intrinsic neuronal signal $\tilde{s}^i$ with coefficients

$$
\begin{aligned}
\boldsymbol{F^i} &= \left[\boldsymbol{f^i_1}, \dots, \boldsymbol{f^i_M}\right]^T \\
&= \left[a_{1i} \cdot \tilde{s}^i, \dots, a_{Mi} \cdot \tilde{s}^i\right]^T
\end{aligned} \tag{10}
$$

The mixing coefficients $a_{1i}, \dots, a_{Mi}$ describe how $\tilde{s}^i$ is mixed across the electrodes. If the neuron templates are known, the demixing coefficients in **A** can be directly derived by

$$
a_{ji} = \operatorname{argmin}_a \left\|\boldsymbol{f^i_j} - a_{ji} \cdot \tilde{s}^i\right\| ; \begin{array}{l} i = 1, \dots, N \\ j = 1, \dots, M \end{array} \tag{11}
$$

The average of the template waveforms is used for the intrinsic signal:

$$
\tilde{s}^i = \frac{1}{M} \sum_{j=1}^{M} \boldsymbol{f^i_j} \tag{12}
$$

2.5.2 ICA-based spike sorting algorithm

This section describes the individual steps of the spike sorting algorithm and the parameters that were used for spike sorting of the simulated datasets.

1) All data is band-pass filtered between 500 and 3000 Hz.

2) *FastICA is applied to the full length data and the number of estimated ICs equals the electrode number. The following steps 3-5 are successively performed for every IC signal.*

3) *Spikes are detected on the IC by threshold detection. The noise level is estimated based on the median (Donoho and Johnstone, 1994)*

$$\sigma_n = \text{median} \left\{ \frac{|x|}{0.6745} \right\} \qquad (13)$$

which has been shown to be robust for variable firing rates (Quiroga et al., 2004). A threshold level of $5 \cdot \sigma_n$ is used.

4) *PCA is applied to the aligned IC spike waveforms. The scores from the first three resulting principal components are clustered using KlustaKwik, which automatically estimates the number of clusters. The cluster with the largest average IC spike signal is selected for further processing and other clusters are discarded.*

5) *As spike traces from a well-isolated cluster are expected to have low variation, the standard deviation of the traces is used as a measure of cluster quality. The traces on the three electrodes with highest spike signals are normalized by the peak-to-peak amplitude of the cluster template and the standard deviation of the normalized traces is computed (relative standard deviation, RSTD). The RSTD has been experienced to be a robust quality measure, as it compensates for the effect that the degree of spike trace variation also depends on spike amplitude. The resulting cluster from step 4 is discarded if the RSTD exceeds a threshold of 0.12.*

6) *After repeatedly conducting steps 3-5 for all ICs, pair-wise comparisons between the obtained clusters are performed and two clusters A and B are merged if they appear to belong to the same neuronal unit according to the following criteria:*

   a. *If the number of spikes shared by both clusters exceeds 30% of the number of spikes in cluster A or B.*

   b. *The similarity between the aligned average waveforms of clusters A and B is measured by means of their normalized Euclidian distance*

$$D = \sqrt{\frac{1}{M} \cdot \frac{1}{L} \cdot \sum_{j} \sum_{\tau} \left(f_{j\tau}^{A} \cdot f_{j\tau}^{B} \right)^{2}} \qquad (14)$$

where $f_{j\tau}^{A}$ is the τ-th sample of the cluster template for cluster A at the j-th electrode, M is the number of electrodes considered and L is the waveform length. For this measure, only electrodes on which the clusters had significant energy were considered. The threshold value for merging was set empirically (merge if $D < 4.3$). The merging is organized in the following way. In a first step the clusters are compared for the criterion of common spike times and accordingly merged. In a second steps, the distances for all cluster pairs are calculated and the cluster pair with the smallest distance is merged if the condition is fulfilled. After merging, the cluster-pair distances are recalculated and the merging condition is checked again for the pair with smallest distance.

7) The STA waveforms of the identified neuronal clusters are subtracted from the raw data and steps 2-6 are subsequently applied to the residual data. This iterative scheme is repeated for a total of five iterations. After each iteration, newly identified clusters are aggregated with previously obtained clusters using the merging method described in step 6.

2.5.3 Computing the overlap-specific error probability

From the spike sorting results, the observed probabilities of a FN error for non-overlapping, p_E, and for overlapping spikes, p_{OE}, can be extracted. The observed probability of missing an overlapping spike can also be formulated as:

$$p_{OE} = p_E + (1 - p_E) \cdot p_O. \qquad (15)$$

p_o is the specific error probability for overlapping spikes, i.e. the probability to miss a spike participating in an overlap although it would have been detected if the other spike was not there:

$$p_O = \frac{p_{OE} - p_E}{(1 - p_E)}. \qquad (16)$$

2.6 Acknowledgments

CHAPTER 3 Mapping Synaptic Connections by Using Combined High-density Microelectrode Array and Patch Clamp recordings

David Jäckel[1], Thomas Russell[1], Douglas Bakkum[1], Jan Müller[1], Felix Franke[1], Urs Frey[2], and Andreas Hierlemann[1]

1 ETH Zurich, Department of Biosystems Science and Engineering, 4058 Basel, Switzerland

2 RIKEN, Quantitative Biology Center, 650-0047 Kobe, Japan

Abstract

The functional properties of synaptic transmission between presynaptic and postsynaptic neurons have been studied in great detail. Typically, the postsynaptic neuron is recorded in the whole-cell patch clamp configuration, while action potentials (APs) at a presynaptic cell are evoked. Since cortical neurons typically receive input from thousands of synapses, the functional characterization of multiple combined synaptic inputs into neurons is of great importance. Therefore, techniques for measuring and stimulating APs at multiple presynaptic neurons and the postsynaptic neuron are required, which would allow to characterize interactions between multiple presynaptic inputs. Complementary-metal-oxide-semiconductor-based microelectrode arrays featuring high electrode density represent a novel tool to stimulate and record firing activity of large numbers of neurons simultaneously. In this work, we present a system which combines the whole-cell patch clamp technique with high-density microelectrode arrays (HD-MEAs). By recording spiking activity of multiple neurons on the array and by simultaneously measuring the intracellular membrane potential of a patched postsynaptic neuron, we were able to identify individual presynaptic neurons and their contributions to average postsynaptic potentials (PSPs). This technique allows for observing interactions between different inhibitory and excitatory synaptic inputs during spontaneous activity. Furthermore, neurons were stimulated with voltage pulses, and stimuli evoking individual monosynaptic PSPs were identified. The identified stimuli can be used to evoke PSPs in multiple neurons in various patterns to study interactions between presynaptic inputs in a controlled environment.

3.1 Introduction

The excellent signal-to-noise ratio of intracellular recordings with the whole-cell patch clamp technique, which allows measuring very small synaptic currents, has been a key to study the functional properties of synaptic transmission. In paired-recordings, for example, a presynaptic and a postsynaptic neuron are simultaneously patched, and action potentials (APs) are evoked in the presynaptic cell triggering synaptic signals at the postsynaptic cell. This technique was used to characterize different types of short-term plasticity at inhibitory (Poncer et al., 1997) and excitatory (Debanne et al., 1996) synaptic connections and long-term plasticity effects such as long-term potentiation (LTP), long-term depression (LTD) (Debanne et al., 1998) and spike-timing dependent plasticity (STDP) (Markram et al., 1997; Bi and Poo, 1998).

Cortical neurons, however, typically receive synaptic input from many, up to thousands of cells. For this reason, it seems evident that the functional characterization of how *multiple* synaptic inputs integrate and interact is of great importance. Various forms of interaction effects between individual synaptic inputs have been identified, such as the summation properties of multiple inputs through dendrites (Polsky et al., 2004; Branco and Häusser, 2011; Hang and Dan, 2011), temporal precision and reliability of combined synaptic inputs (Nawrot et al., 2009), heterosynaptic long-term plasticity effects (Royer and Paré, 2003; Chen et al., 2013) where nonactivated synaptic contacts were modulated by plastic changes of activated synapses, as well as heterosynaptic forms of short-term plasticity (Fuentealba et al., 2004).

Only a few electrophysiological techniques have been introduced, which allow measuring synaptic inputs from multiple presynaptic cells. Paired-recordings from multiple simultaneously-patched neurons in a preparation represent a powerful measurement configuration, as the full multidirectional connectivity can be accurately characterized. Some studies have reported as many as 8-12 simultaneously patched neurons in brain slices (Perin et al., 2011; Jiang et al., 2013). Reliably achieving such high numbers of simultaneously patched neurons is, however, extremely challenging and requires highly specialized recording setups and technical skills. Thus, only a few laboratories

have established recordings for more than 2-3 simultaneously patched cells.

The main principle of the alternative approaches is to patch an individual neuron while simultaneously either detecting APs of presynaptic cells or directly evoking them through different stimulation techniques. The presynaptic spike times and stimulus timings, respectively, are used for spike-triggered-averaging (STA) of the intracellular signal in order to compute the average postsynaptic potentials (PSPs).

The 'reverse optical probing' technique (Aaron and Yuste, 2006; Sasaki et al., 2009) combines calcium imaging of a neural population during spontaneous or glutamate-evoked activity with patch clamp recordings and makes use of the reverse correlation analysis to identify neurons firing APs time-locked with detected synaptic events. It is a powerful approach to identify synaptic projections (Takahashi et al., 2010), but the limited temporal resolution in the calcium signals poses major challenges on measuring the PSPs accurately.

Introduced by Callaway and Katz 1993, 'photostimulation scanning' is another optical approach where an individual neuron is patched, while many other neurons are sequentially stimulated by photolytic release of caged glutamate. Recent implementations featured the possibility to dynamically control the light beam and to thus generate spatio-temporally structured synaptic input patterns (Boucsein et al., 2005; Nawrot et al., 2009). A combination of this technique with two-photon excitation has demonstrated that single-cell photostimulation in acute slices can be achieved, even across different focal planes (Nikolenko et al., 2007). The high spatial resolution allows for stimulating large numbers of neurons, which makes it an attractive technique for mapping functional circuits within brain slices. However, the technique also has some substantial limitations. Direct stimulation of the postsynaptic cell must be avoided, and the laser power and pulse duration must be carefully calibrated. Still, evoking single presynaptic APs is difficult to achieve reliably and the temporal stimulation resolution is limited. Furthermore, caged neurotransmitters were found to block $GABA_A$ receptors to some extent (Fino et al., 2009; Ellis-Davies, 2013), which can lead to epileptiform events and prevents the study of inhibitory synaptic transmission. Due to these limitations, the

method is not suitable for short- and long-term plasticity experiments (Lübke and Feldmeyer, 2007).

Alternatively, the stimulation of presynaptic cells can be carried out by electrical means with extracellular electrodes. Extracellular stimulation of presynaptic neurons was performed with individual bipolar electrodes (Fuentealba et al., 2004; Chen et al., 2013), or with arrays of stimulating microelectrodes (Royer and Paré, 2003). Electrical stimulation allows for evoking activity in a temporally precise and reproducible way, but lacks, however, spatial resolution. For this reason, the number and selectivity of activated presynaptic cells is limited and largely depends on number, dimension and location of the extracellular electrodes.

Recently developed high-density microelectrode arrays (HD-MEAs) (Eversmann et al., 2003; Berdondini et al., 2005, 2009; Hutzler et al., 2006; Frey et al., 2010; Ballini et al., 2014) based on complementary metal oxide semiconductor (CMOS) feature addressing and signal conditioning circuitry on the same chip and incorporate up to thousands of electrodes at unprecedented spatial resolution. As a result of the high spatial density, for neuronal cultures grown on the array, virtually every neuron is surrounded by multiple electrodes. This fact has great impact on the stimulation and recording capabilities of HD-MEAs. For some HD-MEA devices (Frey et al., 2010; Eversmann et al., 2011; Ballini et al., 2014), every electrode can be used to apply temporally precise and spatially confined stimuli (Bakkum et al., 2013) which provides the possibility to reliably evoke neuronal APs of many different neurons. Due to the closely spaced microelectrodes, activity of individual neurons is always measured by multiple electrodes. This factor is essential for analyzing the recorded activity at single-cell and single-AP resolution, as recording extracellular signals of individual neurons with multiple electrodes greatly improves spike sorting performance (Gray et al., 1995; Einevoll et al., 2012; Fiscella et al., 2012).

In this work, we combine the particular capabilities of HD-MEAs to record and stimulate at high spatiotemporal resolution with the patch clamp technique, in order to precisely map and evoke synaptic signals from multiple presynaptic cells. The HD-MEA (Frey et al., 2010) features 11,011 densely packed electrodes (3,161 electrodes/mm^2) on

an area of 1.99 x 1.75 mm^2, which can be used for electrical stimulation and recording (up to 126 electrodes simultaneously) of neuronal activity. The working principle is, as for the methods discussed above, to patch a neuron in the whole-cell configuration and to record or to evoke APs in presynaptic cells.

The experimental procedure is comparably simple, as only one neuron needs to be patched at a time. By combining the acquisition of the intracellular and extracellular signals at hardware-level, the presented system allows fast and efficient data processing during the experiment, in order to e.g. scan and identify synaptic connections within a short time. As opposed to the optical methods, our HD-MEA-based approach allows detecting and evoking APs at the resolution of tens of microseconds in order to accurately average the PSPs. Furthermore, the experiments do not require any special dyes, chemicals compounds or uncaging agents, which might introduce side-effects such as blockage of receptors, phototoxicity or influencing the affect the intracellular calcium dynamics.

Two approaches for measuring individual synaptic inputs are presented. In the first approach, spontaneous extracellular activity from many neurons is recorded with the HD-MEA, while, at the same time, the intracellular signal of an individual patched neuron is measured. The sorted spike times of the recorded neurons are then used for apply spike-triggered averaging (STA) on the intracellular signal in order to identify monosynaptic connections.

The second approach makes use of the stimulation capabilities of the HD-MEA. APs of neurons are evoked by sequentially stimulating at HD-MEA electrodes with different stimulation amplitudes, while a neuron is patched. A semi-automatic algorithm is then used to identify which electrodes evoked monosynaptic PSPs through the respective presynaptic neurons. A technique is introduced, in order to identify whether individual presynaptic neurons had been stimulated.

3.2 Methods

3.2.1 HD-MEA system

We used a microsystem-based HD-MEA system (Frey et al., 2009, 2010) for extracellular neuronal recording and stimulation. The electrode array is integrated into a microsystem chip, which has been fabricated in a 0.6 µm CMOS process; the chip accommodates a total of 11,011 electrodes in an area of 1.99 x 1.75 mm^2 (17.8 µm center-to-center pitch, 3'161 electrodes/mm^2 density, 8.2 x 5.8 µm^2 electrode size). Out of all electrodes, 126 can be simultaneously recorded from, by connecting them to the 126 read-out channels by means of a flexible switch matrix located underneath the array. The switch-matrix approach provides low-noise (7-9 µV$_{rms}$) recordings and high routing flexibility to select almost arbitrary electrode configurations. Furthermore, electrodes can be connected to stimulation channels for voltage or current stimulation (Livi et al., 2010) and can be stimulated with arbitrary stimulation waveforms (up to 20 kHz), which are provided by two individual digital-to-analog converter units.

The recorded signals are amplified (0–80 dB programmable gain), filtered (high pass: 0.3-100 Hz, low pass: 3.5-14 kHz) and digitalized (8 bit, 20 kHz) on-chip, and sent to a field-programmable gate array (FPGA) board. The data are then streamed to a host PC for data storage and real-time visualization with an adapted version of the MeaBench software (Wagenaar et al., 2005). MATLAB (The Mathworks) was used for online data analysis and visualization during the experiments, as well as for controlling and sending commands to the chip (i.e., for electrode selection, recording and stimulation protocols).

In order to effectively reduce the electrode impedance and improve recording and stimulation conditions by increasing the effective electrode surface area, platinum black was deposited on the electrode by applying a current of 180 µA simultaneously to all electrodes for 45-75 s by using a platinum wire as a ground electrode immersed in the deposition solution (0.7 mM hexachloroplatinic acid and 0.3 mM lead (II) acetate anhydrous). Deposition uniformity was improved by wiping

the platinum black from the electrode area with a cotton stick and repeating the procedure 1 or 2 times.

3.2.2 Setup for combined HD-MEA and Patch Clamp Recordings

The experimental set-up is a combination of the HD-MEA system with an upright microscope (Leica DM6000B) and a conventional patch clamp system. The HD-MEA chip and the patch clamp micromanipulator (Sutter Instruments) are positioned on a fixed stage (Scientifica), whereas the microscope is mounted on a motorized XY stage (Scientifica UMS), which allows for imaging a large area. Image acquisition and XY stage position are controlled by the microscope controller (CTR7000 HS) through the imaging software (Leica LAS AF), which allows for storing the precise microscope position for every acquired image. Custom image alignment software (written in MATLAB) was developed to automatically align the acquired images with the corresponding HD-MEA coordinates. This feature was particularly important to identify the electrodes underneath a patched cell, or to localize a particular neuron based on the activity measurements with the HD-MEA.

For synchronizing the recording of the analog signals through the patch clamp amplifier (Multiclamp 200B), the FPGA was equipped with four analog-to-digital conversion channels (ADCs, AD974 Analog Devices) on a custom printed-circuit board. The ADCs provide 16 bit conversion for a ±10 V input range and are synchronized to the HD-MEA sampling rate. The digitalized signals are inserted into the HD-MEA data stream, so that the patch clamp signals can be visualized together with the HD-MEA signals in real-time (MeaBench), which is crucial for correlating intra- and extracellular measurements during the experiment.

3.2.3 Cortical neuron culture preparation

Embryonic-day 18 Wistar rat cortices were dissociated in 2 ml of trypsin with 0.25% EDTA (Invitrogen) with trituration. The array was pre-coated with a thin layer of poly(ethyleneimine) (Sigma), 0.05% weight/weight, in borate buffer (Chemie Brunschwig) at a pH of 8.5, followed by a drop of 0.02 mg ml^{-1} laminin (Sigma) in Neurobasal

(Invitrogen). 15000-20000 cells in a 30 μl drop were seeded over the array. 1 ml of Neurobasal medium was added after 30 minutes. The cultures were maintained inside an incubator under controlled environmental conditions (37 °C, 65% humidity, 9% O_2, 5% CO_2) in 1 ml of Neurobasal medium (partially replaced twice per week).

3.2.4 Patch Clamp Electrophysiology

Patch clamp experiments were performed after 2-5 weeks in culture. For the patch clamp experiments, the cultivation medium was removed, and the chip was perfused with a HEPES-buffered external bath solution containing (in mM:) NaCl 149, KCl 3.25, $CaCl_2$ 2, $MgCl_2$ 2, HEPES 10, Glucose 11 (pH: 7.35 adjusted by using NaOH 1M). The bath was constantly perfused during the experiment at a low rate, and all experiments were performed at room temperature. Neurons on top of the MEA electrodes were visualized in bright field mode by using difference interference contrast (DIC) optics of the upright microscope. We found that the deposited platinum black reduced the strong contrast of the electrodes by darkening the array electrode surfaces, which resulted in greatly improved visibility of the cells. The micropipettes had resistances of 5-7 MΩ and were filled with an internal solution containing (in mM): potassium gluconate 135, KCl 20, $MgCl_2.6H_2O$ 2, HEPES 10, EGTA 0.1 Na_2ATP 2, Na_3GTP 0.3, adjusted to a pH of 7.3 with KOH. In most cases, 0.02 mM Alexa Fluor 594 (Life Technologies) was added to the internal solution, and fluorescence images were acquired during and after the patch clamp experiment. The patched cells used in this paper had holding potentials below -50 mV, and the junction potential was not corrected for. All recordings shown in this study were performed in the current clamp mode, and the patch clamp amplifier was controlled through the open-source software WinWCP (John Dempster, University of Strathclyde, UK).

To block excitatory synaptic activity, 100 μM of the AMPA antagonist 6-cyano-7-nitroquinoxaline-2 3-dione (CNQX), and 10 μM of the selective NMDA receptor antagonist DL-2-amino-5-phosphonovaleric acid (AP5) were added to the bath solution. Addition of 50 μM Bicuculline methiodide (BIC), a $GABA_A$ antagonist, was used to block Inhibitory synaptic signaling.

3.2.5 Extracellular Recording and Stimulation

During cultivation, extracellular activity could be recorded inside the incubator in culturing medium. Spontaneous firing activity was typically observed after one week in culture. One day before a patch clamp experiment, the following recording protocols were routinely performed:

Spontaneous Spike Map: The complete array was scanned for spontaneous activity. For this purpose, signals were recorded sequentially by 146 electrode configurations for 30 − 60 s per configuration, where each configuration consisted of a high-density electrode block (6 x 17 electrodes). Spikes at every electrode were detected by thresholding (threshold level of 5.5 x standard deviation of the signal). The 'spontaneous spike map', as shown in Figure 3.2b and Figure 3.6a displays the amplitude of the negative-peak, recorded for each electrode, and can be used for visualization of the activity.

Electrodes with Large Negative Signals in the Spike Map: In the 'spontaneous spike map', local peaks with negative signals exceeding a predefined threshold were automatically identified, and the closest electrodes to these peaks were selected, as visualized by all black dots in Figure 3.6a. Such electrodes recording local negative signal peaks were used as recording spots for recording network activity, as shown in Figure 3.3a, and as stimulation spots for stimulation-triggered PSP mapping as shown in Figure 3.6a.

Spontaneous Scan: The spike-triggered average extracellular action potential (STA-EAP) is a cell-specific extracellular signature and visualized e.g. in Figure 3.1c and e and in Figure 3.2a. The array-scale STA-EAPs including axonal signals were acquired by selecting groups of 2-4 electrodes around electrodes that featured large negative signal amplitudes and by then recording spontaneous activity with multiple configurations covering the whole array, while the preselected groups of electrodes were read out in every configuration. Spikes at the selected groups were manually sorted and used to calculate chip-wide STA extracellular potential distribution. The automated routine allowed for detecting 10 − 12 neurons within 2.5 hours of recorded spontaneous activity.

For manual spike sorting the Ultramegasort software (Hill et al., 2011) was used. In stimulation experiments, all applied voltage pulses had a biphasic, positive-first waveform with 200 µs phase width of variable amplitude.

3.3 Results

3.3.1 Simultaneous HD-MEA and Patch clamp Recordings of Cultured Cortical Neurons

Cortical neurons cultured on HD-MEAs (see Figure 3.1a) were patched in the whole-cell configuration, and intracellular recordings were made in the current clamp mode. Spontaneous and evoked intracellular and extracellular action potentials (APs) were recorded simultaneously, whereas the extracellular spikes of the individual neurons were always seen on multiple electrodes. The neurons had been plated and cultivated at low densities so that, in most cases, the patched cells were located directly on the array surface. However, extracellular spikes from patched neurons could be measured also for neurons lying up to 30-40 µm above the electrodes if these neurons were located on top of cell aggregations.

We used the intracellular APs to detect the spike times and to compute the distribution of the spike-triggered average extracellular waveforms of the patched neurons. Figure 3.1b shows recordings from a spontaneously firing neuron that has been patched on the array. Individual extracellular spikes are measured on multiple electrodes (colored in black) whenever the patched neuron fires an AP. Figure 3.1b *right* shows the average extracellular spike waveforms on selected electrodes, and the spatial distribution of the STA waveforms, as measured with the array, is depicted in Figure 3.1c. The distribution of STA waveforms represents a cell-specific, extracellular signature of the neurons and will be referred to as *spike-triggered average extracellular action potential* (*STA-EAP)*.

Since many of the patched neurons did not fire spontaneously, fired at very low rates or only in bursts, we routinely applied the following technique for obtaining the STA-EAP of any patched cell. After successfully patching a neuron, a bright-field image of the patched cell
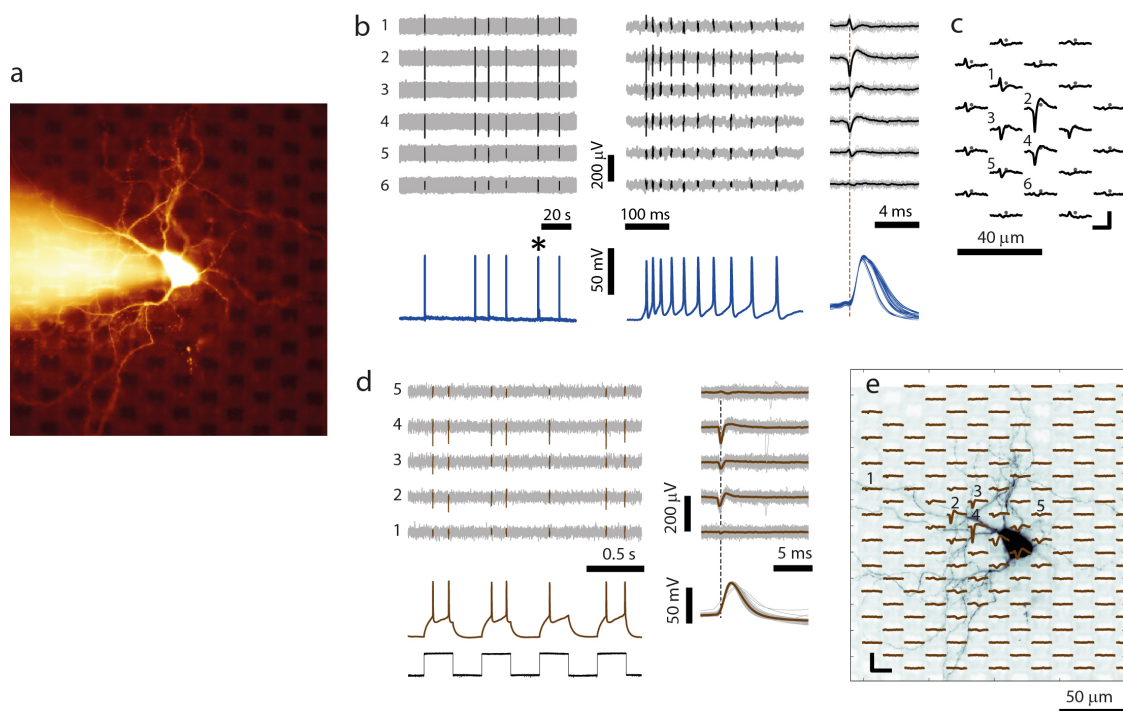

Figure 3.1 Patch-clamping neurons on top of HD-MEAs.

(a) Fluorescence image of a neuron on the array patched in the whole-cell configuration. In the background, the Pt-black electrodes can be seen as black squares. (b) *Left:* Intracellular (*bottom*) and extracellular recordings from six selected MEA electrodes (*top*) of another example neuron. During the two minutes displayed, the neuron spontaneously fired APs in six bursts. *Center:* Close-up view of one individual burst marked with an asterisk. *Right:* superposition of all detected spike waveforms. The black traces represent the spike-triggered average (STA) waveforms. The dashed lines in b and d are aligned to the negative peak of the largest extracellular spike for timing visualization. (c) Spatial distribution of STA waveforms, the gray dots represent the electrode positions. Scale bars: 100 µV and 2 ms. (d) Extracellular and intracellular recordings of the neuron shown in (a). *Left:* APs were evoked by injecting current pulses (100 pA / 250 ms / 2Hz, black signal at the *bottom*), where every pulse evoked 1-2 APs. *Right:* Extracellular and intracellular STA waveforms of the evoked spikes. (e) STA-EAP superimposed to a fluorescence image of the patched neuron (same as in d), showing the location of the recorded extracellular signals with respect to neuron morphology. Scale bars: 100 µV / 5 ms.

was acquired and automatically aligned with the HD-MEA electrode coordinates (see Methods). Electrodes were selected in the area around the patched neuron with a custom MATLAB-based GUI, and electrode configurations were generated, so that each of the selected electrodes could be recorded from. Intracellular current pulses were applied typically at 2 Hz (with the current adjusted to evoke 1-2 APs per pulse, Figure 3.1d *left*), while each configuration was recorded for approximately 30 s. The overall, combined STA-EAP was then computed based on the spike times obtained from the detected APs in the intracellular signal (Figure 3.1d-e).

The method allowed us to obtain a comprehensive mapping of the intracellular signal, the STA-EAP, and the neuronal morphology for any patched cell on the array. Interestingly, as can be seen in Figure 3.1b and e, the STA-EAP was usually not found to be centered at the soma, but to be spatially offset by up to tens of micrometers. Furthermore, the timing of the extracellular spikes was slightly before or at the very beginning of the intracellular AP, which is visualized by the dashed lines in Figure 3.1b and d. These findings are in accordance with the assumption that the largest extracellular signals are located around the axon initial segment (AIS), which features the highest density of voltage-gated sodium channels, and where electrical activity is initialized. In Section 4.3.6 (page 110) of this thesis, immunohistochemistry images of the AIS position relative to the extracted neuronal STA-EAP are shown, which further support our assumption.

3.3.2 HD-MEA Capabilities: Neuronal Network Recording, Axonal Signal Tracking and Direct Stimulation

We have shown (Figure 3.1) that a single neuron is recorded from by multiple electrodes of the HD-MEA. The array resolution and capability to record extracellular signals from different neuronal compartments is further exemplified in Figure 3.2a. Here, the STA-EAP of a neuron at electrodes close to the cell soma (gray circle) and at groups of electrodes along two axonal branches is shown, which have been recorded by using the 'spontanous scan' protocol (see Methods). AP latency (determined by the timing of the negative peak) is indicated by the color code, and the gray dashed line was drawn in order to

visualize axonal propagation. Individual average waveforms at the soma (electrode 1) and along one axonal branch (electrodes 2 to 10) are shown in the inset.
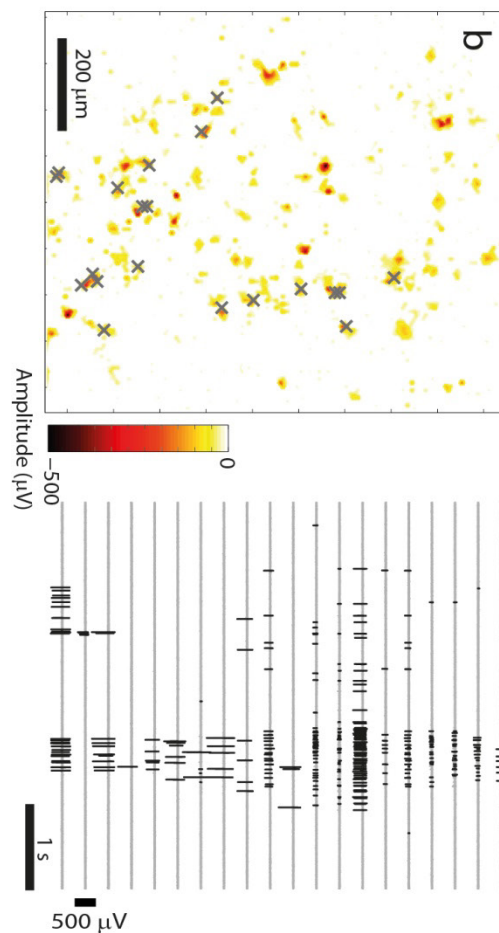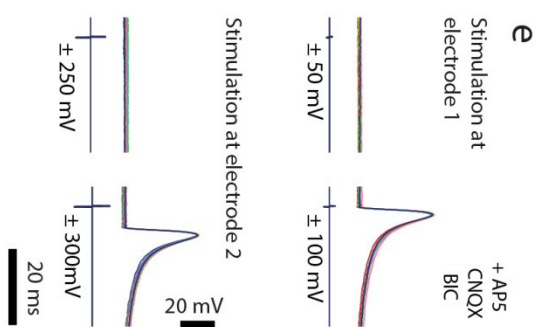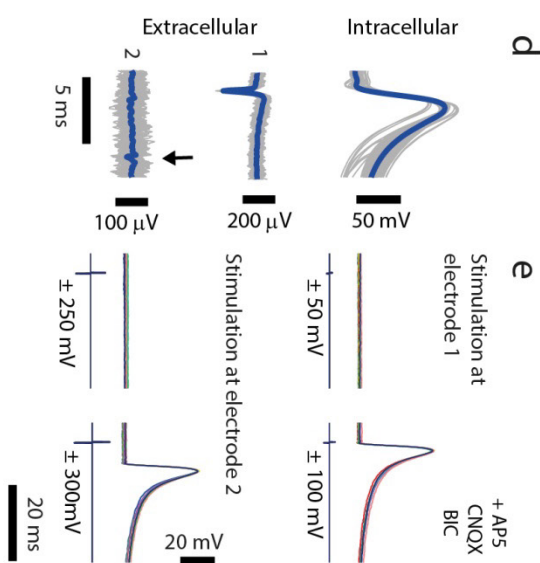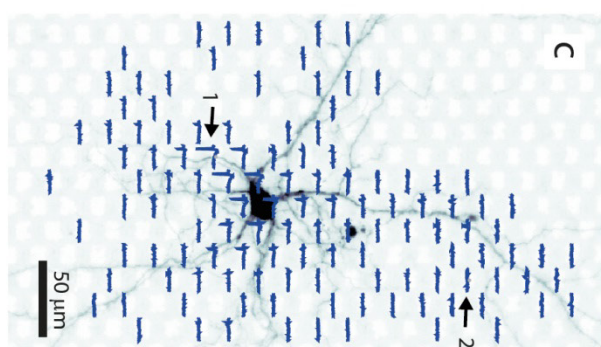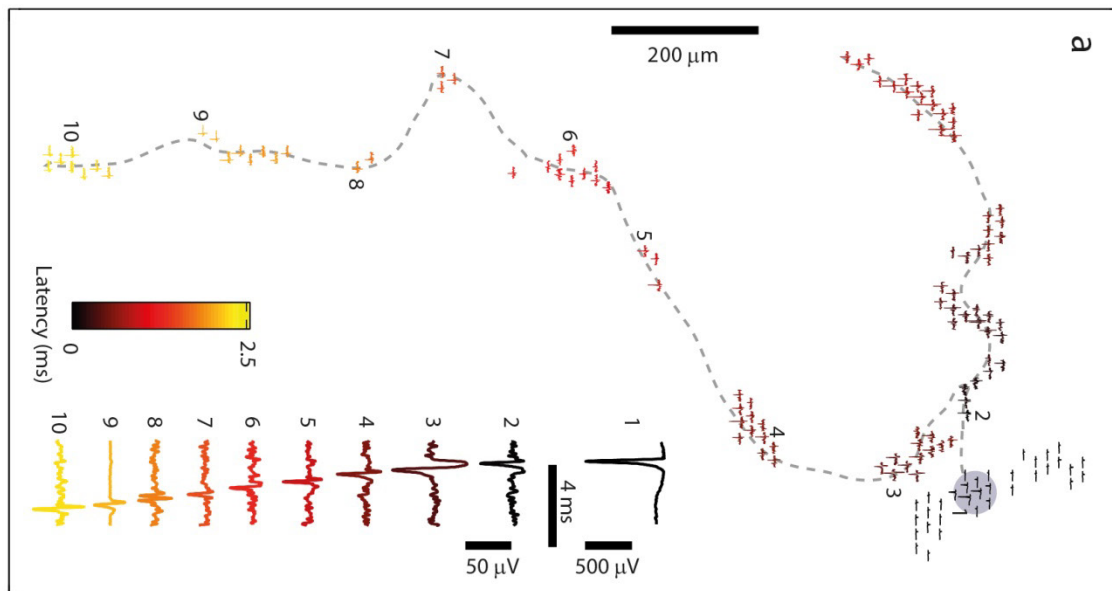
Figure 3.2 Axonal AP propagation recordings, network activity recordings, and direct electrical stimulation of cultured neurons on HD-MEAs.

(a) STA-EAP of a neuron showing a somatic compartment (gray circle), dendritic compartments (black traces above and below gray circle) and axonal waveforms along two identified branches, indicated by the gray dashed lines. Note that the somatic and axonal waveforms are differently scaled for better visualization. Propagation latency of the axonal traces was determined with respect to the timing of the negative peak and is indicated by the color code. The inset visualizes one somatic STA waveform (electrode 1) and STA waveforms along one axonal branch (electrodes 2-10). (b) *Left*: Example of an amplitude signal map of the complete MEA, with the color code indicating the negative peak amplitude of the spikes at each electrode. This map was obtained by scanning the complete array for spontaneous activity with HD-blocks. *Right*: Electrodes with local maxima of spike amplitudes were automatically identified, and electrode configurations were generated to record from these electrodes simultaneously. The plot shows extracellular signals on 20 electrodes (black crosses in the amplitude map), which showed spikes belonging to a network burst. For visualization purposes, spikes exceeding 5 times the signal standard deviation were colored black. (c) Morphology and STA-EAP of a patched neuron on the array. (d) STA of the intracellular signal (*top*), of an electrode with a somatic extracellular signal (*center*, electrode 1) and of an electrode showing an axonal spike after a substantial delay of 5 ms (*bottom*, arrow). The positions of the electrodes are shown in d. (e) Extracellular stimulation of the neuron shown in c-d as verified by intracellular recordings, the stimulus waveform is represented by the blue traces. APs are evoked for amplitudes of ±100 mV but not for ±50 mV, when electrode 1 is stimulated, and for ±300 mV but not for ±250 mV, when electrode 2 is stimulated (10 trials per electrode and voltage). Note that at electrode 1, the AP occurs instantaneously, whereas the AP at electrode 2 appears after a significant delay (5.6 ms). All data in d-f were acquired in the presence of synaptic blockers.

Besides recording from different compartments of individual neurons with many electrodes, we also used the HD-MEA to simultaneously record from many neurons in the network. Figure 3.2b shows the amplitude signal map, which was acquired by scanning the complete array for spontaneous activity with HD configurations, where the color code indicates the negative peak amplitudes at the electrodes. Based on this map, individual electrodes or groups of 2-4 electrodes at locations of large extracellular amplitudes can be selected and configured for simultaneous recording of network activity. An example showing extracellular signals from 20 electrodes containing APs is

illustrated in Figure 3.2b *left*. Due to the limitation to 126 read-out channels, there is a trade-off for the electrode selection while trying to record from multiple cells within a network: On the one hand fewer electrodes per recording position allow to record from more sites and, therefore, from more cells. On the other hand more electrodes per site are advantageous for spike sorting. Typically, three electrodes around sites of significant extracellular amplitudes (> 100 µV peak-to-peak) yielded, in most cases, satisfactory spike sorting results (judged by visual inspection).

Another important HD-MEA capability is the possibility to stimulate at every electrode location on the array. APs can be evoked by stimulating a neuron either near the soma, where the STA-EAP shows large amplitudes, or along its axon. These two types of direct extracellular stimulation are demonstrated in Figure 3.2d-f. A neuron was patched, and, in the presence of synaptic blockers, the STA-EAP was determined by STA, as described in the previous section. At electrode 1, the neuron produced a large-amplitude extracellular signal, whereas at electrode 2, a small axonal AP (arrow in Figure 3.2e) was observed, delayed by 5 ms (determined with respect to the timing of the negative peak). As shown in Figure 3.2f, stimulating electrode 1 led to instantaneously evoked APs, and stimulating electrode 2 evoked APs with a latency of 5.6 ms, which indicates antidromic AP propagation from the stimulation site to the soma.

Electrodes yielding large extracellular signal amplitudes were many times found to be also efficient stimulation sites for evoking neuronal activity. However, as directly evoked APs cannot be recorded with the array nearby the stimulation site due to the stimulation artifact, it is not possible to reliably determine, without additional control measurements, which neurons were stimulated. For this study, electrodes for evoking neuronal activity were selected at sites of large extracellular signals, and, in most cases, we did not control which neurons were activated and whether AIS or axonal stimulation was the case. Characteristics of extracellular stimulation of cultured neurons with HD-MEAs are further investigated in Chapter 4 of this thesis, which provides more detailed experimental results.

3.3.3 Mapping Postsynaptic Signals based on Spontaneous Presynaptic Spikes

The first method to map synaptic input signals exploits the ability of the HD-MEA to simultaneously record from many neurons at high spatiotemporal resolution. Individual neurons were patched in the whole-cell configuration, while the spontaneous activity of cells on the array was recorded by sparsely distributed groups of 2-4 closely spaced electrodes (black dots in Figure 3.3a). By spike sorting the extracellular signals of the electrode groups and correlating the obtained spike times with intracellular membrane potential signals, we identified presynaptic neurons, which were presumably monosynaptically connected to the patched cell. Monosynaptic connections were assumed, in cases where the evoked PSPs were observed with high temporal precision.

Figure 3.3 illustrates this approach with two examples of patching neurons one after the other on the same HD-MEA chip. The positions of the patched cells are indicated in Figure 3.3a in the background and by the pipette drawings. For the first patched neuron ('post A'), two presynaptic cells (blue and green) were identified, which caused EPSPs after every presynaptic spike. Spikes of a third cell (red), which did not cause PSPs, were also included in the Figure. Figure 3.3b-c show individual presynaptic spikes and recorded PSPs during spontaneous activity. To better visualize the mapping between PSPs and presynaptic APs, the intracellular signals immediately after spikes of the blue and green neuron were colored accordingly in Figure 3.3c *top*. Figure 3.3c *top center* shows, how individual EPSPs superimpose during spontaneous activity, and the presence of other EPSPs (indicated by black arrows) for which the presynaptic cells were not identified.

Spike-triggered average postsynaptic potentials (STA-PSPs) were computed by averaging the intracellular MP values, based on the presynaptic spike times of sorted neurons, and represent a measure of the synaptic connectivity from respective presynaptic cells to the postsynaptic cell. Figure 3.3d shows the STA presynaptic extracellular signals and Figure 3.3e shows the resulting STA-PSPs. During bursts of network activity, the patched cell was in a depolarized state, making it difficult to detect individual PSPs during these periods. Therefore, to

calculate the average PSPs, only traces that started at a MP value close to the holding potential were used (black traces in Figure 3.3e). All other PSP traces following presynaptic spikes, for which the patched neuron was in a depolarized state, are colored gray in the bottom plot
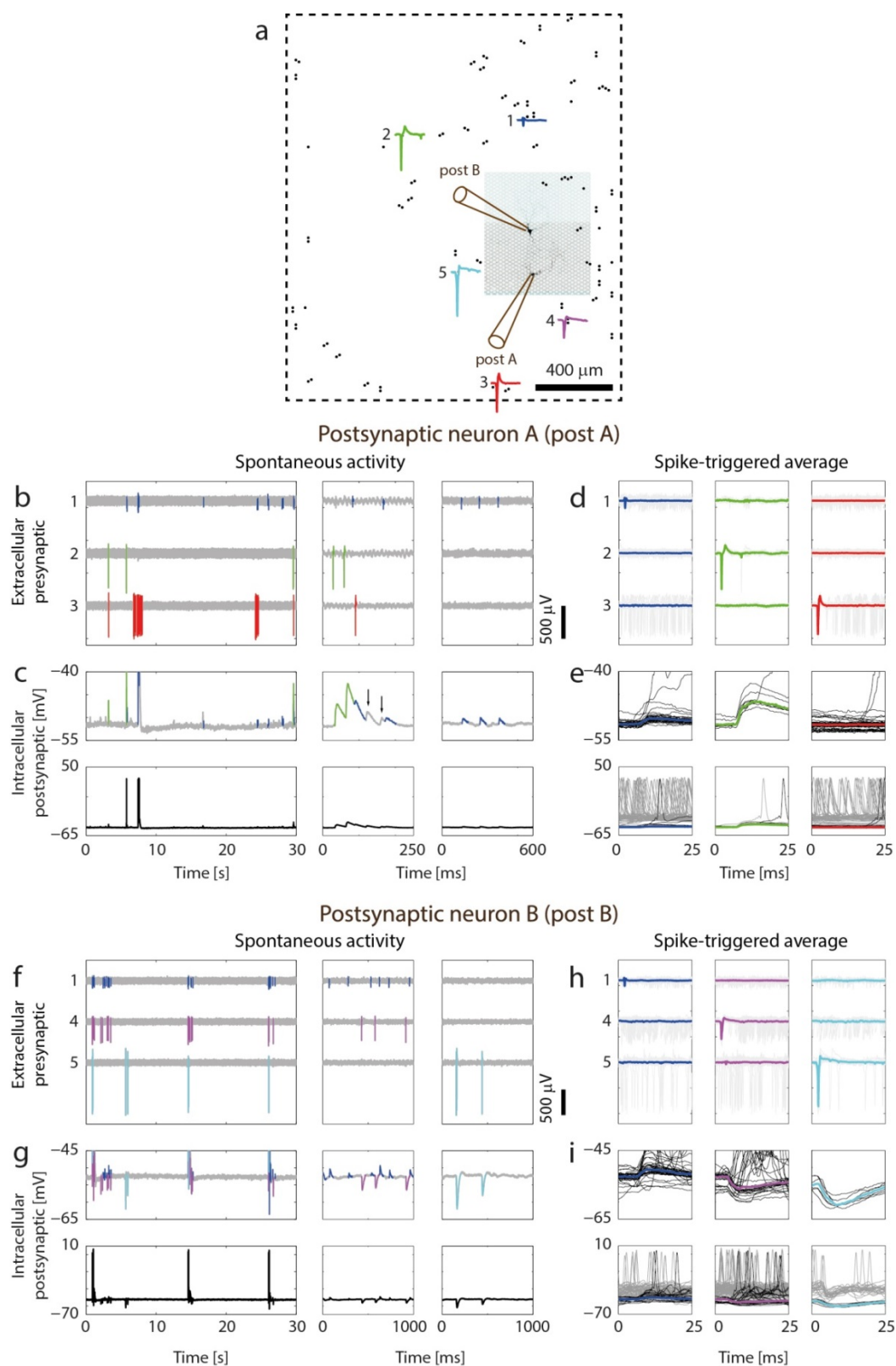
Figure 3.3 Mapping excitatory and inhibitory intracellular postsynaptic signals to extracellular HD-MEA recordings of spontaneous activity.

(a) Visualization of the array area (dashed box). Two neurons (post A and post B, fluorescence image in the background) were consecutively patched on the array, while spontaneous extracellular activity was recorded by sparsely distributed electrodes (black dots). Numbers and colored STA waveforms indicate positions and identities of identified presynaptic neurons in b-i. (b) 3 data segments with different time scales (*left, center, right*) of recorded extracellular data from 3 electrodes (electrode positions 1, 2, 3 as labeled in a). Spikes from 3 neuronal units were sorted and colored, where the blue and the green neuron were identified as presynaptically connected to the patched neuron A, while the red neuron was not. (c) *Top*: Intracellular recordings from postsynaptic neuron A. The signal trace after spikes from the blue and green neuron was colored, visualizing excitatory PSPs originating from these two neurons, as determined by PSP averaging in d. Note the summation of the synaptic events in the center plot, and note that two additional EPSPs were measured, which did not originate from the blue or green neurons (black arrows). *Bottom*: The same signal displayed with a larger amplitude range so that also postsynaptic APs can be seen. (d) Spike-triggered average of the extracellular spikes extracted from a total of 2.5 minutes of recorded data (individual traces: light gray; averaged waveforms: colored lines). (e) *Top*: Intracellular postsynaptic traces for the spikes of the colored neurons. Only traces that started from a baseline MP value (i.e. did not exceed -48 mV during the first 5 ms) are shown here. Note that the blue and the green neurons evoked EPSPs of different magnitude, and that no PSPs were seen following spikes of the red neuron. The colored waveforms show the median MP trace. *Bottom*: The same traces on a wider MP range. Additionally, traces which were recorded at depolarized state (exceeding -48 mV during the first 5 ms) are plotted in gray. (f) – (i) Equivalent plots for postsynaptic neuron B. In this example the violet and the cyan neurons (4 and 5 in a) evoked inhibitory PSPs (IPSPs) of different magnitudes, whereas the blue neuron (1 in a) evoked EPSPs. Note that the blue presynaptic neuron is the same than the one for post A. Spikes in f and h were extracted from 6 minutes of recorded data.

of Figure 3.3e. For stimulations of the blue and red presynaptic neurons, elicited postsynaptic APs interfere with many of these PSPs.

PSP mapping according to spontaneous activity for the second cell ('post B') is shown in Figure 3.3f-i. For this postsynaptic cell, one excitatory and two inhibitory presynaptic cells were identified, whereat the blue excitatory presynaptic neuron was the same as identified for first patched cell ('post A'). EPSPs and IPSPs co-occurred

spontaneously (Figure 3.3g), and the STA-PSPs could be computed for the inhibitory as for the excitatory inputs (Figure 3.3i). For all presynaptic neurons in Figure 3.3b-i, the relative positioning and the average extracellular spikes are plotted in Figure 3.3a.

Since averaged PSPs represent a precise estimate of the synaptic input strength, they can be used to compare and judge other estimates of functional connectivity. We performed, prior to the patch clamp recordings, recordings of the spontaneous network activity inside the incubator. Out of 30 minutes of activity, spike times of the three presynaptic neurons in Figure 3.3b-e were extracted by manual spike sorting, as well as the spike times of the postsynaptic cell ('post A') by using signals from two electrodes underneath that neuron (Figure 3.4a-b). Information about the firing dynamics is captured by these spike times, visualized in Figure 3.4c-d. Correlated activity due to bursting dynamics was found for the blue, the red, and the postsynaptic (brown) neuron, as is evident from temporally correlated peaks of the firing rates over time in Figure 3.4d. The green neuron fired uncorrelated from the other cells and, more specifically, showed non-spiking periods when the other neurons were bursting.

Next, the cross-correlograms between the blue, green, respectively red neuron and the brown postsynaptic neuron were computed (Figure 3.4e). The blue and red neurons showed correlation peaks centered close to zero, with slow decays along hundreds of milliseconds, and their correlation curves featured similar, slightly asymmetric shapes. These correlations are presumably caused by correlated bursting activity, even though the asymmetric shape suggests more complex underlying network dynamics that regulate the firing activities. Although the blue neuron was identified as synaptically connected and the red one was identified as not synaptically connected to the patched cell, the correlation curves did not show significant differences. These measurements demonstrate the difficulties of using spike cross-correlations as a measure for functional connectivity, especially in the case of correlated bursting in the network.
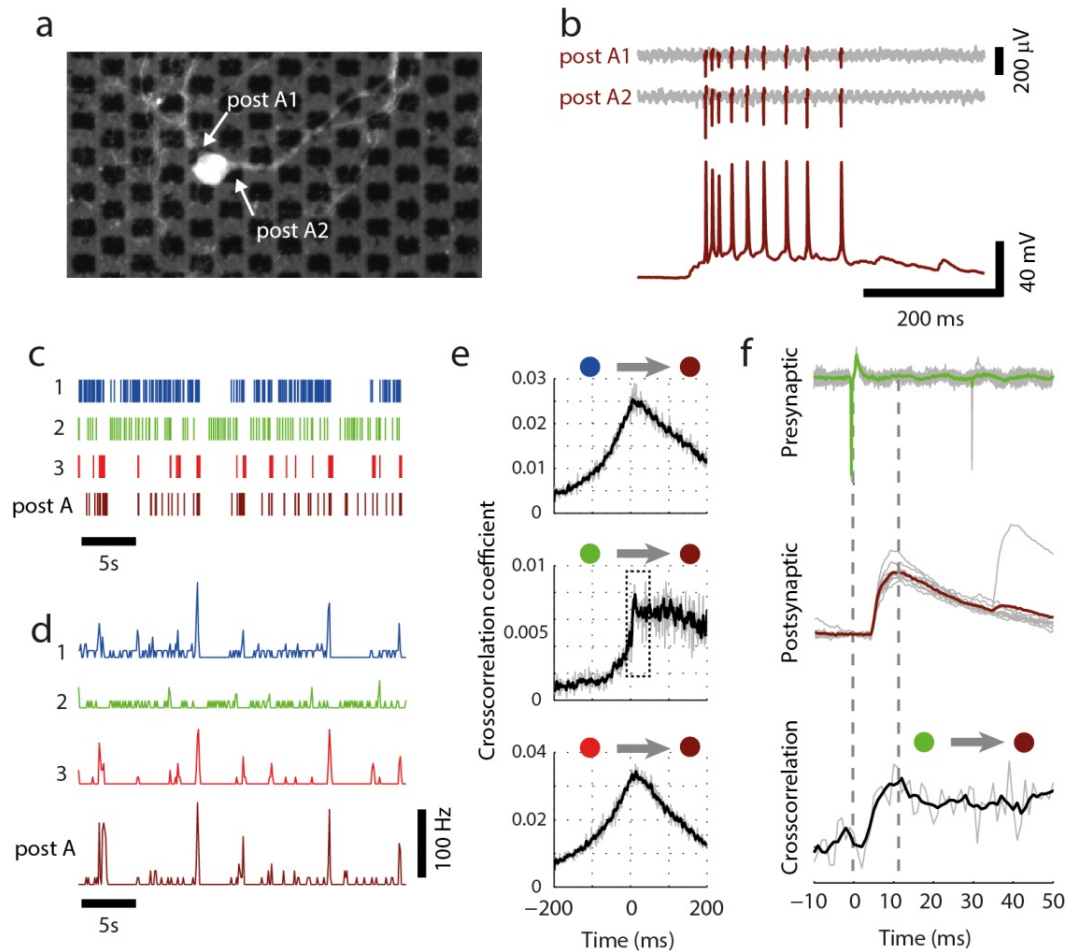
Figure 3.4 Comparison between mapped synaptic connections and correlations in spontaneous activity.

(a) Fluorescence image of the postsynaptic neuron A from Figure 3.3, with the arrows pointing on two electrodes that recorded from the patched cell. (b) Intra- and extracellular recordings showing that the selected electrodes (post A1 and post A2) recorded spikes from postsynaptic neuron A. (c) Raster-plots showing spike times of the 3 presynaptic neurons in Figure 3.3b and the postsynaptic neuron. The extracellular data were recorded in the incubator prior to the patch clamp experiment. Out of 30 minutes of recorded spontaneous activity, spikes from 30 seconds are displayed. (d) Firing rates over time for the data shown in c. The bin size was set to 100 ms. (e) Cross-correlograms (gray: raw data, black: smoothed data) between presynaptic (blue, green, red neuron) and postsynaptic spikes (1 ms bins). From 30 minutes recording 13062, 6491, 12663, and 4977 spikes for the blue, green, red, and brown (postsynaptic) neurons were extracted and used. (f) *Top:* Extracellular traces and average presynaptic spike waveform of the green neuron, centered at 0. *Center:* Intracellular traces and average PSPs recorded at the postsynaptic cell for spikes of the green neuron. *Bottom:* Segment of the cross-correlogram surrounded by the dashed rectangle in e.

The cross-correlation of spike times between the green presynaptic and the postsynaptic neuron showed a more asymmetric distribution, which was attributed to the non-spiking periods of the green neuron when the other cells bursted. Figure 3.4f shows a direct comparison between the average PSPs evoked by the green at the brown neuron, as derived in Figure 3.3e, and the cross-correlation curve derived from spontaneous spikes. The presynaptic spike (*top*) is centered at zero, and the average PSP (*center*) shows the timing of the synaptic excitatory signal with respect to the presynaptic spike. The cross-correlation curve (*bottom*), extracted from the dashed rectangle in Figure 3.4e, exhibits a peak, which temporally matches with the peak of the STA-PSP. This example illustrates how the presented method can be used to establish a comparison between mapped postsynaptic signals and connectivity estimates.

3.3.4 Stimulation-triggered Postsynaptic Potentials

The number of mapped synaptic connections for the method presented in the previous section strongly depends on the characteristics of the spontaneous activity. Presynaptic neurons with tonic firing can be mapped more easily, whereas neurons featuring a high degree of activity that is correlated to that of the postsynaptic neuron or other neurons are difficult to map.

In order to increase the number of presynaptic cells for which the average PSP could be determined, we investigated strategies for stimulation-evoked PSP mapping. In Figure 3.5, examples are shown for detecting postsynaptic signals by stimulating presynaptic neurons through the HD-MEA for the cases of excitatory and inhibitory presynaptic cells.

Figure 3.5a shows the morphology of a patched neuron and the position of the electrode (circled, black x) used for electrical stimulation with biphasic voltage pulses. A ±50 mV pulse did not evoke any response, as depicted in Figure 3.5b (gray: ten individual traces, blue: median MP signal). For stimulations with ±100 or ±150 mV, single and presumably monosynaptic PSPs were measured at the patched neuron. When the stimulation amplitude was further increased to ±200 mV, some trials showed PSPs with higher activation, indicating that multiple presynaptic cells were simultaneously activated.

Stimulation pulses of ±250 mV finally evoked additional presynaptic sites, resulting in suprathreshold synaptic signals, which caused the postsynaptic neuron to fire APs for most trials. The postsynaptic signals were completely blocked by the addition of synaptic blockers (APV, CNQX and BIC).
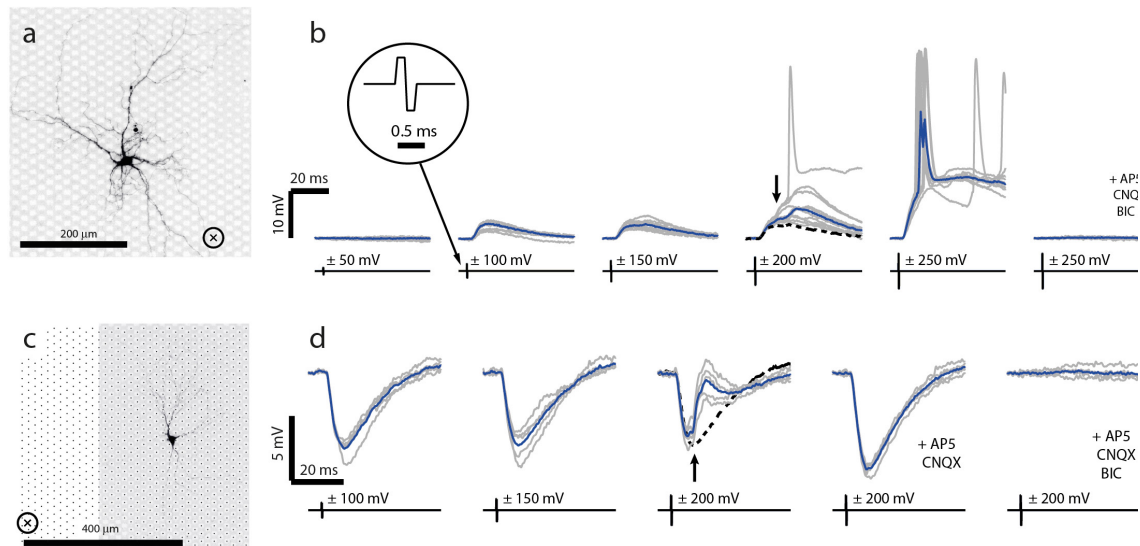

Figure 3.5 Evoking postsynaptic signals through HD-MEA electrical stimulation.

(a) Fluorescence image of a neuron patched on the array, the circled x indicates the position of the stimulating electrode. Note the relative proximity between the stimulation electrode and the neuronal dendritic processes in this example. (b) Stimulating voltage pulses with increasing amplitudes. Stimulation waveforms at the bottom and evoked intracellular responses at the top (10 individual traces in gray, median response in blue). The inset shows a single biphasic voltage pulse. A presynaptic neuron was evoked with stimulation amplitudes of ±100 and ±150 mV leading to PSPs. Increasing the amplitude to ±200 mV resulted in additional PSPs for some trials (indicated by the black arrow, the dashed line represents the median response for ±150 mV pulses). Yet larger PSPs were seen for ±250 mV, along with evoked postsynaptic APs in most of the trials. Addition of synaptic blockers resulted in complete blockade of any evoked signals, indicating that all observed responses involved synaptic transmission. (c) Image of a different neuron (postsynaptic neuron B in Figure 3.3) and positioning of the stimulation electrode. Each black dot represents the position of a MEA electrode. (d) PSPs from an inhibitory presynaptic neuron were triggered by stimulating at ±100 and ±150 mV. An additional excitatory presynaptic neuron was evoked at ±200 mV (black arrow, dashed line represents the median response for ±150 mV). Application of excitatory blockers blocked the EPSPs at ±200 mV, whereas addition of BIC completely blocked all responses.

The second example in Figure 3.5c-d shows an inhibitory postsynaptic response to electrical stimuli, evoked with ±100 mV and ±150 mV pulses at the electrode indicated in Figure 3.5c. Increasing the stimulation amplitude to ±200 mV additionally activated a second, excitatory neuron that evoked EPSPs, which then superimposed to the IPSPs (indicated by the black arrow). The EPSPs were suppressed upon adding APV and CNQX (AMPA and NMDA receptor antagonists) to the bath solution. Further addition of BIC, a selective GABA$_A$ antagonist, also blocked the initial IPSPs.

3.3.5 Identification of and Measuring from Multiple Presynaptic Inputs

Based on the measurements shown in Figure 3.5, a suitable strategy to obtain stimulation-evoked, monosynaptic PSPs from individual neurons is to stimulate electrodes at different voltages and to then select the lowest voltage, for which PSPs are evoked reliably. Figure 3.6 illustrates the steps performed in order to identify stimuli which activated individual distinct presynaptic cells. Electrodes with large negative signal peaks were identified based on spontaneous
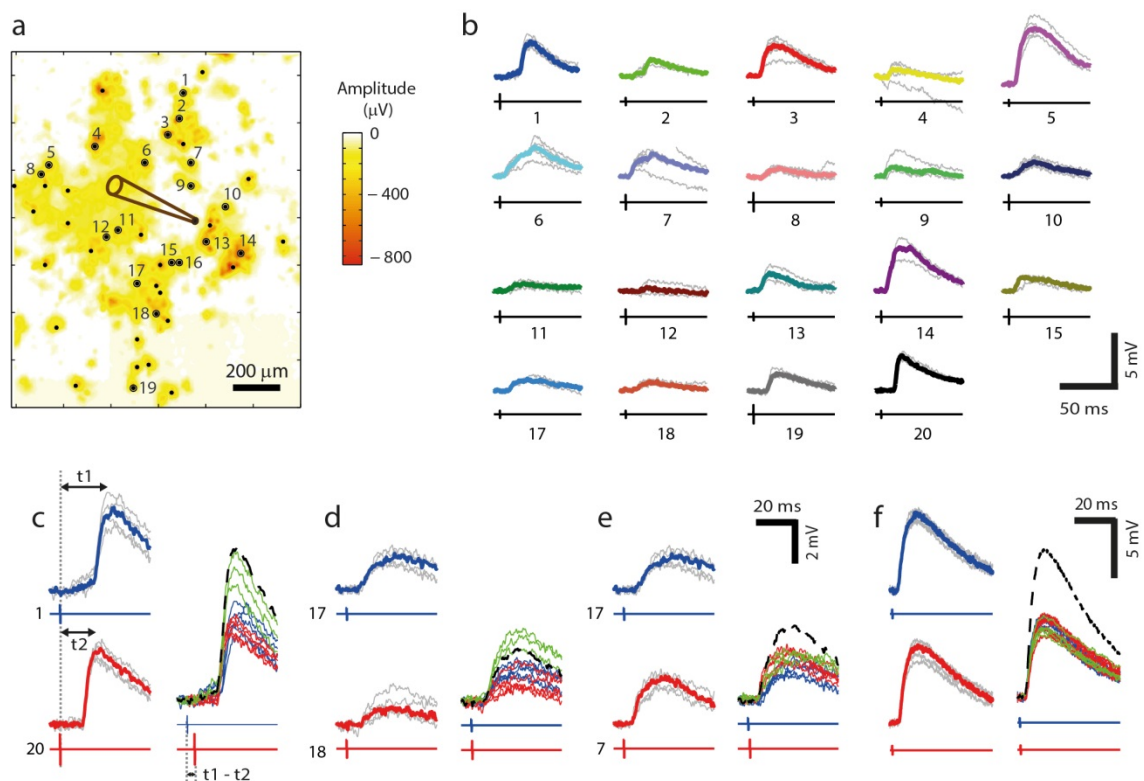
Figure 3.6 Stimulation-triggered PSP from multiple presynaptic inputs.

(a) Amplitude signal map of a MEA region, with the color code indicating the negative peak amplitude of the spikes at each electrode. The position of the patched cell is visualized by the brown pipette drawing. Electrode locations were selected according to large negative peaks in the amplitude map (depicted as black dots) and stimulated with voltage pulses of ±100, ±150, ±200 and ±250 mV. Small dots mark electrodes that did either not evoke any PSP response or could not be attributed to individual monosynaptic PSPs, and large dots mark electrodes for which stimulation yielded individual PSPs. (b) PSP responses (gray: individual traces; colored: median trace) for stimulation at numbered electrodes in a, where the lowest PSP-evoking stimulation amplitude was chosen for every electrode. The stimulation signal timing and amplitude are visualized by the black signals below the PSPs. (c) *Left*: PSPs and stimulation waveform for electrodes 1 and 20 in b, which exhibited similar signal amplitudes but different latencies (t1, t2: time between stimulation pulse and PSP maximum). *Right*: Paired stimulation for electrodes 1 and 20, where the timing between the two stimuli was t1 − t2 = 3.65 ms. The green traces show responses to paired stimulation, and red, respectively blue traces display the PSP responses to individual stimuli shown *left*. The responses to paired stimulation (green) showed clearly larger amplitudes than the responses to individual stimuli, suggesting that the PSPs obtained through stimulation at electrodes 1 and 20 originated from two different presynaptic inputs. The black dashed line visualizes the theoretical sum of individual average PSP responses. (d) Second example showing responses to paired stimulation that are significantly larger than responses to individual stimuli, thus indicating two different presynaptic sources. (e) Example where paired stimulation responses do not show larger amplitudes than responses to individual stimuli, indicating that stimulation of electrodes 17 and 7 activated the same presynaptic neuron. Note the large spatial distance between the two electrodes in a. (f) Example from another dataset, where two individual PSP responses originated from a single presynaptic neuron.

activity recordings from the complete array ('spontaneous spike map', see Methods), as shown in Figure 3.6a by all black dots. The electrodes were stimulated with different amplitudes (±100 − ±250 mV, 5 trials per amplitude and electrode) in randomized order.

Stimulation at some electrodes evoked postsynaptic signals in the patched neuron, and a subset of individual electrodes could be identified (numbered black dots in Figure 3.6a, traces in Figure 3.6b), which reliably yielded PSPs. Each PSP presumably originated from individual stimulated presynaptic neurons displaying a monosynaptic

connection to the patched cell. As described in Section 3.3.2, neurons can be stimulated at different sites close to the soma and along the axon. Furthermore, axons may grow across large distances on the array, as shown in Figure 3.2a. Therefore, it cannot be ruled out that an individual presynaptic neuron can be activated by multiple electrodes. For investigating interactions between multiple synaptic inputs, however, it is necessary to identify and measure distinct inputs. We controlled for the identity of the synaptic inputs by applying paired presynaptic stimulation (Royer and Paré, 2003).

PSPs with similar amplitudes were stimulated in combination, where individual stimuli timings were adjusted so that the maxima of both PSP traces would occur simultaneously (Figure 3.6c). In cases where PSPs were originating from distinct presynaptic cells, the individual PSPs summed up, and the measured synaptic signals resulting from paired presynaptic stimulation were significantly larger than the individual PSP signals (synaptic inputs in Figure 3.6c-d). Figure 3.6e-f shows two examples, where the PSPs evoked from stimulating different electrodes originated from the same presynaptic neuron. Such stimulations of individual presynaptic neurons by two electrodes were also seen for electrodes with large spatial distances, as in the case of Figure 3.6e.

3.3.6 Reconstructing the Dynamics of Pre- and Postsynaptic Transmission

It was shown in Figure 3.2a how axonal signals of individual neurons can be recorded at hundreds of electrode locations by HD-MEAs. These axonal signals provide information about the axon positioning and about the AP timing along the axon. The cross points between a presynaptic axonal signal and the dendritic morphology of a correspondent postsynaptic neuron, can be used to estimate putative synaptic locations. Figure 3.7 visualizes this concept for the presynaptic neuron recorded at electrode 5 in Figure 3.3 and the postsynaptic neuron ('post B'). The complete STA-EAP of the presynaptic neuron had been identified during spontaneous activity recordings ('spontaneous scan', see Methods) in the incubator prior to the patch clamp experiment. In Figure 3.7a-b, the latency of the extracellular presynaptic APs including its propagation along two

axonal branches, as recorded by the array, is indicated by the color code of the electrodes and superimposed to an image of the postsynaptic neuron. The region where the presynaptic axonal signal crosses the postsynaptic apical dendrites is shown in Figure 3.7b and the positions of the active synapses between the two neurons are likely to be found in that region. In Figure 3.7c, extracellular STA waveforms of the presynaptic neuron at selected electrodes (black rectangles in Figure 3.7a) are shown on the *top*, whereas the average inhibitory PSP is plotted on the *bottom*. In this example, a significant delay between the timing of the axonal presynaptic AP (at electrode 4 in Figure 3.7c) and the actual PSP onset was found in the range of 2 ms.
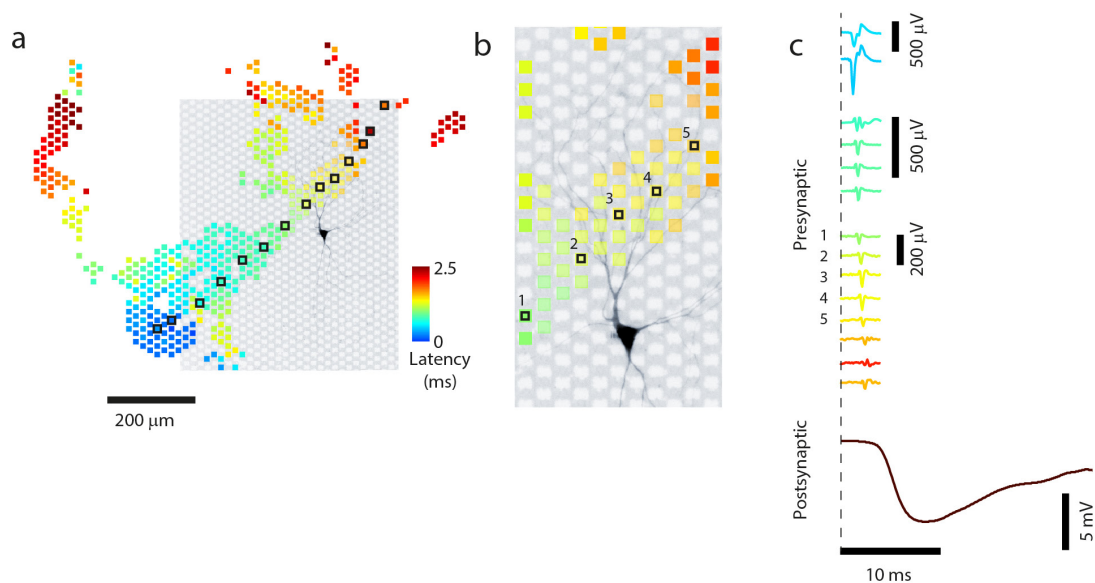

Figure 3.7 Combining signals of a propagating presynaptic AP and an evoked IPSP.

(a) Fluorescence image of a patched neuron and AP propagation timing along the axonal arbor of an identified presynaptic cell. Electrodes featuring spikes in the STA STA-EAP were colored, and the color code indicates AP latency based on the timing of the negative peak. The soma of the presynaptic cell is at the bottom left in the blue-colored electrode area. (b) Close-up of the region, where the presynaptic extracellular axonal signal passes over the postsynaptic apical dendrites. (c) *Top*: Individual STA waveforms obtained from the electrodes marked by black rectangles in a. The numbering of the waveforms corresponds to the numbering of the electrodes in b. *Bottom*: Average IPSP as evoked by the presynaptic cell.

85

3.4 Discussion

Cortical pyramidal neurons typically receive inputs from a few thousands of synapses (Kandel et al., 2000). Therefore, a characterization of the functional properties of combined synaptic inputs from multiple presynaptic cells appears to be fundamental to a better understanding of mechanisms and working principles of neuronal networks. However, methods are needed to measure and to evoke synaptic signals that originate from multiple presynaptic cells. In this paper, we combined the techniques of extracellular HD-MEA stimulation/recording and intracellular patch clamp recording and presented two methods for identifying multiple presynaptic inputs to individual neurons in culture.

The first method uses the HD-MEA chip to simultaneously record spiking activity of many cells, while an individual neuron is patched. The spike times of extracellularly recorded neurons are then sorted and used to calculate STA-PSPs. Since this measurement does not interfere with the intrinsic neuronal activity, it is a suitable approach to observe interactions and summation properties of multiple spontaneous excitatory and inhibitory inputs that produce PSPs, as well as to monitor spontaneous plasticity effects. Another advantage of this method is that the presynaptic neurons can be identified based on their STA extracellular waveforms. As shown in Figure 3.4, the STA-PSPs can be then compared to an estimate of the functional connectivity, which was derived from the presynaptic and postsynaptic spike times only. The STA-PSPs can thus serve as ground-truth data for evaluating and improving methods to estimate functional connectivity based on spike times.

A difficulty of PSP-mapping, based on spontaneous activity, is the requirement of spontaneous, non-synchronous activity. Typically, cultures of dissociated cortical neurons oftentimes show a high degree of synchrony and collective bursting activity. During network bursts, the postsynaptic cell is in a depolarized state so that individual PSPs cannot be properly measured. The use of voltage clamp recording instead of current clamp may help to reduce this problem.

In the second method presented here, neuronal APs were evoked by extracellular voltage stimulation through the HD-MEA electrodes,

while the intracellular signal of an individual neuron was recorded. The stimuli were applied on preselected electrodes at different amplitudes, allowing us to identify stimuli that reliably evoked PSP from individual presynaptic cells. This method represents a fast approach, as the patterned stimuli can be programmed arbitrarily, and no spontaneous activity is required. Effective voltage stimuli always evoked single APs at high temporal precision, which is an advantage of electrical stimulation over optical stimulation techniques. The HD-MEA can, once a set of stimuli to evoke PSPs has been identified, be programmed to apply any pattern of stimuli. Therefore, the method allows for conducting a wide range of electrophysiological experiments, which involve the activation of multiple presynaptic cells at high spatiotemporal precision.

Both presented methods for measuring PSPs in spontaneous and evoked activity do not exclude each other, but could be also used in a complementary way. The spontaneously recorded inhibitory presynaptic neuron at electrode 5 in Figure 3.3f-i, for example, was the same as the one evoked in Figure 3.5c-d by stimulation. Therefore, the capability of HD-MEAs of recording and stimulating at the same electrodes could also allow for performing experiments that combine spontaneous and evoked activity. In such an experiment, the synaptic properties of multiple identified presynaptic neurons could be characterized (e.g. by paired-pulse stimulation) or manipulated (e.g. plasticity protocols) by using stimulation through HD-MEA electrodes. Subsequently, combined spontaneous recordings of presynaptic extracellular and postsynaptic intracellular activity could be performed. This experiment would allow for investigating how measured or manipulated synaptic properties of multiple presynaptic neurons affect intrinsic neuronal activity.

Furthermore, we have shown in Figure 3.7 that the presynaptic axonal signal combined with the postsynaptic morphology and the PSP, can be used to identify the putative positioning of synapses between two neurons. Paired patch clamp recordings generally allow to record the time between a presynaptic somatic AP and its evoked PSP on a second neuron (Boudkkazi et al., 2007). Experiments, as the one presented in Figure 3.7, allow to also measuring the timing of the presynaptic AP at the axon in the region of the putative synapses. Such

experiments may provide more insights into the precise timing of synaptic transmission.

CHAPTER 4 Highly Localized Extracellular Stimulation of Cultured Cortical Neurons using High-density Arrays of Subcellular-size Microelectrodes

David Jäckel[1§], Milos Radivojevic[1§], Douglas Bakkum[1], Jan Müller[1], Thomas Russel[1], Felix Franke[1], Urs Frey[2], and Andreas Hierlemann[1]

1 ETH Zurich, Department of Biosystems Science and Engineering, 4058 Basel, Switzerland

2 RIKEN, Quantitative Biology Center, 650-0047 Kobe, Japan

§ contributed equally.

Abstract

Measuring and manipulating neuronal activity within complex networks is important for a wide range of electrophysiological experiments. Over the last decade, novel high-density microelectrode arrays (HD-MEAs), based on complementary metal oxide semiconductor technology, have been developed. Featuring large numbers of readout channels and high electrode densities, HD-MEAs allow for recording extracellular activity of large numbers of neurons at subcellular resolution. Devices that additionally include stimulation circuitry also have the potential to selectively stimulate neurons by targeting them through the optimal electrode location. In this study, the effects of HD-MEA stimulation on cultured neurons were investigated by using a combination of intra- and extracellular recording and optical imaging. While many stimulation electrodes in different locations could be used to evoke activity of individual neurons, the somatodendritic neuronal compartment was identified as a region of low excitability for extracellular stimulation. In contrast, electrode array regions in which large extracellular neuronal signals were measured, were also comparably efficient in exciting the respective neurons through subsets of electrodes. Immunohisto-chemical imaging was combined with extracellular spontaneous recordings to map the exact location of recorded extracellular signals to the respective neuronal morphology. Our findings indicate that the largest extracellular signals of cultured neurons on HD-MEAs can be recorded at the axonal initial segment (AIS), an area of high neuronal excitability. Therefore, the region with large extracellular signals is highly suitable for targeted stimulation of identified neurons.

4.1 Introduction

The ability to measure and to manipulate the activity of large numbers of neurons in complex networks is key to performing a wide range of electrophysiological experiments aimed at revealing network mechanisms and dynamics. Planar microelectrode arrays (MEAs) are 2D arrangements of metal electrodes on a substrate and represent a promising technique for measuring and stimulating many cells simultaneously. The combined recording and stimulation capabilities of MEAs have been used to investigate, e.g., learning effects, induced by repetitive stimulation (Shahaf and Marom, 2001), long-term dynamics of neuronal excitability (Gal et al., 2010) and plasticity of axonal propagation (Bakkum et al., 2008). The associated studies relied on cultures of dissociated primary neurons as model system, which have shown to remain stable under experimental conditions for up to weeks or months (Wagenaar et al., 2006; Gal et al., 2010). Furthermore, the non-invasive nature of the MEAs allowed for conducting electrophysiological recording and stimulation experiments over extended time scales. Another important feature of MEAs is the high temporal resolution, which allows for extraction of precise spike times, as well as for evoking activity in a temporally precise and reproducible way through electrical stimuli.

In the studies cited above, traditional "passive" MEAs were used, which typically featured 50-200 electrodes, arranged at center-to-center distances of 100–200 μm. The relatively large distances between the electrodes impose limitations on both recording and stimulation capabilities. Concerning the recordings, large distances between neighboring electrodes enable only a small subset of cells to be measured, namely the neurons close to the respective electrodes. With respect to stimulation capabilities of passive MEAs, it has to be noted that neurons are typically stimulated at the location of the axon, which evokes antidromic propagation of action potentials (APs) that are then detected close to the soma, where the extracellular AP features the largest signal-to-noise ratio (SNR). Therefore, mainly the effects of antidromic stimulation can be detected and the possibility to target individual cells is limited.

Over the last decade, "active" MEAs based on complementary metal oxide semiconductor (CMOS) technology have been developed (Eversmann et al., 2003; Berdondini et al., 2005, 2009; Hutzler et al., 2006; Frey et al., 2010; Ballini et al., 2014). These devices feature addressing and signal conditioning circuitry on the same chip and provide much larger electrode densities. For the recording capabilities, three major advantages result from the high spatial electrode density:

1. Center-to-center electrode distances in the range of 10-20 µm allow for recording from many, or potentially all cells on the HD-MEA, as every neuron is in close proximity to several electrode. This feature has been exploited to, e.g., estimate functional connectivity in neuronal cultures (Maccione et al., 2012), to record from defined populations in the retina (Fiscella et al., 2012), and to characterize activity waves in retinae (Maccione et al., 2014).

2. Due to the closely spaced microelectrodes, activity of individual neurons is always measured by multiple electrodes. This allows for recording from different compartments of individual cells (Zeck et al., 2011; Bakkum et al., 2013).

3. It has been shown that recording extracellular signals of individual neurons with multiple electrodes greatly improves spike sorting performance (Gray et al., 1995; Einevoll et al., 2012; Fiscella et al., 2012).

A high electrode density also entails substantial advantages for stimulating neurons. First, many if not all neurons can be targeted. Moreover, individual neurons can be stimulated at different sites, allowing for optimization of stimulation by finding the most effective electrode. Effective and selective stimulation with two devices incorporating densely arrayed, sub-cellular-size electrodes has been demonstrated for cultured neurons (Braeken et al., 2010; Lei et al., 2011). These devices, however, only featured stimulation, but no recording capabilities. Therefore, it was not possible to correlate measured neuronal signals to locations of stimulation electrodes.

HD-MEAs featuring both recording and stimulation circuitry (Frey et al., 2010; Eversmann et al., 2011; Ballini et al., 2014) enable measuring and stimulating neuronal activity at high spatiotemporal resolution.

Some HD-MEA devices allow recording and stimulating neurons with the same electrodes. They can be therefore used to record extracellular AP waveforms of individual neurons at specific electrodes and to apply electrical stimuli at those electrodes, in order to find the most effective position to stimulate identified neurons. Such non-invasive, targeted stimulation in combination with the recording capabilities makes HD-MEAs a unique tool for long-term experiments, in which individual neurons can be selectively stimulated and recorded at single-spike resolution.

In this study, we investigated the effects of extracellular voltage stimulation on cultured cortical neurons that were grown on HD-MEAs. The high spatial electrode density allowed for stimulating a certain individual neuron through different sites. We applied a combination of techniques including extracellular HD-MEA recordings, intracellular patch clamp recordings and optical imaging in order to address the following questions:

1. Which intracellular effects are caused by extracellular stimulation?

2. Which are effective sites for stimulating cultured neurons by means of HD-MEA electrodes? Moreover, can the extracellular waveforms of the identified neurons, as recorded by the multiple electrodes, be used to determine the most effective stimulation site?

4.2 Methods

4.2.1 HD-MEA system

A CMOS-based HD-MEA system, fabricated in a 0.6-µm CMOS 3M2P process (Frey et al., 2009, 2010) was used for extracellular neuronal recording and stimulation. The electrode array is integrated into a microsystem chip and features a total of 11,011 electrodes in an area of 1.99 x 1.75 mm^2 (17.8 µm center-to-center pitch, 3'161 electrodes/mm^2 density, 8.2 x 5.8 µm^2 electrode size). Up to 126 electrodes can be simultaneously recorded from, by connecting the electrodes to read-out channels through a flexible switch matrix underneath the electrode array. The switch-matrix approach provides

low-noise recordings (7-9 μV_{rms}) and high routing flexibility to select almost arbitrary electrode configurations. Furthermore, up to 42 electrodes can be stimulated simultaneously by connecting them to stimulation channels. Two digital-to-analog (DAC) converter units provide arbitrarily selectable stimulation waveforms (max. 20 kHz) to the stimulation channels.

On-chip circuitry is used to amplify (0-80 dB programmable gain), filter (high pass: 0.3-100 Hz, low pass: 3.5-14 kHz), and digitalize (8 bit, 20 kHz) the recorded signals, which are then sent to a field-programmable gate array (FPGA) board. Finally, the data are streamed to a host PC for data storage and online visualization. Data analysis and programming of the extracellular stimulation protocols were performed by using MATLAB.

The electrode impedance was reduced by depositing platinum black on the electrodes, which increased the effective electrode surface area, concurrently decreased the electrode impedance, and, therefore, significantly improved recording and stimulation conditions. For Pt-black deposition, a current of 180 μA was simultaneously applied to all electrodes for 45-75 s while using a platinum wire as a ground electrode immersed in the deposition solution (0.7 mM hexachloroplatinic acid and 0.3 mM lead (II) acetate anhydrous). By wiping the platinum black from the electrode area with a cotton stick and repeating the procedure 1 or 2 times, deposition uniformity was improved.

4.2.2 Cortical Neuron Culture Preparation

Embryonic day 18 Wistar rat cortices were dissociated in 2 ml of trypsin with 0.25% EDTA (Invitrogen) with trituration. The array was pre-coated with a thin layer of poly(ethyleneimine) (Sigma), 0.05% weight in borate buffer (Chemie Brunschwig) at a pH of 8.5, followed by a drop of 0.02 mg ml^{-1} laminin (Sigma) in Neurobasal (Invitrogen). 15'000-20'000 cells in a 30 μl drop were seeded over the array and 1 ml of Neurobasal media was added after 30 minutes. The cultures were maintained inside an incubator to control environmental conditions (37 °C, 65% humidity, 9% O_2, 5% CO_2) in 1 ml of Neurobasal medium (partially replaced twice per week). Animal experiments were

approved by the Basel City Cantonal Veterinary Office according to Swiss Federal Laws on animal welfare.

4.2.3 Extracting Array-wide Extracellular Action Potentials from Spontaneous Activity

In order to identify spike-triggered average (STA) waveforms of neuronal units on the complete array (or *STA-EAP*, see Section 4.3.1), an automated routine was implemented. In the first step, spontaneous activity was recorded by partially overlapping HD electrode blocks or by using configurations with random electrode subsets. Local spots of large extracellular signal amplitudes in the recordings were identified and selected. In the following, the complete array was scanned by electrode configurations, where 2-4 electrodes at the selected sites were always connected to read-out channels. Spikes from the electrodes at the selected sites were then manually sorted using the Ultramegasort software (Hill et al., 2011), and array-wide STA signals were computed. This method allowed for identification of 10-12 neurons within 2-3 hours based on their recorded spontaneous activity.

4.2.4 Combined HD-MEA and Patch Clamp Recordings

The experimental setup includes the HD-MEA system, combined with an upright microscope (Leica DM6000B) and a conventional patch clamp system (Multiclamp 200B amplifier, Sutter Instruments micromanipulator). The microscope is mounted on a motorized XY-stage (Scientifica UMS) allowing for imaging of a large working area and storage of the precise microscope position for every acquired image. Custom image alignment software (written in MATLAB) was developed to automatically align acquired images with the corresponding HD-MEA coordinates. The alignment software was used to identify the electrodes underneath a patched cell for stimulation experiments and for imaging. The FPGA was equipped with four analog-to-digital conversion channels (ADCs, AD974 Analog Devices) on a custom printed-circuit board for synchronous acquisition of the patch clamp signals together with the HD-MEA data.

For the patch clamp experiments, the cultivation medium was removed, and the chip was perfused with a HEPES-buffered external

bath solution containing (in mM:) NaCl 149, KCl 3.25, CaCl$_2$ 2, MgCl$_2$ 2, HEPES 10, Glucose 11 (pH 7.35 adjusted using 1M NaOH). The bath was constantly perfused during the experiment at slow rate, and all experiments were performed at room temperature. Neurons on top of the MEA electrodes were visualized in bright-field illumination using difference interference contrast optics on the upright microscope. The patch clamp micropipettes (borosilicate glass, Sutter Instruments) had resistances of 5-7 MΩ and were filled with an internal solution containing (in mM): potassium gluconate 135, KCL 20, MgCl$_2$.6H$_2$O 2, HEPES 10, EGTA 0.1, Na$_2$ATP 2, Na$_3$GTP 0.3, adjusted to a pH 7.3 with KOH. In most cases, 0.02 mM Alexa Fluor 594 (Life Technologies) was added to the internal solution, and fluorescence images were acquired during and after the patch clamp experiment. The patch clamp amplifier was controlled using the open-source software WinWCP (John Dempster, University of Strathclyde, UK).

To block synaptic activity during stimulation experiments, 100 μM of the AMPA antagonist 6-cyano-7-nitroquinoxaline-2 3-dione (CNQX), 10 μM of the selective NMDA receptor antagonist DL-2-amino-5-phosphonovaleric acid (AP5), and 50 μM Bicuculline methiodide (BIC), a GABA$_A$ antagonist, were simultaneously added to the bath solution.

4.2.5 Immunohistochemistry

Immunohistochemistry was used to compare the neuronal morphology with the distribution of extracellular recorded signals. Cultures were seeded at very low densities (2000 cells/chip), and spontaneous activity was recorded with overlapping high-density electrode blocks. After the recordings, the cultures were immediately fixed in 4% paraformaldehyde (Invitrogen) in phosphate-buffered saline (PBS; Sigma) at pH 7.4 for 5 min at room temperature and washed twice with ice-cold PBS. They were then permeabilized with 0.25% Triton X-100 (Sigma) in PBS for 10 min and washed in PBS three times for 5 min each time. Next, unspecific binding of antibodies was blocked by adding a blocking medium (PBS with 1% bovine serum albumin (BSA; Sigma) and 0.1% Tween 20 (Sigma)) for 30 min. The primary antibodies to MAP2 (Abcam ab5392, diluted to 1:500 in blocking medium) and to Ankyrin G (diluted to 1:500 in blocking medium) were added and incubated for 2 h at 37 °C, followed by three

washes in PBS for 5 min, each on a shaker. Next, the secondary antibodies containing Alexa Fluor 647 and Alexa Fluor 488 (Invitrogen), each diluted to 1:200 in PBS with 1% BSA, were added. After 30 min at 37 °C, the medium was washed out three times with PBS for 5 min each on the shaker in the dark.

4.3 Results

4.3.1 High-density Recordings and Spike Sorting

Cultured neurons were grown on top of HD-MEAs and their spontaneous activity was recorded at high spatiotemporal resolution. Figure 4.1a shows extracellular signals recorded on 6 HD-MEA
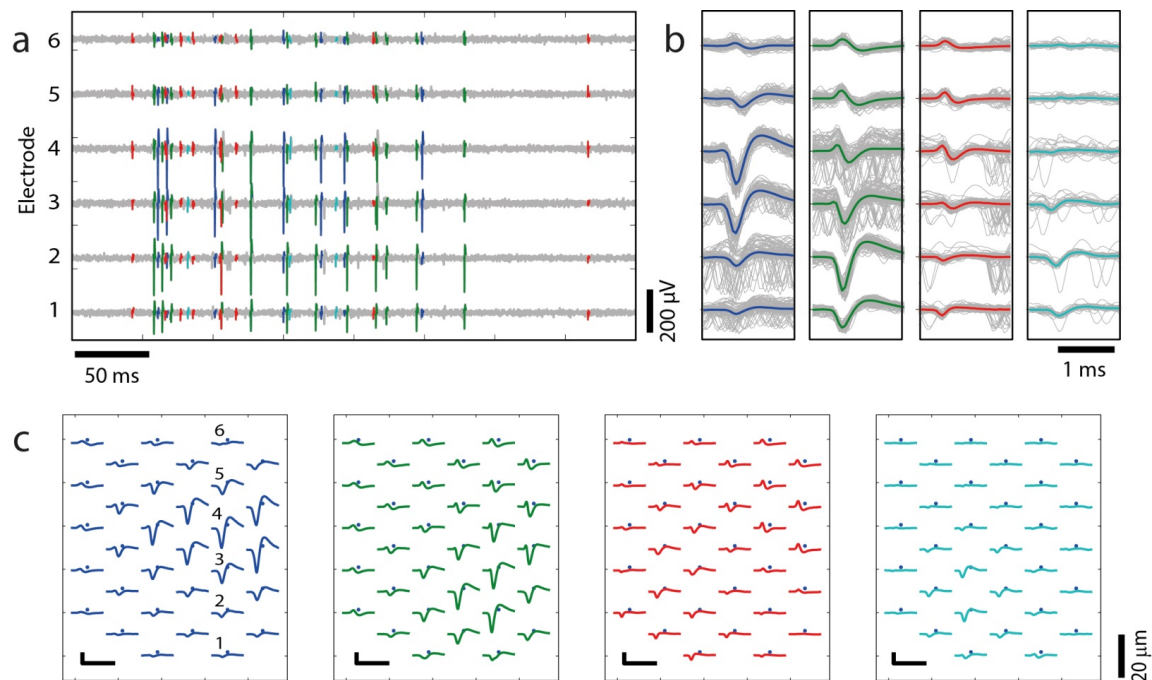

Figure 4.1 Identification of neuronal units based on high-density recordings.

(a) Traces showing 0.4 s of spontaneous activity recorded by 6 electrodes (electrode positions are indicated in c). 4 neuronal units were identified and their spike waveforms were colored. (b) Superposition of all detected spike waveforms for each neuronal cluster (gray: individual traces, colored: average waveform). (c) Cell-specific STA-EAP. The dots indicate electrode positions, the colored traces correspond to the STA waveforms of the neuron on the respective electrodes. Scale bars: 100 µV/1.6 ms.

electrodes. Spikes were detected and classified into 4 different groups by means of principal-component-analysis-based spike sorting (Jäckel et al., 2012). For each cluster, the STA waveforms on the 6 electrodes are shown in Figure 4.1b. It can be seen that the spike waveforms, captured by these 6 electrodes, are sufficiently different to allow for a clear separation. The spatial distribution of the STA waveforms, as displayed in Figure 4.1c, represents the cell-specific, extracellular signature of a neuron, and will be referred to as neuronal *spike-triggered average extracellular action potential (STA-EAP)*.

The measurements in Figure 4.1 illustrate the importance of the high electrode density of HD-MEAs for spike sorting and that several closely-spaced units of cultured cortical neurons can be identified and separated based on their extracellular signals.

Another feature of HD-MEA recordings is the possibility to record from individual neurons across multiple sites, and, more specifically, to record the propagation of APs along the axon over hundreds to thousands of micrometers (Zeck et al., 2011; Bakkum et al., 2013).

Figure 4.2 shows the STA-EAP of a neuron recorded over the complete array area. The individual STA-EAP was computed based on spikes at electrodes with large amplitudes (see *Methods*). This method allows for identifying multiple axonal branches and to characterize their corresponding propagations latencies, ranging up to 1.3 ms in the example in Figure 4.2. Near to the neuronal soma, typically extracellular signals with larger amplitudes are measured (black traces in Figure 4.2a), whereas along the axon, the extracellular amplitudes are significantly lower (colored traces). In the following, we will refer to the STA-EAP near the soma as the *near-somatic STA-EAP*, and to the waveforms along the axon as the *axonal STA-EAP*.
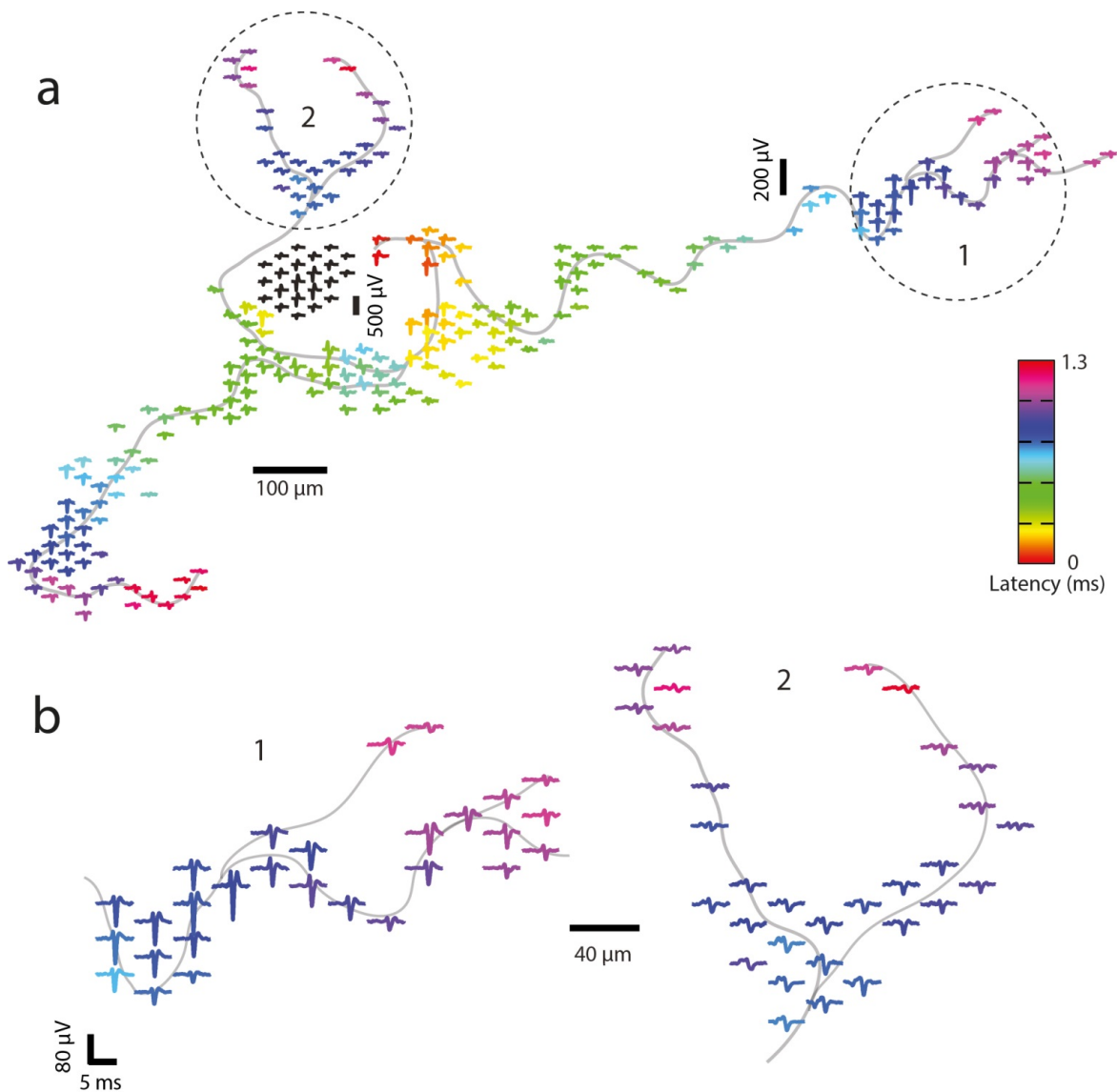
Figure 4.2 STA-EAP of a cortical neuron, including propagating APs along axonal branches.

(a) Full STA-EAP of a neuron on the array. Near-somatic STA-EAP (black traces) and axonal STA-EAP (colored traces) are plotted with different amplitude scale bars. Propagation latency of the axonal traces was determined by the timing of the negative peak and visualized by the color code. The gray lines were drawn to visualize the propagation of the axonal AP. (b) Close-up view on two branching points from a, where the axon divided into several individual branches.
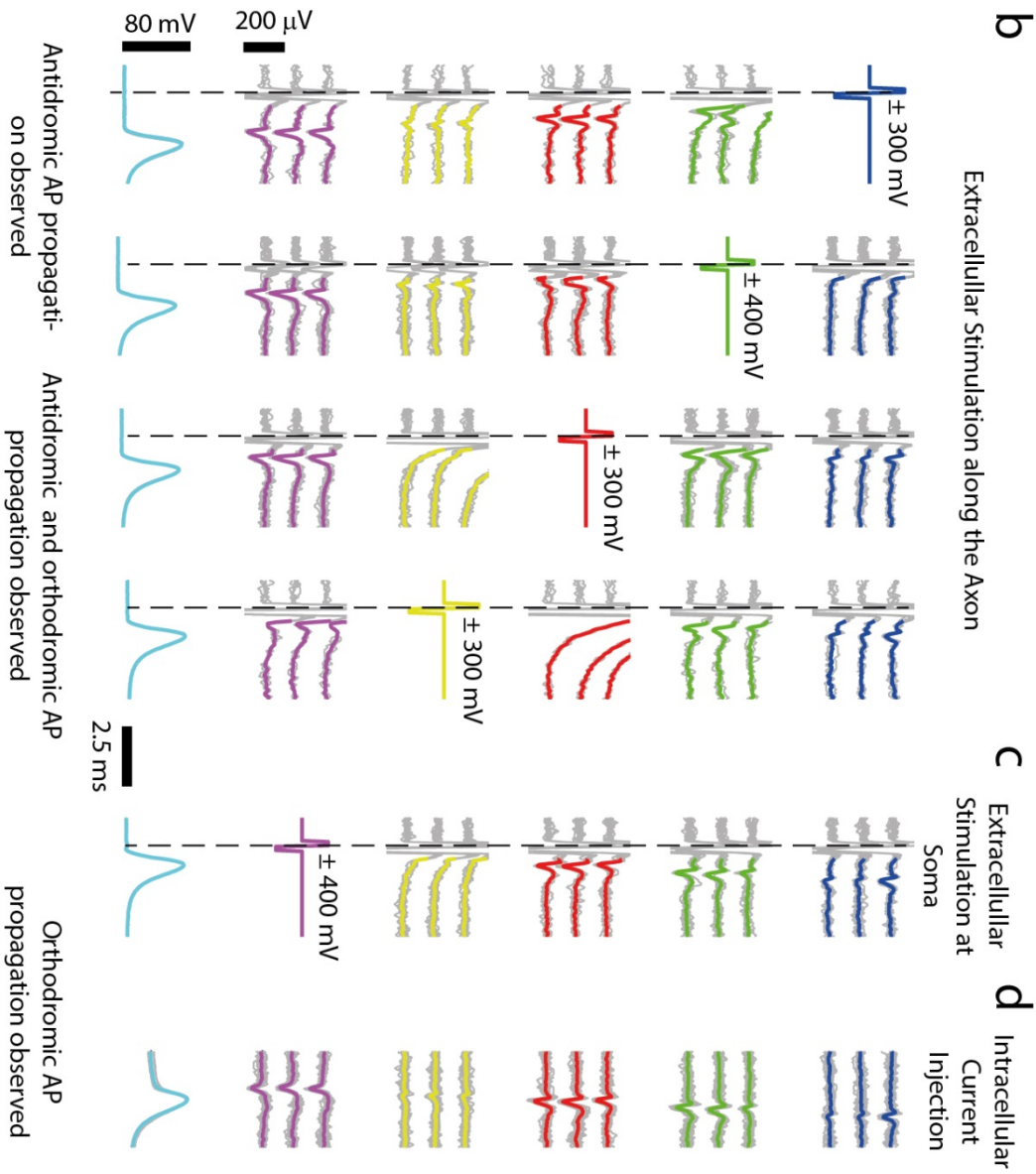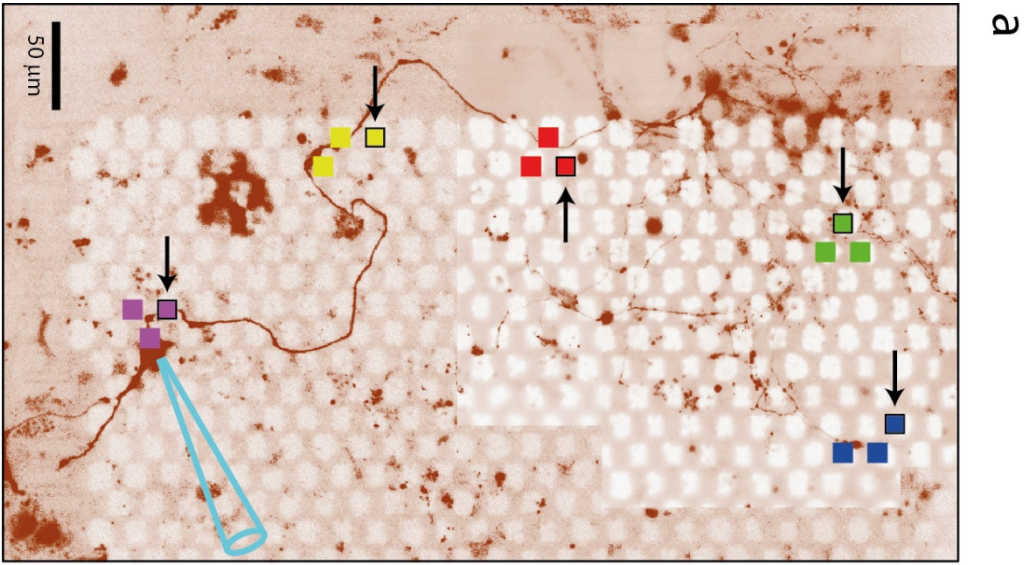
Figure 4.3 Example of multi-site extracellular neuronal stimulation.

(a) Fluorescence image (Fluo4 calcium dye, background) indicating the morphology of a neuron at one corner of the array; white squares are MEA electrodes. Five groups of three electrodes were selected (violet: at the soma, other colors: along the axon) for HD-MEA recording. The cell was patched at its soma (illustrated by the cyan pipette). (b-c) Every column represents an experiment where 4 extracellular stimulation pulses (stimulus represented by biphasic waveforms along the matrix diagonal) were applied through one electrode (indicated by black arrows in a) of each 3-electrode group. Gray traces: individual recorded signals; colored traces: average signals (colored only after the stimulation artifact for better comparison). The dashed black lines indicate the timing of the falling stimulus edge. Bottom: Intracellular signals. (b) When stimulating along the axon, antidromic (blue and green stimulation sites) as well as combined anti- and orthodromic AP propagations (red and yellow stimulation sites) were measured. Note the difference in timing of the intracellular somatic AP for the different stimulation sites. (c) When stimulating close to the soma, the intracellular AP is initiated immediately and only orthodromic AP propagation is observed. (d) APs evoked by intracellular current injection (240 pA pulses at 2 Hz), followed by orthodromic AP propagation.

4.3.2 Antidromic and Orthodromic Propagation of Stimulus-Evoked Action Potentials

The measurements shown in Figure 4.2 indicate that axonal processes of cultured cortical neurons can extend over long distances and can reach different and distant areas of the array. Besides recording from individual neurons across multiple axonal sites, also the possibility to stimulate cells at many points along the axon has been used as a method to characterize spatial extension of and signal propagation latency in axonal branches. In Bakkum et al., 2013, electrodes of the near-somatic STA-EAP measuring large extracellular amplitudes were used to record and detect APs that were evoked at the axon and antidromically propagated towards the soma. If the stimulating electrodes, however, were too close to the recording electrodes, the evoked APs could not be detected anymore due to stimulation artifacts.

In order to overcome this limitation and to also detect APs that have been evoked near the soma, neurons were patched on top of the HD-

MEAs and their intracellular signals were recorded in current-clamp mode. Figure 4.3a shows the morphology of a neuron, stained with a Fluo4 calcium dye, which was patched in the whole-cell configuration on the HD-MEA. Intracellular current injection (240 pA pulses at 2 Hz) was used to evoke APs, while the extracellular signals were recorded from a large area of electrodes. Then, the STA-EAP was computed based on the intracellular spike times. Five groups of three electrodes each were selected: one at the near-somatic (violet) and four along the axonal STA-EAP (other colors). Stimulating one electrode (marked by a black arrow in Figure 4.3a) from the blue group, and similarly from the green group, evoked APs that propagated antidromically down the axon (first two columns in Figure 4.3b) and finally elicited APs at the soma as recorded by the extracellular and intracellular electrodes. The stimulation pulses in this particular experiment, as well as in the following experiments, had a biphasic, positive-first, waveform with 200 µs phase width of variable amplitude.

When electrodes from the red and yellow groups were stimulated, antidromic and orthodromic AP propagation was detected. The latency of the intracellular AP decreased accordingly, when the stimulation electrode was closer to the soma.

Stimulation at the violet electrode, led to immediately evoked APs, as seen by the intracellular trace on the bottom of Figure 4.3c. This example shows that APs can be evoked by stimulating neurons within their near-somatic STA-EAP and that these APs are followed by orthodromic propagation along the axon.

For comparison, Figure 4.3d shows APs which were evoked by intracellular current injection and were followed by orthodromic AP propagation. Note that the extracellular AP at the violet electrodes temporally preceded the intracellular AP, which was consistently found for different patched neurons. The electrodes record the AP at its initiation site (see 4.3.6), whereas the patch pipette measures the AP after its backpropagation to the soma (Stuart et al., 1997).

4.3.3 Intracellular Response Profiles to Extracellular Stimulation

In order to obtain a better understanding on how extracellular HD-MEA stimulation affects cultured neurons, the different intracellular responses to extracellular HD-MEA stimulation near the cell body were investigated. For this purpose, neurons were patched on the MEA and their STA-EAP was measured by evoking APs intracellularly through the patch pipette. Electrodes at and around the near-somatic STA-EAP were then identified and selected, and biphasic voltage stimulation pulses were applied at different amplitudes (between ±100 and ±400 mV, 50 mV intervals) in random order through these selected electrodes.

A variety of intracellular response behaviors upon HD-MEA stimulation at different electrodes was observed. Figure 4.4 shows the electrode positions with respect to the neuronal morphology, and the corresponding intracellular responses to extracellular stimulation for two neurons. The subset of stimulation electrodes and stimulation amplitude was selected for the plots in Figure 4.4b and d, which illustrate the different types of responses. For the neuron in Figure 4.4a-b, stimulation at electrode 1 resulted in immediately evoked APs, whereas stimulation at electrode 2 led to evoked APs within substantial, reproducible delays. When stimulating at electrode 3 underneath the soma, a fast small depolarization of the membrane potential (MP) was observed. Some electrodes, such as electrode 4, activated reliably a presynaptic neuron and evoked postsynaptic potentials (PSPs) in the patched cell. Finally, electrode 5, even though located in close proximity to other activating electrodes, did not evoke any intracellular response.

In order to discriminate between direct neuronal activation and activation involving synaptic signaling, stimulation of the neuron in Figure 4.4c-e was performed first under control conditions and then repeated after addition of synaptic blockers. Intracellular responses to stimulation at electrodes 1-4 in Figure 4.4d are of the same type as the ones shown in Figure 4.4b. In the case of electrodes 1-2, the neuron was stimulated directly, as the addition of synaptic blockers did not obviate the APs. In both cases, however, some stimulation trials under

the control conditions also evoked PSPs, which overlapped with the APs. These PSPs were suppressed in the presence of synaptic blockers. The timing of the AP onset upon stimulation at electrode 2 showed a significant delay compared to the AP timing for stimulation at electrode 1 (Figure 4.4e). Stimulation of electrode 2, which is located distantly to the cell body (see Figure 4.4c), thus evoked antidromically propagating APs in the axon, such as in the example shown in Figure 4.3. We observed consistently that stimulation at electrodes located at the near-somatic STA-EAP produced immediate APs without any delay.

The small depolarization caused by stimulating at electrode 3 was seen also after addition of synaptic blockers, and, therefore, can be categorized as direct neuronal activation. Stimulation at electrodes 4 and 5 in Figure 4.4d evoked postsynaptic signals in the patched neuron, which were then completely suppressed after application of synaptic blockers. In the case of electrode 4, subthreshold PSPs were reliably measured, whereas stimulation at electrode 5 evoked suprathreshold PSPs leading to postsynaptic APs in most trials.

In some cases, an artifact in the intracellular signal was measured upon HD-MEA stimulation. This was the case for the neuron in Figure 4.4b but not for the cell in Figure 4.4d, as shown in the insets. The artifacts had amplitudes of up to several millivolts and were temporally confined to the stimulus timing. A likely reason for the variability of intracellular artifacts for different cells is the difference in the quality of the patch. It can be expected that superior patches with very high leak resistances will show no intracellular artifact at all, whereas a leaky recording with a low leak resistance will exhibit a large intracellular artifact, when extracellular stimulation is applied.
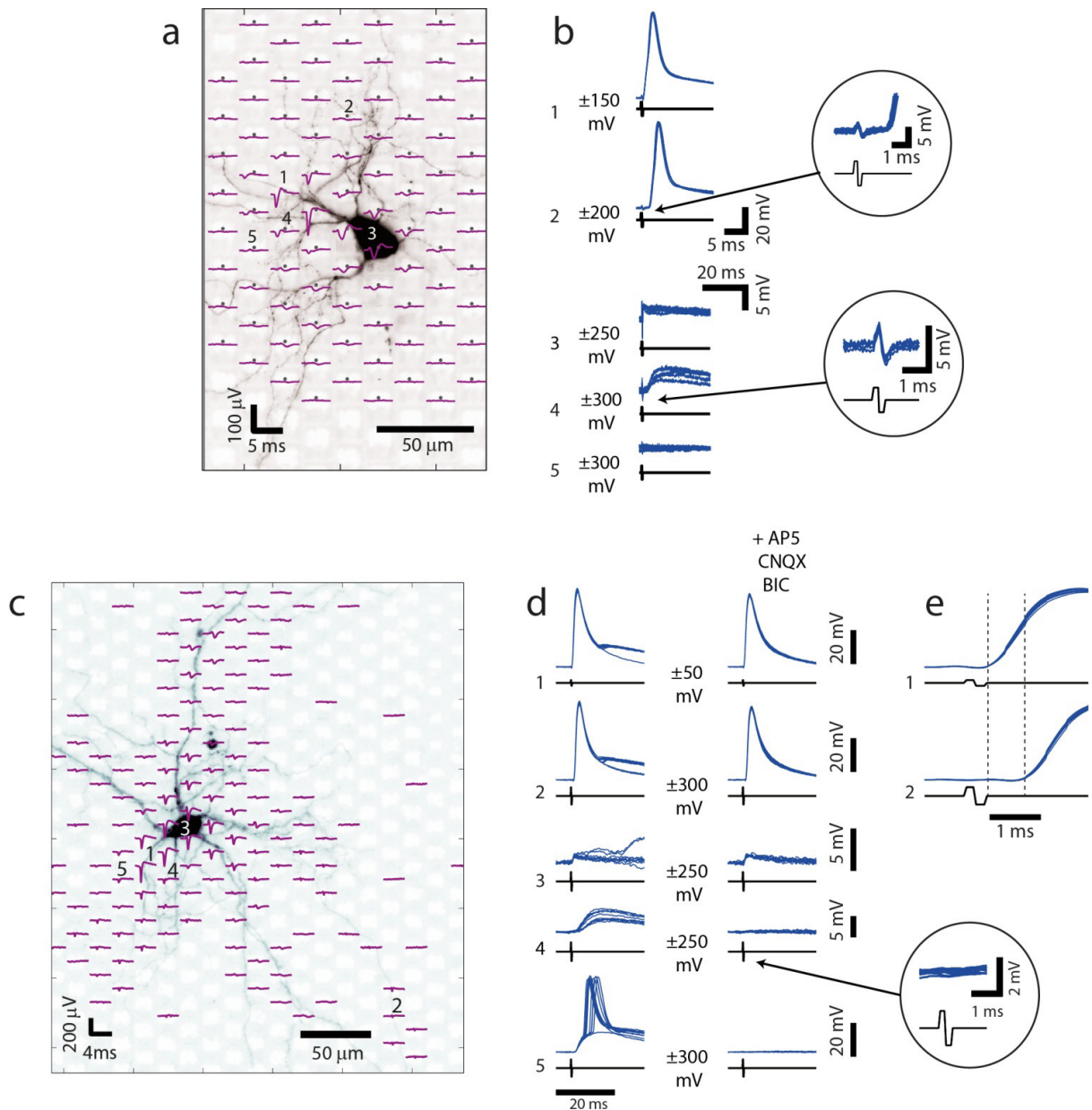
Figure 4.4 Distinct intracellular responses to extracellular stimulations at the near-somatic STA-EAP.

(a) Fluorescence image of a patched neuron (background) and STA-EAP (violet traces) and 5 numbered electrodes at which stimulation was applied. (b) Intracellular responses to extracellular stimulation at these 5 electrodes. Each electrode was stimulated 5 times. Blue traces are individual responses; black waveforms indicate timing of the biphasic voltage stimulation pulses. The insets visualize the stimulation artifacts for electrodes 2 and 4. (c) Fluorescence image and STA-EAP for a second neuron. (d) *Left:* Intracellular responses (10 trials each) to extracellular stimulations at the 5 numbered electrodes under control conditions. *Right:* Responses in the presence of synaptic blockers. For this cell, no stimulus artifact was seen (inset). (e) Zoom-in on responses to stimulation at electrodes 1 and 2 under control conditions to visualize the delay between the respective AP onsets (marked by the dashed lines).

4.3.4 Extracellular Stimulation at the Cell Soma induces Fast Membrane Potential Depolarizations but No Action Potentials

In both examples from Figure 4.4, stimulating directly underneath the cell soma did not evoke APs but only caused small depolarizations of the MP (largest stimulus for neurons in Figure 4.4 ±300 mV). Fast subthreshold depolarizations were also observed when a neuron was stimulated underneath the dendrites close to the soma (Figure 4.5c). The depolarization amplitude was found to increase approximately linearly with the stimulation voltage (Figure 4.5a-b) and to be largest at the soma, while decaying with increasing distance (Figure 4.5c). At some electrodes, for which low amplitudes evoked subthreshold depolarizations, APs were elicited by increased amplitudes.

The distances between electrodes evoking fast MP depolarizations and the soma centers are shown in Figure 4.5d *top*, for a total of 6 neurons. Fast depolarizations were mainly induced near somata, but, in some cases, even at up to 80 µm distance from the soma center. The stimulation voltages used for Figure 4.5d amounted to up to 300 mV and the detection of the fast MP depolarizations was performed manually (depolarizations larger than 1 mV were considered).

The same neurons were analyzed with respect to the electrodes evoking APs when stimuli of up to 300 mV were applied. Electrodes located very close to the soma centers did not elicit APs (Figure 4.5d *bottom*) in any instance. The nearest electrode that successfully evoked APs was at 17 µm distance from the soma center. The first significant peak in the histogram in Figure 4.5d occurred for a distance of 35 µm from the soma centers. Electrodes evoking APs in the neuronal axons were also found at larger distances (as also shown in Figure 4.3 and Figure 4.4), but those are not well-represented in this histogram, as mainly electrodes at the near-somatic STA-EAP were stimulated for this experiment.
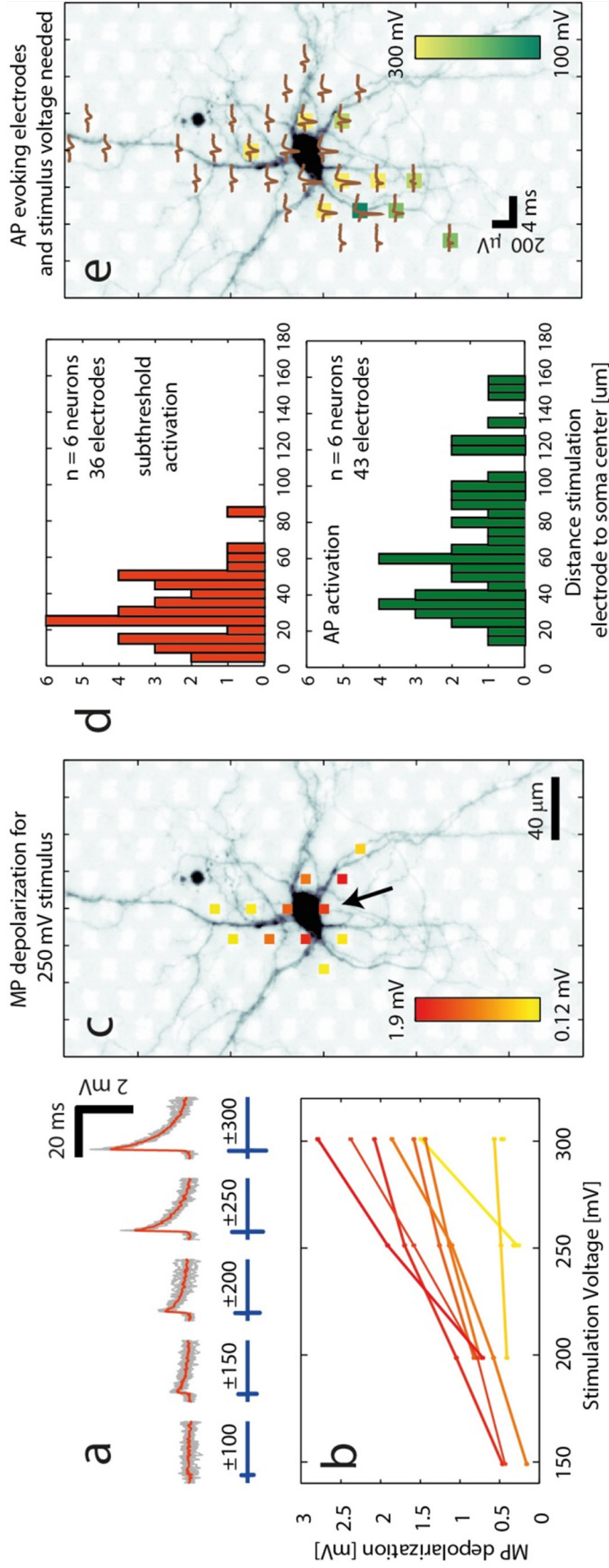
Figure 4.5 Induced membrane potential depolarizations when stimulating by the somatodendritic compartment.

(a) Induced fast MP depolarization when stimulating a neuron at the electrode denoted by the black arrow in (c) with bipolar voltage pulses of different amplitudes (±100-300 mV). Individual trials are shown in gray, the average signal is colored orange. (b) Peak depolarization amplitudes for stimulation through individual electrodes with different voltages. The color code corresponds to the colored electrodes in c. (c) Fluorescence image of a patched neuron. Electrodes evoking MP depolarizations were color coded, with the color code indicating the depolarization amplitude for a 250 mV stimulus. (d) *Top*: Histogram of the distances between electrodes evoking fast MP depolarizations and the center of the respective somata for a total of 6 neurons. *Bottom*: For the same 6 neurons, histogram of the distances between electrodes evoking APs and the center of the respective somata. Note that in the close vicinity of the cell bodies no APs were evoked. For all cells, stimulation voltages up to 300 mV were used. (e) Image of the same neuron in c overlayed with its STA-EAP (brown traces). Electrodes which did evoke APs are colored, with the color code indicating the activation threshold.

107

4.3.5 Excitability Profiles at the Location of the STA-EAP

HD-MEA recordings allow for identification of the neuronal units according to their extracellular signals. Therefore, a method for targeted stimulation of identified cells would ideally allow for selecting electrodes for effective stimulation based on the extracellular signals measured at the HD-MEA electrodes.

Figure 4.5e shows the positions of the electrodes that evoked APs superimposed with the morphological neuron image and the STA-EAP. At a first glance, many electrodes that recorded large-amplitude extracellular signals also could effectively be used to stimulate APs. Some electrodes at the sometodendritic region, however, which recorded significant extracellular spike amplitudes, were not effective in stimulating the neurons. On the other hand the dark green-colored electrode featuring the largest extracellular signal requires a relatively low threshold voltage of only 100 mV to reliably elicit APs. Therefore, the characteristics of the near-somatic STA-EAP may provide useful information for targeted stimulation.

Stimulation artifacts saturate the recorded signals on electrodes within a range of 80-100 μm distance from the stimulation site for 1-5 ms (Bakkum et al., 2013). Therefore, it is not possible to record directly evoked APs close to the stimulation site with the current HD-MEA recording circuitry. However, it is possible to obtain detailed excitability profiles of neurons without the need of patch clamp recordings by making use of the large number of available electrodes to identify neurons and their full STA-EAPs including axonal compartments. Once the STA-EAPs of neurons were identified, electrodes at axonal compartments were used to record from, while electrodes at the near-somatic STA-EAP were stimulated. Combining the extracellular signals from multiple electrodes along the axons allowed then to identify evoked APs for individual stimuli, despite the relatively small SNR of the axonal signals. In this way, neuronal excitability could be studied without the temporal restriction that would apply to patch clamp experiments.

Comparisons between near-somatic STA-EAPs and required threshold voltages for evoking APs are shown in Figure 4.6. These excitability maps show the relation between recorded average extracellular

waveforms and stimulation thresholds for individual electrodes (Figure 4.6a and c). In all recorded cases (n = 13 neurons), several electrodes at the near-somatic STA-EAP were found to reliably evoke APs at stimulation amplitudes below 100 mV. The excitability curves shown in Figure 4.6b indicate how reliably APs were evoked when the respective electrodes were stimulated at different amplitudes. Different electrodes showed variable slopes of the transition phase between 0% and 100% reliability of evoking spikes.

The excitability maps in Figure 4.6c again visualize the highly localized excitability characteristics of cultured neurons on HD-MEAs. Despite the fact that many electrodes within the region of the near-somatic
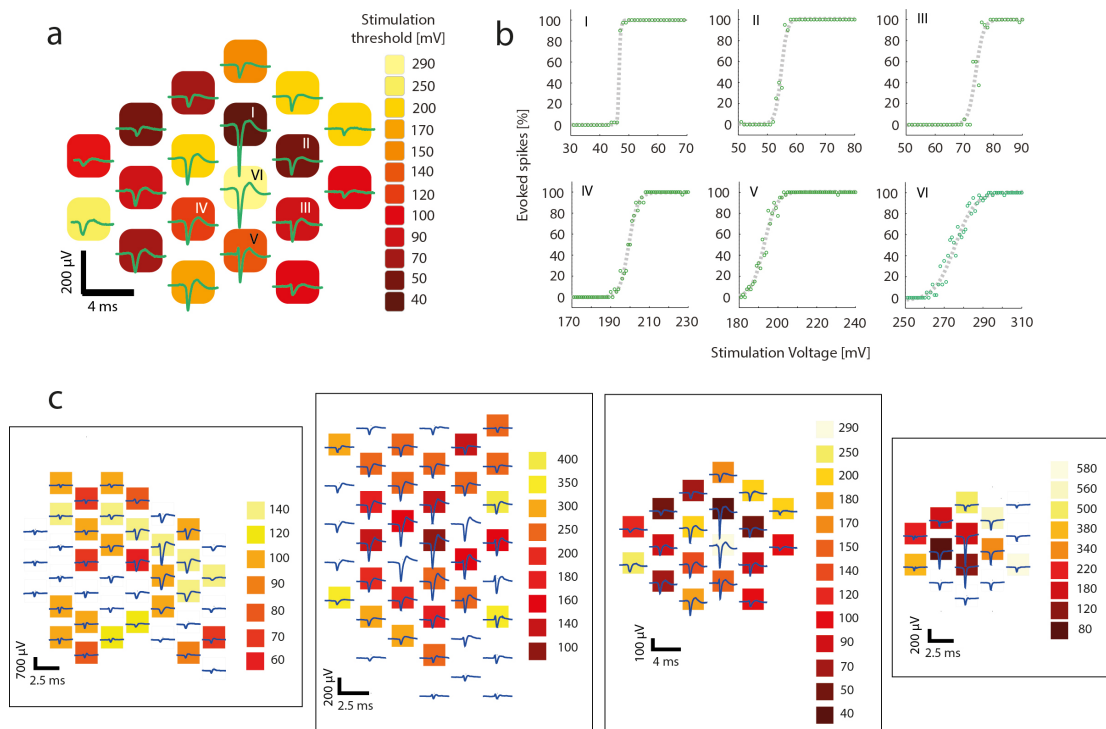

Figure 4.6 Combined measurements of the excitability map and the extracellular STA-EAPs.

(a) STA-EAP of an identified neuron (green traces) and stimulation thresholds needed to reliably evoke spikes at the individual electrodes (colored squares, threshold value was taken at 100% reliability). (b) Excitability curves for the 6 electrodes labeled in (a). Note the different slopes in the transition phases between 0 and 100% evoked spikes for different electrodes. (c) Four examples of excitability maps and the corresponding STA-EAPs.

STA-EAP did effectively stimulate the neurons, the threshold voltages were not always homogeneously distributed. Furthermore, in many cases we found electrodes that did not evoke the neuron at all. Oftentimes such non-effective electrodes where surrounded by electrodes with comparably low activation thresholds.

4.3.6 The Near-somatic STA-EAP is Positioned at the Axon Initial Segment

We have shown that the neuronal soma is a region with comparably low excitability. Our excitability map measurements have shown, however, that subsets of electrodes located within the near-somatic STA-EAP require only low stimulation thresholds for successfully evoking APs of the measured neurons.

In order to more precisely correlate the position of the STA-EAP with the neuronal morphology, sparse neuronal cultures on HD-MEAs were stained after spontaneous activity had been recorded. Fluorescence images of the neuronal dendrites, stained with MAP2 (black), and the position of the AIS, stained with AnkG (violett) are shown in Figure 4.7a and c. The superpositions of the morphology and the near-somatic STA-EAP, shown in Figure 4.7b and d, reveal a correlation between the location of the AIS and the extracellular EAP characteristics: Regions of electrodes with large extracellular signal amplitudes are collocated with the AIS or near the AIS. This holds for both examples: For the case of the AIS originating at the apical dendrite distal to the cell body (Figure 4.7b), as well as for the case of the AIS originating close to the soma (Figure 4.7d).
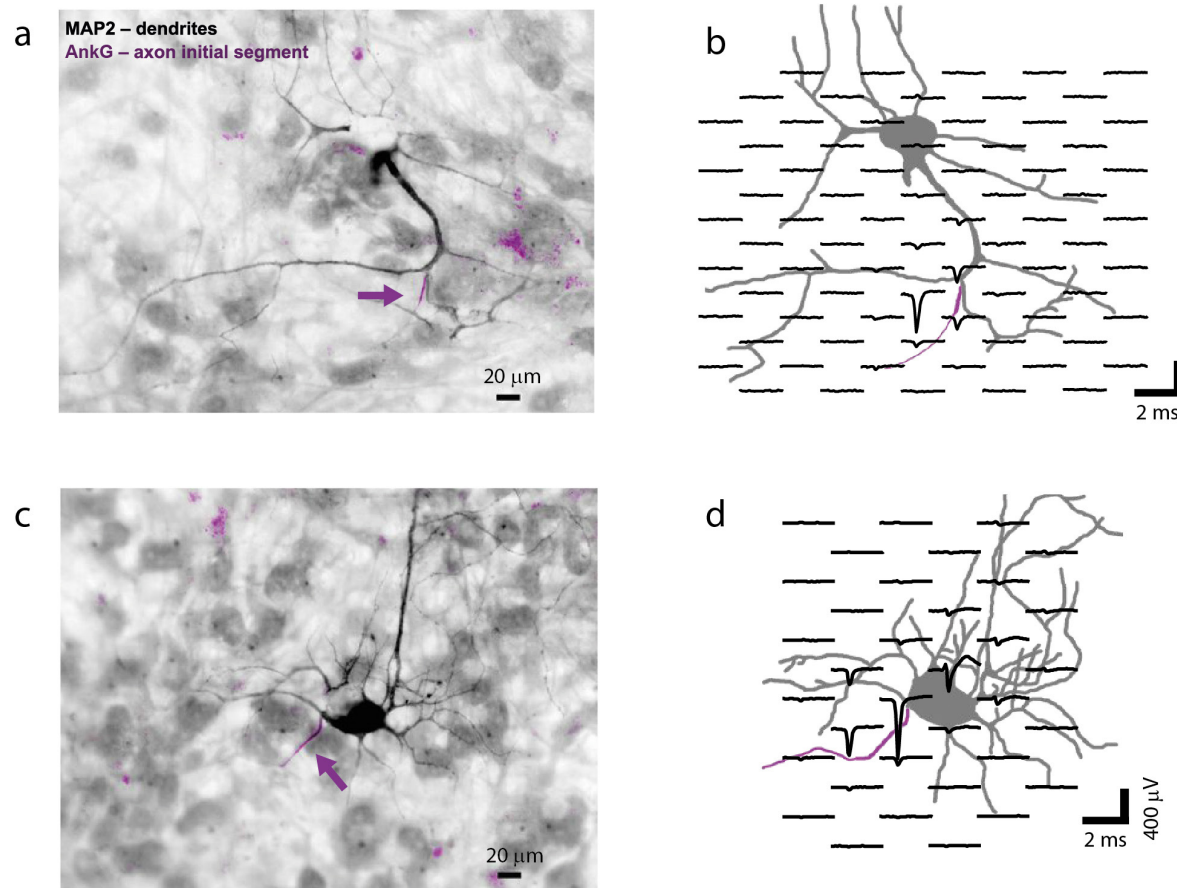
Figure 4.7 Correlating AIS location with the STA-EAP.

(a) Florescence image of an isolated neuron stained with MAP2 for dendrites (black) and the AIS-specific antibody AnkG (violet, indicated by arrow). The AIS originated from an apical dendrite and was located at approximately 80 μm distance from the cell body. (b) Morphological contour of the neuron (background, gray) and AIS (violet) superimposed with the STA-EAP. (c) – (d) Plots showing a second neuron, for which the AIS originated at the soma.

4.4 Discussion

The capability to simultaneously record the activity of large numbers of cells in networks of neurons at single-spike resolution renders HD-MEAs powerful tools for studying cell interactions and firing dynamics in order to better understand the information processing of neuronal networks. Additionally, the possibility to perform targeted stimulation of several individually identified neurons over extended time-scales of weeks to months, will enable a wide range of interesting and relevant experiments, particularly in the field of long-term plasticity dynamics.

Here, we analyzed possibilities and effects of extracellular stimulation on cortical neurons grown and cultured on HD-MEAs. HD-MEAs provided us the experimental means to conduct stimulation experiments at subcellular resolution, in order to (a) investigate the potential of stimulating neurons at different sites and (b) develop strategies for a direct and precise targeting of identified neurons.

One of the main findings of this study is that the effects of electrical voltage stimulation on cultured neurons by means of HD microelectrodes are highly localized. In particular, we found that stimulation thresholds in the excitability maps of neurons were not distributed homogeneously but showed irregularities and that, in many instances, stimulation of electrodes next to highly excitable sites did not evoke any APs. This highly nonlinear observation contrasts the near-somatic extracellular potential distribution, which typically features a center maximum and then a continuous decay into all directions.

Similarly, the different response profiles in Figure 4.4 have shown that stimulation at two neighboring electrodes can lead to different intracellular responses. A potential argument for the location-specificity is the electrode-to-neuron distance. Simulation studies have shown that the extension of regions activated through extracellular stimulation (in the case of current stimuli) increases with distance from the stimulating electrode (Rattay et al., 2012). In the case of cultured neurons grown on HD-MEAs, the distances between electrodes and the neuronal compartments are very small, as the neurons are located directly on top of the electrodes. As a consequence, comparably low stimulation voltages are necessary to

evoke activity, and applied electrical stimuli can be assumed to act particularly local on the neuronal compartments.

The soma and dendrites were found to be places of low excitability. However, all measured neurons could be stimulated with relatively low threshold voltages at small subsets of the electrodes located within the near-somatic STA-EAP. We have furthermore shown that the near-somatic STA-EAP of cultured neurons on HD-MEAs collocates with the position of the AIS. Finally, neurons could also almost always be stimulated through electrodes that recorded axonal signals.

Our findings are in accordance with recent simulations (Rattay and Wenger, 2010; Rattay et al., 2012) and experimental work (Nowak and Bullier, 1998; Histed et al., 2009), which showed that the AIS and the axon, but not the cell bodies, are activated by electrical stimulation. The HD-MEA technology, which allows for localized recording and stimulation of these regions, represents therefore a promising technique to achieve targeted, selective activation of individual neurons. The fact that high sodium channel densities are concentrated in small areas, especially in the region of the AIS, constitutes a plausible explanation for the low stimulation threshold in this area, and, more general, for the inhomogeneous distribution of the stimulation threshold values in the excitability maps.

The most suitable region to identify and to extracellularly record from neurons is, in most cases, in the region of the AIS near the soma, within the near-somatic STA-EAP. This region is also highly suitable for targeted stimulation. We have shown that subsets of the electrodes at the near-somatic STA-EAP always feature high excitability. Ideally, one could identify highly excitable electrodes by means of their extracellular potential distribution. Due to the irregularities in the excitability maps, however, we could not in all cases unequivocally identify the best electrodes for stimulation. Despite this fact, three features of the extracellular waveforms were found to correlate with the measured excitability. First, electrodes with large extracellular amplitudes were found to be generally excitable. Second, electrodes close to the center of mass of the near-somatic STA-EAP - which is not equivalent with the center of the soma - also often featured high excitability values. Finally, we looked at the timing of the extracellular AP waveforms based on the time point of their negative peak (Jäckel

et al., 2012). Electrodes with early AP timing turned out to be more excitable than others. These electrodes are close to the position of the AP initiation site (AIS), which is a very excitable location.

Upon evoking APs through different stimulation electrodes, we detected different AP latencies. If a neuron was stimulated at its axon, stimulation was followed by antidromic propagation so that a delayed somatic AP was observed. However, if the stimulation electrode was located in the area of the near-somatic STA-EAP, APs were always evoked more or less instantaneously. This behavior could be expected, as the AIS is, in most cases, close to the soma and features a high probability of successful AP initiation.

For certain experiments it may be important to stimulate neurons directly at the AIS. If stimulated at the AIS, the evoked AP propagates orthodromically down the respective axon in the same way as an AP arising from natural neuronal activity. In particular, the relative timing between the AP at the soma and at all axonal branches is, in this case, preserved. In the case of axonal stimulation, the relative timings are not preserved, as the initiated AP will propagate in both directions, anti- and orthodromically along the stimulated axon (Figure 4.3).

An important requirement for many applications is stimulation selectivity. For all neurons (n=13), for which we identified complete STA-EAPs and excitability maps, we subsequently selected the most excitable electrode for stimulation. The neuron was stimulated with the threshold voltage amplitude, while the complete array area was scanned. A comparison of the signals evoked by the stimuli with the STA-EAP was used to control if other cells had been activated as well. In all cases, only signals from the target neurons were measured, which was an indication for selective stimulation. It has to be noted, however, that the immediate vicinity of the stimulation electrode could not be recorded immediately after the stimulus. Therefore, unselective activation of other nearby neurons could not be excluded completely.

In future investigations, we will repeat the experiments of targeted stimulation while simultaneously recording the calcium signals of the neurons via optical means. This will allow us to verify that selective stimulation can be achieved if neurons are stimulated at the

electrodes featuring the lowest stimulation thresholds. So far, our preliminary results indicate that, when a neuron is targeted at the optimal stimulation site, single neuron stimulation can be achieved with a high probability.

CHAPTER 5 Conclusions and Outlook

Spike sorting is a complex but indispensable task to exploit the potential of extracellular recording data. Simultaneous recordings from hundreds of densely-arrayed microelectrodes pose even more challenges to devising suitable spike sorting techniques.

In this thesis, data from two different preparations were analyzed: recordings from acute retinae, as well as recordings from long-term cultures of embryonic cortical neurons. Spike sorting of data recorded from cultured cortical neurons in Chapters 3 and 4 was mainly performed by use of a manual spike sorting tool (Hill et al., 2011), as there was typically one target neuron which had to be sorted. In order to sort the simultaneous activity of a population of RGCs, however, a spike sorting algorithm is needed, since it is very challenging and time consuming to manually sort very large numbers of neurons. The specifications for spike sorting techniques are demanding: they need to be adaptable to different devices and preparations, modular, automatic or automatable, and user friendly. Newly developed HD-MEAs with eight times more recording channels than the device used in this work (e.g. Ballini et al. 2014) generate amounts of data, which cannot be processed anymore by manual spike sorting. There is increasing pressure on scientists or laboratories to devote considerable time and efforts solely to spike sorting.

A system combining extracellular HD-MEA recordings, intracellular patch clamp recordings, and optical imaging was realized and used to do measurements in cultures of dissociated cortical neurons. It was shown that postsynaptic potentials (PSPs) can be evoked through extracellular stimulation of multiple presynaptic neurons, making this a powerful system to investigate interactions between multiple synaptic inputs. A variety of experiments in the field of long-term

plasticity could be performed by using the presented technique. Heterosynaptic plasticity effects (Royer and Paré, 2003; Chen et al., 2013) have been found in acute slice preparations, which represent changes of non-activated synaptic inputs due to plasticity at activated synapses. Such effects can be studied and investigated in a straightforward way with the presented combination system due to the possibility to measure many PSPs in parallel. Organotypic slice cultures, in which the neuronal morphology is much better preserved, may be used instead of dissociated cultures in such experiments.

Effects of stimulation through HD-MEA electrodes have been measured and investigated. Selective, targeted stimulation of previously identified neurons is a prerequisite for many experiments. Further analysis is required on the question, how to detect the most suitable electrode for effective stimulation, based on the recorded extracellular neuronal spike shapes and signal amplitudes. A major obstacle is the stimulation artifact, which does not allow for detecting evoked APs in the surrounding of the stimulation site. As soon as improved circuits and stimulation strategies for artifact suppression will allow for detecting directly evoked APs in immediate vicinity of the stimulation electrode, the technique will be very impactful. Advances in this field will also allow for conducting synaptic mapping experiments in much more detail.

A very promising field of application for HD-MEAs is to record axonal signals and to track their propagation across the array (Bakkum et al., 2013). Recent studies indicate that the axon may have an 'analog' component and may feature signal modulations (Sasaki et al., 2011; Debanne et al., 2013), rather than serving as a pure 'digital' transmission device. The combination of patch clamping and HD-MEAs holds great potential for such experiments: while the membrane potential of a patched neuron is precisely controlled by the patch pipette, the neuronal output (the axon) is measured by means of the HD-MEA at hundreds of sites so that modulation of signal amplitude, velocity, or conduction failures can be assessed.

Furthermore, the existing system could be extended by an additional second patch clamp micropipette. The paired-patch configuration, where a presynaptic and a postsynaptic neuron are patched simultaneously, would allow for precisely controlling the presynaptic

membrane potential, for recording its output signal along the axon by the HD-MEA and, at the same time, observe how modulations of the axonal signal affect the postsynaptic neuron on a single-trial basis.

CHAPTER 6 References

Aaron G, Yuste R. Reverse optical probing (ROPING) of neocortical circuits. *Synapse* 60: 437–440, 2006.

Bakkum DJ, Chao ZC, Potter SM. Long-term activity-dependent plasticity of action potential propagation delay and amplitude in cortical networks. *PLoS One* 3, 2008.

Bakkum DJ, Frey U, Radivojevic M, Russell TL, Müller J, Fiscella M, Takahashi H, Hierlemann A. Tracking axonal action potential propagation on a high-density microelectrode array across hundreds of sites. *Nat Commun* 4: 2181, 2013.

Ballini M, Muller J, Livi P, Chen Y, Frey U, Stettler A, Shadmani A, Viswam V, Jones IL, Jackel D, Radivojevic M, Lewandowska MK, Gong W, Fiscella M, Bakkum DJ, Heer F, Hierlemann A. A 1024-Channel CMOS Microelectrode Array With 26,400 Electrodes for Recording and Stimulation of Electrogenic Cells In Vitro. *IEEE J Solid-State Circuits* 49: 1–15, 2014.

Berdondini L, Imfeld K, Maccione A, Tedesco M, Neukom S, Koudelka-Hep M, Martinoia S. Active pixel sensor array for high spatio-temporal resolution electrophysiological recordings from single cell to large scale neuronal networks. *Lab Chip* 9: 2644–51, 2009.

Berdondini L, van der Wal PD, Guenat O, de Rooij NF, Koudelka-Hep M, Seitz P, Kaufmann R, Metzler P, Blanc N, Rohr S. High-density electrode array for imaging in vitro electrophysiological activity. *Biosens Bioelectron* 21: 167–74, 2005.

Bi GQ, Poo MM. Synaptic modifications in cultured hippocampal neurons: dependence on spike timing, synaptic strength, and postsynaptic cell type. *J Neurosci* 18: 10464–72, 1998.

Boucsein C, Nawrot M, Rotter S, Aertsen A, Heck D. Controlling synaptic input patterns in vitro by dynamic photo stimulation. *J Neurophysiol* 94: 2948–2958, 2005.

Boudkkazi S, Carlier E, Ankri N, Caillard O, Giraud P, Fronzaroli-Molinieres L, Debanne D. Release-Dependent Variations in Synaptic Latency: A Putative Code for Short- and Long-Term Synaptic Dynamics. *Neuron* 56: 1048–1060, 2007.

Braeken D, Huys R, Loo J, Bartic C, Borghs G, Callewaert G, Eberle W. Localized electrical stimulation of in vitro neurons using an array of sub-cellular sized electrodes. *Biosens Bioelectron* 26: 1474–7, 2010.

Branco T, Häusser M. Synaptic integration gradients in single cortical pyramidal cell dendrites. *Neuron* 69: 885–92, 2011.

Brown GD, Yamada S, Sejnowski TJ. Independent component analysis at the neural cocktail party. *Trends Neurosci* 24: 54–63, 2001.

Callaway EM, Katz LC. Photostimulation using caged glutamate reveals functional circuitry in living brain slices. *Proc Natl Acad Sci* 90: 7661–7665, 1993.

Chen J-Y, Lonjers P, Lee C, Chistiakova M, Volgushev M, Bazhenov M. Heterosynaptic plasticity prevents runaway synaptic dynamics. *J Neurosci* 33: 15915–29, 2013.

Csicsvari J, Henze DA, Jamieson B, Harris KD, Sirota A, Bartho P, Wise KD, Buzsaki G. Massively parallel recording of unit and local field potentials with silicon-based electrodes. *J Neurophysiol* 90: 1314–1323, 2003.

Debanne D, Bialowas A, Rama S. What are the mechanisms for analogue and digital signalling in the brain? *Nat Rev Neurosci* 14: 63–9, 2013.

Debanne D, Gahwiler BH, Thompson SM. Long-term synaptic plasticity between pairs of individual CA3 pyramidal cells in rat hippocampal slice cultures. *J Physiol* 507: 237–247, 1998.

Debanne D, Guérineau NC, Gähwiler BH, Thompson SM. Paired-pulse facilitation and depression at unitary synapses in rat hippocampus: quantal fluctuation affects subsequent release. *J Physiol* 491 (Pt 1: 163–176, 1996.

Donoho DL, Johnstone JM. Ideal spatial adaptation by wavelet shrinkage. *Biometrika* 81: 425–455, 1994.

Dragas J, Jackel D, Hierlemann A, Franke F. Complexity Optimisation and High-Throughput Low-Latency Hardware Implementation of a Multi-Electrode Spike-Sorting Algorithm. *IEEE Trans Neural Syst Rehabil Eng* PP: 1–1, 2014.

Du JG, Riedel-Kruse IH, Nawroth JC, Roukes ML, Laurent G, Masmanidis SC. High-Resolution Three-Dimensional Extracellular Recording of Neuronal Activity With Microfabricated Electrode Arrays. *J Neurophysiol* 101: 1671–1678, 2009.

Einevoll GT, Franke F, Hagen E, Pouzat C, Harris KD. Towards reliable spike-train recordings from thousands of neurons with multielectrodes. *Curr Opin Neurobiol* 22: 11–7, 2012.

Ellis-Davies GC. A chemist and biologist talk to each other about caged neurotransmitters. *Beilstein J Org Chem* 9: 64–73, 2013.

Eversmann B, Jenkner M, Hofmann F, Paulus C, Brederlow R, Holzapfl B, Fromherz P, Merz M, Brenner M, Schreiter M, Gabl R, Plehnert K, Steinhauser M, Eckstein G, Schmitt-Landsiedel D, Thewes R. A 128 x 128 cmos biosensor array for extracellular recording of neural activity. *IEEE J Solid-State Circuits* 38: 2306–2317, 2003.

Eversmann B, Lambacher A, Gerling T, Kunze A, Fromherz P, Thewes R. A neural tissue interfacing chip for in-vitro applications with 32k recording / stimulation channels on an active area of 2.6 mm^2. In: *2011 Proceedings of the ESSCIRC (ESSCIRC)*. IEEE, p. 211–214.

Fee MS, Mitra PP, Kleinfeld D. Variability of extracellular spike waveforms of cortical neurons. *J Neurophysiol* 76: 3823–3833, 1996a.

Fee MS, Mitra PP, Kleinfeld D. Automatic sorting of multiple unit neuronal signals in the presence of anisotropic and non-Gaussian variability. *J Neurosci Methods* 69: 175–188, 1996b.

Fino E, Araya R, Peterka DS, Salierno M, Etchenique R, Yuste R. RuBi-Glutamate: Two-Photon and Visible-Light Photoactivation of Neurons and Dendritic spines. *Front Neural Circuits* 3: 2, 2009.

Fiscella M, Farrow K, Jones IL, Jäckel D, Müller J, Frey U, Bakkum DJ, Hantz P, Roska B, Hierlemann A. Recording from defined populations of retinal ganglion cells using a high-density CMOS-integrated microelectrode array with real-time switchable electrode selection. *J Neurosci Methods* 211: 103–13, 2012.

Frey U, Egert U, Heer F, Hafizovic S, Hierlemann A. Microelectronic system for high-resolution mapping of extracellular electric fields applied to brain slices. *Biosens Bioelectron* 24: 2191–2198, 2009.

Frey U, Sedivy J, Heer F, Pedron R, Ballini M, Mueller J, Bakkum D, Hafizovic S, Faraci FD, Greve F, Kirstein K-U, Hierlemann A. Switch-Matrix-Based High-Density Microelectrode Array in CMOS Technology. *Solid-State Circuits, IEEE J* 45: 467–482, 2010.

Fuentealba P, Crochet S, Timofeev I, Steriade M. Synaptic interactions between thalamic and cortical inputs onto cortical neurons in vivo. *J Neurophysiol* 91: 1990–1998, 2004.

Gal A, Eytan D, Wallach A, Sandler M, Schiller J, Marom S. Dynamics of excitability over extended timescales in cultured cortical neurons. *J Neurosci* 30: 16332–42, 2010.

Gozani SN, Miller JP. Optimal discrimination and classification of neuronal action potential waveforms from multiunit, multichannel recordings using software-based linear filters. *Biomed Eng IEEE Trans* 41: 358–372, 1994.

Gray CM, Maldonado PE, Wilson M, McNaughton B. Tetrodes markedly improve the reliability and yield of multiple single-unit isolation from multi-unit recordings in cat striate cortex. *J Neurosci Methods* 63: 43–54, 1995.

Hang GB, Dan Y. Asymmetric temporal integration of layer 4 and layer 2/3 inputs in visual cortex. *J Neurophysiol* 105: 347–355, 2011.

Harris KD, Henze DA, Csicsvari J, Hirase H, Buzsaki G. Accuracy of Tetrode Spike Separation as Determined by Simultaneous Intracellular and Extracellular Measurements. *J Neurophysiol* 84: 401–414, 2000.

Henze DA, Borhegyi Z, Csicsvari J, Mamiya A, Harris KD, Buzsaki G. Intracellular Features Predicted by Extracellular Recordings in the Hippocampus In Vivo. *J Neurophysiol* 84: 390–400, 2000.

Hermle T, Schwarz C, Bogdan M. Employing ICA and SOM for spike sorting of multielectrode recordings from CNS. *J Physiol Paris* 98: 349–356, 2004.

Hill DN, Mehta SB, Kleinfeld D. Quality metrics to accompany spike sorting of extracellular signals. *J Neurosci* 31: 8699–705, 2011.

Hill ES, Moore-Kochlacs C, Vasireddi SK, Sejnowski TJ, Frost WN. Validation of independent component analysis for rapid spike sorting of optical recording data. *J Neurophysiol* 104: 3721–31, 2010.

Histed MH, Bonin V, Reid RC. Direct activation of sparse, distributed populations of cortical neurons by electrical microstimulation. *Neuron* 63: 508–22, 2009.

Hutzler M, Lambacher A, Eversmann B, Jenkner M, Thewes R, Fromherz P. High-resolution multitransistor array recording of electrical field potentials in cultured brain slices. *J Neurophysiol* 96: 1638–45, 2006.

Hyvärinen a, Oja E. Independent component analysis: algorithms and applications. *Neural networks* 13: 411–30, 2000.

Hyvärinen a. Fast and robust fixed-point algorithms for independent component analysis. *IEEE Trans neural networks* 10: 626–34, 1999.

Jäckel D, Frey U, Fiscella M, Franke F, Hierlemann A. Applicability of independent component analysis on high-density microelectrode array recordings. *J Neurophysiol* 108: 334–348, 2012.

Jiang X, Wang G, Lee AJ, Stornetta RL, Zhu JJ. The organization of two new cortical interneuronal circuits. *Nat Neurosci* 16: 210–8, 2013.

Kandel ER, Schwartz JH, Jessell TM. *Principles of neural science*. 4th ed. New York: McGraw-Hill, Health Professions Division, 2000.

Lei N, Ramakrishnan S, Shi P, Orcutt JS, Yuste R, Kam LC, Shepard KL. High-resolution extracellular stimulation of dispersed hippocampal culture with high-density CMOS multielectrode array based on non-Faradaic electrodes. *J Neural Eng* 8: 044003, 2011.

Levine MW. The distribution of the intervals between neural impulses in the maintained discharges of retinal ganglion cells. *Biol Cybern* 65: 459–467, 1991.

Lewicki MS. A review of methods for spike sorting: the detection and classification of neural action potentials. *Network* 9: R53–78, 1998.

Litke AM, Bezayiff N, Chichilnisky EJ, Cunningham W, Dabrowski W, Grillo AA, Grivich M, Grybos P, Hottowy P, Kachiguine S, Kalmar RS, Mathieson K, Petrusca D, Rahman M, Sher A. What does the eye tell the brain?: Development of a system for the large-scale recording of retinal output activity. *IEEE Trans Nucl Sci* 51: 1434–1440, 2004.

Livi P, Heer F, Frey U, Bakkum DJ, Hierlemann A. Compact voltage and current stimulation buffer for high-density microelectrode arrays. In: *2010 IEEE International Solid-State Circuits Conference - (ISSCC)*. Ieee, p. 240–241.

Lübke J, Feldmeyer D. Excitatory signal flow and connectivity in a cortical column: Focus on barrel cortex. *Brain Struct. Funct.* 212: 3–17, 2007.

Maccione A, Garofalo M, Nieus T, Tedesco M, Berdondini L, Martinoia S. Multiscale functional connectivity estimation on low-density neuronal cultures recorded by high-density CMOS Micro Electrode Arrays. *J Neurosci Methods* 207: 161–71, 2012.

Maccione A, Hennig MH, Gandolfo M, Muthmann O, van Coppenhagen J, Eglen SJ, Berdondini L, Sernagor E. Following the ontogeny of retinal waves: pan-retinal recordings of population dynamics in the neonatal mouse. *J Physiol* 592: 1545–63, 2014.

Markram H, Lubke J, Frotscher M, Sakmann B. Regulation of synaptic efficacy by coincidence of postsynaptic APs and EPSPs. *Science (80-)* 275: 213–215, 1997.

Molleman A. Patch Clamping: An Introductory Guide to Patch Clamp Electrophysiology. 2003. .

Mukamel EA, Nimmerjahn A, Schnitzer MJ. Automated analysis of cellular signals from large-scale calcium imaging data. *Neuron* 63: 747–60, 2009.

Nawrot MP, Schnepel P, Aertsen A, Boucsein C. Precisely timed signal transmission in neocortical networks with reliable intermediate-range projections. *Front Neural Circuits* 3: 1, 2009.

Neher E, Sakmann B. Single-channel currents recorded from membrane of denervated frog muscle fibres. *Nature* 260: 799–802, 1976.

Nikolenko V, Poskanzer KE, Yuste R. Two-photon photostimulation and imaging of neural circuits. *Nat Methods* 4: 943–50, 2007.

Nowak LG, Bullier J. Axons, but not cell bodies, are activated by electrical stimulation in cortical gray matter. I. Evidence from chronaxie measurements. *Exp brain Res* 118: 477–88, 1998.

Perin R, Berger TK, Markram H. A synaptic organizing principle for cortical neuronal groups. *Proc Natl Acad Sci U S A* 108: 5419–24, 2011.

Pine J. Recording action potentials from cultured neurons with extracellular microcircuit electrodes. *J Neurosci Methods* 2: 19–31, 1980.

Polsky A, Mel BW, Schiller J. Computational subunits in thin dendrites of pyramidal cells. *Nat Neurosci* 7: 621–7, 2004.

Poncer JC, McKinney RA, Gähwiler BH, Thompson SM. Either N- or P-type calcium channels mediate GABA release at distinct hippocampal inhibitory synapses. *Neuron* 18: 463–472, 1997.

Pouzat C. Using noise signature to optimize spike-sorting and to assess neuronal classification quality. *J Neurosci Methods* 122: 43–57, 2002.

Prentice JS, Homann J, Simmons KD, Tkačik G, Balasubramanian V, Nelson PC. Fast, scalable, Bayesian spike identification for multi-electrode arrays. *PLoS One* 6: e19884, 2011.

Quiroga RQ, Nadasdy Z, Ben-Shaul Y. Unsupervised spike detection and sorting with wavelets and superparamagnetic clustering. *Neural Comput* 16: 1661–1687, 2004.

Rattay F, Paredes LP, Leao RN. Strength-duration relationship for intra- versus extracellular stimulation with microelectrodes. *Neuroscience* 214: 1–13, 2012.

Rattay F, Wenger C. Which elements of the mammalian central nervous system are excited by low current stimulation with microelectrodes? *Neuroscience* 170: 399–407, 2010.

Reidl J, Starke J, Omer DB, Grinvald A, Spors H. Independent component analysis of high-resolution imaging data identifies distinct functional domains. *Neuroimage* 34: 94–108, 2007.

Royer S, Paré D. Conservation of total synaptic weight through balanced synaptic depression and potentiation. *Nature* 422: 518–522, 2003.

Sasaki T, Matsuki N, Ikegaya Y. Action-potential modulation during axonal conduction. *Science* 331: 599–601, 2011.

Sasaki T, Minamisawa G, Takahashi N, Matsuki N, Ikegaya Y. Reverse Optical Trawling for Synaptic Connections In Situ. *J Neurophysiol* 102: 636–643, 2009.

Segev R, Goodhouse J, Puchalla J, Berry MJ. Recording spikes from a large fraction of the ganglion cells in a retinal patch. *Nat Neurosci* 7: 1154–61, 2004.

Shahaf G, Marom S. Learning in Networks of Cortical Neurons. *J Neurosci* 21: 8782–8788, 2001.

Shiraishi Y, Katayama N, Takahashi T, Karashima A, Nakao M. Multi-neuron action potentials recorded with tetrode are not instantaneous mixtures of single neuronal action potentials. *Conf Proc IEEE Eng Med Biol Soc* 2009: 4019–22, 2009.

Shoham S, Fellows MR, Normann RA. Robust, automatic spike sorting using mixtures of multivariate t-distributions. *J Neurosci Methods* 127: 111–122, 2003.

Snellings A, Anderson DJ, Aldridge JW. Improved signal and reduced noise in neural recordings from close-spaced electrode arrays using independent component analysis as a preprocessor. *J Neurosci Methods* 150: 254–264, 2006.

Stasheff SF. Emergence of sustained spontaneous hyperactivity and temporary preservation of OFF responses in ganglion cells of the retinal degeneration (rd1) mouse. *J Neurophysiol* 99: 1408–21, 2008.

Stett A, Egert U, Guenther E, Hofmann F, Meyer T, Nisch W, Haemmerle H. Biological application of microelectrode arrays in drug discovery and basic research. *Anal Bioanal Chem* 377: 486–495, 2003.

Stone J V. Independent component analysis: an introduction. *Trends Cogn Sci* 6: 59–64, 2002.

Stuart G, Spruston N, Sakmann B, Hausser M. Action potential initiation and backpropagation in neurons of the mammalian CNS [Online]. *Trends Neurosci* 20: 125–131, 1997.

Takahashi N, Sasaki T, Matsumoto W, Matsuki N, Ikegaya Y. Circuit topology for synchronizing neurons in spontaneously active networks. *Proc Natl Acad Sci* 107: 10244–10249, 2010.

Takahashi S, Anzai Y, Sakurai Y. Automatic sorting for multi-neuronal activity recorded with tetrodes in the presence of overlapping spikes. *J Neurophysiol* 89: 2245–58, 2003.

Takahashi S, Sakurai Y. Real-time and automatic sorting of multi-neuronal activity for sub-millisecond interactions in vivo. *Neuroscience* 134: 301–15, 2005.

Vargas-Irwin C, Donoghue JP. Automated spike sorting using density grid contour clustering and subtractive waveform decomposition. *J Neurosci Methods* 164: 1–18, 2007.

Wagenaar D, DeMarse TB, Potter SM. MeaBench: A toolset for multi-electrode data acquisition and on-line analysis. In: *Neural Engineering, 2005. Conference Proceedings. 2nd International IEEE EMBS Conference on*. 2005, p. 518–521.

Wagenaar D, Pine J, Potter S. An extremely rich repertoire of bursting patterns during the development of cortical cultures. *BMC Neurosci* 7: 11, 2006.

Zeck G, Lambacher A, Fromherz P. Axonal transmission in the retina introduces a small dispersion of relative timing in the ganglion cell population response. *PLoS One* 6: e20810, 2011.

Zhang P-M, Wu J-Y, Zhou Y, Liang P-J, Yuan J-Q. Spike sorting in multi-channel extracellular recordings of retinas. In: *Neural Networks and Signal Processing, 2003. Proceedings of the 2003 International Conference on*. 2003, p. 712 – 715 – Vol – 1.

ACKNOWLEDGEMENTS

I would like to thank Prof. Andreas Hierlemann for giving me the unique opportunity to conduct my PhD thesis at BEL. It was extremely enriching for me to be able to work on such different areas as signal processing, engineering and neuroscience and to have the chance to build a complex measurement set-up from scratch. I truly appreciated the work atmosphere and environment at BEL, which allows the PhD students to take initiatives and to independently shape their own research. Finally I am also very grateful for constructive but also for critical comments on my work, as well as for the extensive editing of scientific text, which quite often turned Swiss German shaped sentence fragments into meaningful, concise scientific statements.

It was a great pleasure for me that Prof. Ulrich Egert acted as a co-examiner for my dissertation, since he is an expert in both, neuronal cultures and MEA research. The comments and suggestions I received were very helpful and encouraging.

Great thanks go to Urs Frey who was also a co-examiner and travelled all the way to Basel from Riken, Japan. It was Urs who introduced me to the 'Neurochip'-project in 2007 during my semester thesis at PEL. Already then he infected me with his enthusiasm about the combination of engineering and neuroscience, which then also brought me to BEL and finally lead to this thesis. The HiDens chip, realized by Urs, is a great device to work with, and clearly forms the foundation for this work. But equally important, Urs was always open for my requests and questions, and never got tired of giving back useful feedback. I learned a lot from the way he approached technical challenges and scientific projects.

During my PhD I found myself in the comfortable position to work with three postdoctoral researchers from different areas and to benefit

many interesting discussions and valuable inputs. Furthermore, the current BEL members Ketki Chawla, Sebastian Bürgel, Roland Diggelmann, Olivier Frey, Jinyoung Kim, Patrick Misun, Gregor Schmidt, Amir Shadmani, Sergey Sitnikov, Yonghong Tao and Ben van Lier, but also the former BELers Branka Roscic, Yihui Chen, Marco Ballini, Paolo Livi, Jörg Rothe, Carlos Escobedo, Zhen Zhu, Nils Haandbaek, Nils Goedecke and Ralf Streichan are and were responsible for creating an inspiring atmosphere and a pleasant work environment, and many of them helped me in one way or the other during the last years.

Our cleanroom engineer Alexander Stettler also helped me out many times and he is also acknowledged for establishing a reliable and fast chip preparation procedure. Paul Argast and Peter Buchmann from the D-BSSE workshop are acknowledged for contributing various important parts to the measurement set-up. Furthermore, I thank the whole IT staff and FIS staff for their professional and motivated support and Albert Martel for the rapid chip preparation. I also thank the Master students Yan Sun, for building the analog acquisition module, and Usman Khalid, for his work on the real-time spike sorter.

Very important support for establishing and improving the patch clamp experiments came from three persons outside ETH: Tamas Szikra from the Friedrich Miescher Institute, as well as Pascal Pflimlin and Veronique Graf from Roche helped and supported me in a very friendly, patient and competent way. I am extremely grateful for their generous help.

Finally, I also received great support from my family and friends. Thank you Avner Pinchover for your help with the dissertation layout and with the cover. And thank you David Hadad for providing extensive last-minute editing support with the thesis. I want to thank all the family members and friends for their support during all the years, but especially during the last months of my thesis.

Thank you Eynav, Naveh, Liran for being here and thank you Dalit for everything!

PUBLICATIONS

Journal Articles

J. Dragas, **D. Jäckel**, A. Hierlemann, and F. Franke, **"Complexity Optimisation and High-Throughput Low-Latency Hardware Implementation of a Multi-Electrode Spike-Sorting Algorithm"**, *IEEE Trans. On Neural Systems and Rehabilitation Engineering*, 2014.

M. Ballini, J. Mueller, P. Livi, Y. Chen, U. Frey, A. Stettler, A. Shadmani, V. Viswam, I. Jones, **D. Jäckel**, M. Radivojevic, M. Lewandowska, W. Gong, M. Fiscella, D. Bakkum, F. Heer, and A. Hierlemann, **"A 1024-Channel CMOS Microelectrode Array With 26,400 Electrodes for Recording and Stimulation of Electrogenic Cells In Vitro"**, *IEEE Journal of Solid-State Circuits*, 2014, 49, pp. 2705–2719.

Felix Franke**, David Jäckel**, Jelena Dragas, Jan Müller, Milos Radivojevic, Douglas Bakkum and Andreas Hierlemann, **"High-density microelectrode array recordings and real-time spike sorting for closed-loop experiments: an emerging technology to study neural plasticity"**, *Frontiers in Neural Circuits*, 2012, 6:105,.

Michele Fiscella, Karl Farrow, Ian L. Jones, **David Jäckel**, Jan Müller, Urs Frey, Douglas J. Bakkum, Péter Hantz, Botond Roska, and Andreas Hierlemann, **"Recording from defined populations of retinal ganglion cells using a high-density CMOS-integrated microelectrode array with real-time switchable electrode selection"**, *Journal of Neuroscience Methods*, 2012, Volume 211, Issue 1, pp. 103–113.

David Jäckel, Urs Frey, Michele Fiscella, Felix Franke and Andreas Hierlemann, **"Applicability of Independent Component Analysis on High-Density Microelectrode Array Recordings"**, *Journal of Neurophysiology*, 2012, 108 (1), pp. 334-348.

Conference Contributions

W. Gong, **D. Jäckel**, J. Müller, M. Fiscella, M. Radivojevic, D. J. Bakkum, F. Franke, F. Knoflach, B. Gähwiler, B. Roscic, T. Russell, A. Hierlemann, **"Long-Term Cultivation and Recording from Organotypic Brain Slices on High-density Micro-electrode Arrays"**, in *Proceedings of the 9th International Meeting on Substrate-Integrated Micro Electrode Arrays*, 2014, Reutlingen, Germany, pp. 335-336, ISSN 2199-1596.

D. J. Bakkum, M. Radivojevic, **D. Jäckel**, F. Franke, T. L. Russell, U. Frey, H. Takahashi, and A. Hierlemann, **"3D Finite Element Modeling of Single Neurons and the Microelectrode Array Microenvironment"**, in *Proceedings of the 9th International Meeting on Substrate-Integrated Micro Electrode Arrays*, 2014, Reutlingen, Germany, pp. 160–161, ISSN 2199-1596.

D. Jäckel, J. Müller, T. L. Russell, M. Radivojevic, F. Franke, U. Frey, D. J. Bakkum, and A. Hierlemann, **"Simultaneous Intra- and Extracellular Recordings using a Combined High-Density Microelectrode Array and Patch-Clamp System"**, in *Proceedings of the 9th International Meeting on Substrate-Integrated Microelectrode Arrays*, 2014, Reutlingen, Germany, pp. 153–155, ISSN 2199-1596.

V. Viswam, **D. Jäckel**, M. Ballini, J. Müller, M. Radivojevic, U. Frey, F. Franke, and A. Hierlemann, **"An Automated Method for Characterizing Electrode Properties of High-Density Microelectrode Arrays"** in *Proceedings of the 9th International Meeting on Substrate-Integrated Microelectrode Arrays*, 2014, Reutlingen, Germany, pp. 302–303, ISSN 2199-1596.

J. Dragas, **D. Jäckel**, F. Franke, A. Hierlemann, **"High-throughput, High-performance, Low-latency Spike-Sorting Hardware Platform"**, in *Proceedings of the 9th International Meeting on Substrate-Integrated Microelectrode Arrays*, 2014, Reutlingen, Germany, pp. 185-186, ISSN 2199-1596.

M. Radivojevic, **D. Jäckel**, J. Müller, V. Viswam, I.L. Jones, A. Hierlemann, D. Bakkum, **"Finding the most effective site for extracellular neuronal stimulation"**, in *Proceedings of the 9th International Meeting on Substrate-Integrated Microelectrode Arrays*, 2014, Reutlingen, Germany, pp. 60-61, ISSN 2199-1596.

J. Dragas, **D. Jäckel**, F. Franke and A. Hierlemann **"High-Throughput Hardware for Real-Time Spike Overlap Decomposition in Multi-Electrode Neuronal Recording Systems"**, *Proceedings of the IEEE International Symposium on Circuits and Systems (ISCAS)*, 2014, Melbourne, Australia, pp. 658-661. ISBN: 978-1-4799-3432-4/14.

J. Dragas, **D. Jäckel**, F. Franke and A. Hierlemann, **"An Unsupervised Method for On-Chip Neural Spike Detection in Multi-Electrode Recording Systems"**, *Proceedings of the 35th Annual International Conference of the IEEE EMBS*, Osaka, Japan, 2013, pp. 2535-2538. ISSN 978-1-4577-0216-7/13.

Invited: U. Frey, M. Fiscella, **D. Jaeckel**, and A. Hierlemann, **"CMOS-based Microelectrode Arrays for High-Resolution Electrophysiology of the Retina"**, *2nd HD Physiology International Symposium*, Tokyo, Japan, 2013, p. 24.

D. Jäckel, D. J. Bakkum, M. Radivojevic, J. Müller, M. Fiscella, U. Frey, F. Franke, A. Hierlemann, **"Using extracellular high-resolution microelectrode array recordings to estimate intracellular features of cultured neurons"**, *Annual Meeting of the Society for Neuroscience (SfN)*, 2012, New Orleans, USA.

D. Jäckel, F. Franke, U. Frey, A. Hierlemann, **"Simulator for Realistic High-Density Microelectrode Array Signals"**, *5th INCF Congress of Neuroinformatics 2012*, Munich, Germany.

J. Dragas, **D. Jäckel**, F. Franke, A. Hierlemann, **"FPGA implementation of a template matching-based real-time spike sorter for extracellular multi-electrode recordings of neural signals"**, *5th INCF Congress of Neuroinformatics 2012*, Munich, Germany.

F. Franke, **D. Jäckel**, A. Hierlemann, **"High performance spike sorting for HDMEA recordings"**, in *Proceedings of the 8th International Meeting on Substrate-Integrated Micro Electrode Arrays*, 2012, Reutlingen, Germany, pp. 218-219, ISSN 2194-5519.

M. Fiscella, K. Farrow, I. L. Jones, **D. Jäckel**, J. Müller, U. Frey, D. J. Bakkum, B. Roska, A. Hierlemann, **"Targeting Defined Populations of Retinal Ganglion Cells with CMOS Microelectrode Arrays"**, in *Proceedings of the 8th International Meeting on Substrate-Integrated*

Publications

Micro Electrode Arrays, 2012, Reutlingen, Germany, pp. 114-116, ISSN 2194-5519.

M, Radivojevic, **D. Jäckel**, J. Müller, M. Fiscella, U. Frey, B. Roscic, A. Hierlemann, D. J. Bakkum, **"Methods for Long-term High-resolution Characterization of In Vitro Developing Neuronal Networks Grown over High-density CMOS-based Microelectrode Arrays"**, in *Proceedings of the 8th International Meeting on Substrate-Integrated Micro Electrode Arrays*, 2012, Reutlingen, Germany, pp. 68-69, ISSN 2194-5519.

J. Dragas, **D. Jäckel**, F. Franke, A. Hierlemann, **"Hardware implementation, optimisation and performance analysis of a real-time spike sorter for high-density microelectrode recordings"**, *Proc. of the 8th International Meeting on Substrate-Integrated Micro Electrode Arrays*, 2012, Reutlingen, Germany, pp. 232-233, ISSN 2194-5519.

M. Fiscella. I. L. Jones, **D. Jäckel**, J. Müller, U. Frey, K. Farrow, B. Roska and A. Hierlemann, **"Recording of Light Induced Neural Activity of Mouse Retinal Ganglion Cells on a CMOS-Integrated High-Density Microelectrode Array"**, *Proceedings of the European Retina Meeting (ERM)*, 2011, Amsterdam, The Netherlands, pp. 92.

D. Jäckel, U. Frey, M. Fiscella, and A. Hierlemann, **"Blind Source Separation for Spike Sorting of High Density Microelectrode Array Recordings"**, *Proceedings of the 5th International IEEE EMBS Conference on Neural Engineering*, 2011, Cancun, Mexico, pp. 5-8. ISBN: 978-1-4244-4140-2.

D. Jäckel, J. Müller, M.U. Khalid, U. Frey, D.J. Bakkum, and A. Hierlemann **"High-Density Microelectrode Array System and Optimal Filtering for Closed-Loop Experiments"**, *Proceedings of the 16th IEEE International Conference on Solid-State Sensors, Actuators & Microsystems, Transducers*, 2011, Beijing, China, pp. 1200-1203. ISBN: 978-1-4577-0157-3.

I.L. Jones, M. Fiscella, U. Frey, **D. Jäckel**, J. Müller, B. Roscic, R. Streichan, A. Hierlemann, **"Recording of Neural Activity of Mouse Retinal Ganglion Cells by Means of an Integrated High-density Microelectrode Array"**, *Proceedings of the 16th IEEE International Conference on Solid-State Sensors, Actuators & Microsystems,*

Transducers, 2011, Beijing, China, pp. 186-189. ISBN: 978-1-4577-0157-3.

U. Frey, **D. Jäckel**, M. Fiscella, and A. Hierlemann, **"Spike Sorting Techniques for High-Resolution Microelectrode Array Recordings"**, in *Proceedings of the 26th Symposium on Biological and Physiological Engineering (BPES)*, Shiga, Japan, 2011, pp. 131–134.

M. Fiscella, I.L. Jones, **D. Jäckel**, J. Müller, U. Frey, K. Farrow, B. Roska, A. Hierlemann, **"Recording of Light Induced Neural Activity of Mouse Retinal Ganglion Cells on an Integrated High-density Microelectrode Array"**, *Abstract Book 1st International SystemsX.ch Conference on Systems Biology*, Oct 24th – 26th, 2011, Basel, Switzerland, p.142. ISBN: 978-3-909386-21-5.

F. Franke, **D. Jäckel**, P. Meier, U. Frey, M. Fiscella, A. Hierlemann, K. Obermayer, **"Spike sorting for multielectrode arrays"**, *Annual Meeting of the Society for Neuroscience (SfN)*, 2011, Washington DC, USA.

D. Jäckel, R. Moeckel, and S-C. Liu, **"Sound Recognition with Spiking Silicon Cochlea and Hidden Markov Models",** in *Proc. of the 6th Conference on Ph.D. Research in Microelectronic & Electronics*, Berlin, Germany, 2010

M. Fiscella, U. Frey, **D. Jäckel**, J. Müller, R. Streichan, I. L. Jones, B. Roscic, K. Farrow, B. Roska, A. Hierlemann, **"Recording of Neural Activity of Mouse Retinal Ganglion Cells by Means of an Integrated High-Density Microelectrode Array"**, in *FENS Abstr.*, vol.5, 019.10, 2010, Amsterdam, The Netherlands.

M. Fiscella, U. Frey, **D. Jäckel**, J. Müller, R. Streichan, I. Jones, B. Roscic, C. Farrow, B. Roska, A. Hierlemann, **"Recording of Neural Activity of Mouse Retinal Ganglion Cells by Means of an Integrated High Density Microelectrode Array"**, *Proc. of the 7th International meeting on substrate-integrated micro electrode arrays*, 2010, Reutlingen, Germany, p. 106-107, ISBN 3-938345-08-5.

D. Jäckel, U. Frey, J. Müller, I. Jones, U. Khalid, J. Sedivy, A. Hierlemann, **"Online Spike Extraction for Bidirectional High-Density Microelectrode Arrays using Optimal Filters"**, *Proc. of the 7th International meeting on substrate-integrated micro electrode arrays*, 2010, Reutlingen, Germany, p. 201-202, ISBN 3-938345-08-5.

Publications

J. Sedivy, U. Frey, **D. Jackel**, and A. Hierlemann, "Independent-Component-Analysis-Based Spike Sorting Algorithm for High-Density Microelectrode Array Data Processing," in *Proc. IEEE Sensors Conf.*, Christchurch, New Zealand, pp. 384 – 386, 2009.

U. Frey, U. Egert, **D. Jäckel**, J. Sedivy, M. Ballini, P. Livi, F. Faraci, F. Heer, S. Hafizovic, B. Roscic, and A. Hierlemann,**"Depth Recording Capabilities of Planar High-Density Microelectrode Arrays"**, *Proceedings of the 4th International IEEE EMBS Conference on Neural Engineering*, Antalya, Turkey, 2009, pp. 207–210, ISBN 978-1-4244-2073-5.

CURRICULUM VITAE

David Jäckel

Born November 4th, 1980, Buenos Aires, Argentina

Swiss Citizen

December 2014	Defense of the dissertation entitled *Methods for Synaptic Connectivity Mapping, Neuronal Stimulation and Spike Sorting Using High-density Microelectrode Arrays and Patch Clamp Recordings*
2009 - 2014	PhD candidate at the Bio Engineering Laboratory, ETH Zürich
2008	MSc ETH in Electrical Engineering, Master thesis entitled *Robot Head with Neuromorphic Chips* at the Institute for Neuroinformatics, University of Zürich and ETH Zürich
2007	Internship at Automación Micromecánica, Buenos Aires, Argentina
2002 - 2008	Studies in Information Technology and Electrical Engineering, ETH Zürich
2001 - 2002	Jewish studies, Maale Gilboa, Israel
1996 - 2001	Kantonsschule Enge, Zürich, Switzerland